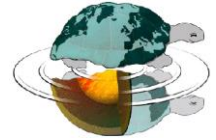




UNIVERSITÀ DEGLI STUDI DI MILANO

Dottorato di Ricerca in Scienze della Terra

Ciclo XXIX



---

**Degradation of organic and mineral phases in buried  
human remains: the Earth Sciences analytical  
characterization**

Ph.D. Thesis

**VALENTINA CARUSO**  
Matricola R10799-R28

---

*Tutor*

**Dott. Luca Trombino**

*Co- Tutor*

**Prof.ssa Cristina Cattaneo**

**Academic Year**

**2015-2016**

*Coordinator*

**Prof.ssa Elisabetta Erba**



# Contents

<b>Abstract</b>	<b>7</b>
<b>1. Introduction</b>	<b>11</b>
1.1 - Bone tissue.....	11
1.2 - Taphonomy and bone diagenesis.....	13
<b>2. Materials and Methods</b>	<b>15</b>
2.1 - Materials.....	15
2.1.1 - Bones coming from four known dating burial locations of Milan.....	15
2.1.1.1 - Site 1: Università Cattolica.....	15
2.1.1.2 - Site 2: Viale Sabotino.....	15
2.1.1.3 - Site 3: Ca' Granda.....	16
2.1.1.4 - Site 4: Cimitero Maggiore.....	16
2.1.1.5 - Samples.....	16
2.1.2 - Archaeological site of Travo (PC).....	18
2.1.2.1 - Necropolis of S.Andrea.....	18
2.1.2.2 - Geology.....	19
2.1.2.3 - Geopedology.....	20
2.2 - Methods.....	20
2.2.1 - Macroscopic analysis.....	20
2.2.2 - Bone conservation after the recovery.....	22
2.2.3 - Biochemical analysis (Luminol test).....	22
2.2.4 - Microscopic analysis.....	24
2.2.4.1 - Histology.....	24

2.2.4.1.1 - Optical light microscopy on calcified thin bone sections.....	25
2.2.4.1.2 - Optical light microscopy on decalcified thin bone sections.....	26
2.2.4.3 - Scanning electron microscopy with energy-dispersive X-ray spectroscopy.....	27
2.2.4.3.1 - Preparation of non-embedded bone sections.....	28
2.2.4.3.2 - Preparation of embedded thin bone sections.....	28
2.2.4.3.3 - Grave soil samples preparation.....	29
2.2.4.3.4 - Elaboration of quantitative data.....	29
2.2.4.3.5 - Elaboration of qualitative data.....	29
2.2.5 - 3D micro-computed tomography.....	30
2.2.5.1 - Samples preparation.....	30
2.2.5.2 - Synchrotron radiation.....	31
2.2.5.3 - Imaging analysis.....	32
2.2.6 - Fourier transform infrared spectrometry (FT-IR) and micro-spectrometry (mFTIR).....	37
2.2.6.1 - Fourier transform infrared spectrometry (FT-IR).....	37
2.2.6.1.1 - Whole bone sample preparation.....	37
2.2.6.1.2 - Bone Acid Insoluble Fraction (AIF).....	37
2.2.6.1.3 - FT-IR Spectra collection.....	38
2.2.6.1.4 - Spectral Analysis.....	38
2.2.6.2 - Fourier transform infrared micro-spectrometry (mFTIR)....	40
2.2.7 - Characterization of grave soil.....	41
2.2.7.1 - Color.....	41
2.2.7.2 - Particle size distribution.....	42
2.2.7.3 - pH.....	43
2.2.7.4 - Organic carbon.....	43
2.2.7.5 - Calcium carbonate equivalent.....	44

### **3. Results**

**45**

3.1 - Macroscopic analysis.....	45
3.2 - Preservation degree of buried human skeletons.....	46
3.2 - Biochemical analysis.....	48
3.3 - Microscopic analysis in optic light.....	49

3.4 - Chemical and morphological analyses performed by scanning electron microscopy coupled with energy-dispersive X-ray spectroscopy (SEM-EDS).....	51
3.4.1 - SEM-EDS results of bone sections from Milan.....	51
3.4.2 - SEM-EDS results of bone sections and grave soils from Travo (PC).....	61
3.5 - Computed tomography imaging.....	62
3.6 - Organic and mineral fraction by FT-IR analysis.....	65
3.7 - Grave soil analyses.....	68

## **4. Discussions 73**

4.1 - Bone tissue conservation in archaeological and contemporary human remains from Milan: the role of degradation of organic and mineral phases.....	73
4.1.1 - Macroscopic scale.....	73
4.1.2 - Biochemical scale.....	73
4.1.3 - Microscopic scale in transmitted and polarized light.....	75
4.1.4 - Quantitative and qualitative analyses by SEM-EDS.....	78
4.1.5 - 3D $\mu$ CT (bone porosity).....	82
4.1.6 - Qualitative and semi-quantitative analyses of organic and mineral matter by FT-IR spectroscopy .....	85
4.2 - How human remains and grave soil interact? The case study of archaeological site of S. Andrea, Travo (PC).....	92

## **5. Conclusions 103**

## **6. References 107**

## **7. Appendices 113**

7.1 - Appendix 1.....	113
7.2 - Appendix 2.....	132
7.3 - Appendix 3.....	134
7.4 - Appendix 4.....	139
7.5 - Appendix 5.....	141
7.6 - Appendix 6.....	144
7.7 - Appendix 7.....	147
7.8 - Appendix 8.....	151
7.9 - Appendix 9.....	153

<i>Acknowledgements</i> .....	159
-------------------------------	-----



# Abstract

The thesis focuses on the characterization of the alteration of the mineral and organic phases, investigated with different approaches, of human bone tissue from different burial contexts, with ages spanning from the Late Roman period to our time. This topic is very important in paleontological, archaeo-anthropological and forensic contexts in order to understand the taphonomic agents and then to provide biological data as possibly to discern human behavior in ancient funerary as well as in recent forensic contexts. It is well-known that *peri* and *post mortem* events may leave marks that have to be interpreted in the light of the state of the conservation or degradation of the skeletal remains.

In fact, physical anthropologists are frequently required to date human bone remains, in order to recognize if osteological samples have an archaeological, historic or forensic interest. The determination of *post mortem interval* (PMI), the time elapsed between the death and the discovery of the corpse or skeletal remains, is extremely difficult to evaluate in absence of direct chronometric dating (e.g. C<sup>14</sup>), since bones might undergo several alterations, both structural and chemical, depending on the environment in which they deposited in. Because of bone tissue is an intimate association of mineral (carbonate-hydroxyapatite) and organic components (collagen) arranged in an ordinary structure, different levels of degradation are possible. Over time *post mortem* degradation is dominated by loss of structural collagen by collagenolytic enzymes, which caused a rapid swelling and hydrolysis of the protein fibers. Collagen dissolution is generally accompanied by the alteration of mineral crystals, which are vulnerable to diagenetic changes due to their small size. During diagenesis, the protein can be totally or partially removed and can be replaced by inorganic precipitates, the most common benign hydroxyapatite, which in the process is subjected to recrystallization, ion

exchange and substitution. As consequence, when depositional conditions are favorable for bone preservation, the mineral crystallinity increase, the porosity and chemical composition change.

The quality and the assesement of organic and inorganic phase, can act positively or negatively both on bone mechanical properties in live, both on decomposition process after death, reducing or accelerating it.

Several studies were performed to better understand the taphonomy of bone material during burial time. It appears that bone degradation depends on a wide range of environmental interactions, including biological, chemical and physical factors. These include: average temperature and humidity, microbilological composition and activity, soil chemistry (mineralogy and pH) and permeability, mechanical pressure and other numerous factors.

Different type of bone degradation are observable at different scale of observation; particularly, in this study, bone preservation was investigated at macroscopic, biomolecular, microscopic, ultramicroscopic and chemical scale.

The aim of this research is thus to further describe the impact of environmental conditions on bone preservation, and the effect of time, by applying and comparing the results from different analitical techniques.

For this study 40 human skeletons of adult individuals from four different dated burial location in the Milan area were analyzed. The first one is a necropolis dated to the Late Roman age (3<sup>th</sup>-4<sup>th</sup> century AD), the second one is a 17<sup>th</sup> century AD mass grave, the third one is an ossuary containing bones dated between 15<sup>th</sup> and 18<sup>th</sup> century AD, and the last one is a modern cemetery.

The macroscopic analysis evaluated the general appearance of the remains and their state of preservation, through the observation of specific macroscopic parameters and morphological characteristics.

The Luminol test, a fast and inexpensive method developed to detect blood traces, was performed to investigate the presence of haemoglobin preserved in bone.

The histological analysis, conducted on calcified thin sections, considered the presence or absence of tunneling and bioerosion, in accordance to the Oxford Histological Index (OHI). Also, to evaluate the state of preservation of the organic component, primarily collagen, the samples were decalcified and stained with Hematoxylin and Eosin. Because of the lack of literature in this field, we created a new Decalcified Histological Index (DHI). Both calcified and decalcified bone thin sections were



observed in transmitted and polarized light microscopy, in order to test the optical properties of structural components.

Scanning electron microscope coupled with energy-dispersive X-ray spectroscopy (SEM-EDS) was used to evaluate exogenous chemical elements and minerals, adsorbed from burial environment, and histological changes, as well as recrystallization, tunnelling and fractures, due to fungal or bacteria action.

X-ray micro-computed tomography of bone sections was performed at the SYRMEP beamline of the third-generation Synchrotron Light Laboratory (ELETTRA) located in Trieste (Italy), with the purpose to evaluate and quantify the preservation of bone structure, such as canals and lacunae, and the porosity changes due to diagenetic process.

Fourier transform infrared spectrometry (FT-IR) and micro-spectrometry (mFTIR) were performed at Simon Fraser University (Burnaby) in Canada to investigate the preservation of both mineral and organic phases.

Finally, 23 skeletons from the archaeological site of Travo (PC), dating from 7<sup>th</sup>-8<sup>th</sup> century AD, and their burial ground sediments were sampled and analyzed. Macroscopic, microscopic and chemical analyses were performed on bones to evaluate the tissue preservation state at different scales; the soil samples collected from the graves were characterized for color, particle size distribution, pH, organic carbon and calcium carbonate concentration.

This study shows that macroscopic, biomolecular, microscopic, ultramicroscopic and chemical alterations follow independent paths that affect the bone preservation at different scales of observation. Therefore, the estimation of the diagenetic process cannot be limited to the macroscopic aspect of the bone tissue but must take into account biomolecular, microscopic and chemical alterations, since these may have affected the bone tissue differently at different scale.

Bone degradation can be employed to estimate the *post mortem interval*, or to reconstruct the burial environment of human remains. As long as the evaluation of taphonomic alterations is performed at different scales with different ad hoc methodologies. In fact, age and environment can play an equal role on the degradation of organic and mineral phases, producing different effects on bone conservation at different levels.



## Chapter 1

# Introduction

### 1.1 - Bone tissue

Bone is a special connective tissue made of inorganic salts (i.e. minerals) impregnated in the organic matrix. Thanks to its rigidity and hardness, it maintains the shape of the body and protects the soft tissues. The minerals act also as a reservoir for ions, particularly calcium.

The macroscopic structure of bone is composed of two architectures, named cortical (or compact) and trabecular (or cancellous). Cortical bone is a dense solid mass whereas trabecular bone appears as a lattice of rods, plates and arches trabeculae.

The 80% of the skeletal mass is composed of cortical bone, which forms the outer shell of all bones; on the contrary, trabeculae bone is limited to the central region of bones and contain marrow.

At microscopic scale, the adult bone is organized in lamellae, with an ordered and organized structure produced by the repeated addition of uniform lamellae. Each lamella is 3-7  $\mu\text{m}$  thick and its collagen fibers are oriented parallel to each other. Groups of circular rings of lamellae with different size (generally between 4 to 20 layers), are arranged concentrically around a longitudinal vascular channel to form a structure called osteon or Haversian system, which is the main bone structural unit of cortical bone. Each canal is 30-70  $\mu\text{m}$  in diameter and contain nutrient vessel, nerves and connective tissue; different Haversian canals are connected with oblique or transvers channels, named Volkmann.

The outer border of osteons is surrounded by a cement line, 1-2  $\mu\text{m}$  thick, constituted by mineral matrix.

Between adjoining lamellae there are small cavities, named lacunae, containing living bone cell (osteocytes) (WEISS, 1983; WEINER, 2010).

Adjacent lamellae have two different orientations, longitudinal and transverse, respect to the osteon major axis. In the first case the collagen fibers are parallel oriented, instead in the second one are perpendicular oriented. Transverse lamellae are made of dense, interwoven collagen fibers (dense lamellae), while the longitudinal ones possess fewer fibers in a coarse weave (a less dense or loose lamellae), with a greater amount of mineral.

The lamellar orientation within an osteon can predict its anisotropic mechanical behavior; osteons with longitudinal lamellae are better for tension and torsion and perhaps stronger in bending, while osteons with alternating lamellae are more suited for compression (RHO *et alii*, 1995).

At the ultramicroscopic scale, human bone is made of three principal components: minerals, organic matrix and water. Organic matrix makes up 24% of cortical bone, and is composed by protein, glycoprotein and polysaccharide. It consists predominantly (90%) of collagenous fibers embedded in an amorphous ground substance, however there are two hundred or more so-called non-collagenous proteins (NCPs) in the organic matter, but together generally comprise less than 10% of the total bone protein content. Bone collagen is composed by type I collagen, characterized by a fibrous nature, that give to living bones tensile strength and small degree of flexibility. Each fibril, generally about 80–100 nm in diameter, is made of three stretched helical polypeptide chains (about 1000 amino acids long), two identical  $\alpha_1$  chain and a single  $\alpha_2$  chain, twisted into a triple helix. A triple-helical molecule is thus a cylindrically shaped, with an average diameter of 1.5nm and length of 300nm. Aligned fibrils make up a larger structure called fibers, that in mature bone are organized in concentric lamellae.

Bone minerals fill the gaps between collagen molecules, and constitute 76% of bone weight. The 50% of minerals is carbonate-hydroxyapatite (CHA), arranged in a plate-shape, 15-30Å thick and 100Å long. CHA crystals are regularly distributed at intervals of 600-700Å along the length of collagen fibers. The mineral crystals grow with a specific crystalline orientation: the *c* axes of the crystals are roughly parallel to the long axes of the collagen fibrils. The average lengths and widths of the plates are ca. 40x25nm, and the crystal thickness is 2–3nm (WEISS, 1983, WEINER, 2010).

## 1.2 - Taphonomy and bone diagenesis

Bones recovered from archaeological or forensic sites might have been subject to marked and complex alterations, both structural and chemical, principally depending on the environment in which the bones were buried. In the archaeological literature, the alteration of bone tissue that occurs during burial is termed diagenesis (GUARINO *et alii* 2006). According to WILSON & POLLARD (2002), diagenesis is “the cumulative physical, chemical, and biological processes that alter all archaeological materials in the burial environment; these processes will modify an inorganic object's original chemical and/or structural properties and will govern its ultimate fate, in terms of preservation or destruction”.

Because of bone tissue is an intimate association of mineral and organic components arranged in an ordinary structure, several levels of degradation are possible: partial or complete dissolution, erosion, precipitation, recrystallization, ion uptake by sorption and diffusion, hydrolysis and repolymerization. Bone tissue preservation is very variable and depends mainly on direct environmental conditions, such as groundwater and soil/sediment composition, pH, soil hydrology and redox potential, temperature, mechanical pressure, biological factors and mechanical transport (REICH *et alii*, 2003). Generally, over time, bones undergo a loss of organic material, an increase of mineral crystallinity, a change in porosity and in trace element composition (TRUEMAN *et alii*, 2004).

The *post mortem* sequence that influence the bone preservation is called taphonomy. BEHRENSMEYER & KIDWELL (1985) defined taphonomy as “... the study of processes of preservation and how they affect information in the fossil record”.

*Post mortem* degradation of bone (chemical and structural) is dominated by loss of structural collagen, which is insoluble under normal physical and environmental condition, but a rapid swelling and hydrolysis can occur when the protein are attacked by collagenolytic enzymes. The deterioration is governed primarily by time and temperature; however, alkaline and aquatic environment can also produce negative effect on bone tissue. Because of the intimate association between collagen and bone minerals, the collagen dissolution is accompanied by the alteration of apatite crystal, which is vulnerable to diagenetic change due to its small size. In fact, during diagenesis, the proteins are totally or partially removed or replaced by inorganic substance, and the carbonate-hydroxyapatite is subjected to recrystallization and ion exchange and substitution. The results of this early stage lead up to a more stable mineral phase, and over time to a total replacement of the collagen by minerals. Removal of minerals allows the extracellular microbial enzymes to access the collagen; microbial attack is probably the most common mechanism of bone deterioration and can occur rapidly after

death, in general optimized at neutral pH conditions. Due to mineral solubilization and re-precipitation by bacterial action, the bone porosity increase and histological changes are possible.

The water content is also important for the future integrity over archaeological time-scales, as the geochemistry of the environment in which the bones are buried (PFRETZSCHNER, 2004, TRUEMAN & MARTIN 2002, COLLINS *et alii*, 2002, TURNER-WALKER, 2002).

On the other hand, the tissue properties, influenced by composition and architecture of organic and mineral phases, can affect the bone response to diagenetic changes. Porosity, density, orientation of the collagen fibers, etc., can act positively or negatively on bone mechanical properties, reducing or accelerating the decomposition process.

Severas studies were performed to better understand the diagenetic and taphonomic alterations of bone material during burial time, which vary from one environment to another, depending on a wide range of interactions, including biological, chemical and physical factors (REICH *et alii*, 2003, HEDGES & MILLARD, 1995).

To understand and characterize the bone tissue alterations in soils and the impact of environmental conditions on its conservation, together with the effect of age, in this research different analytical techniques (mainly used in the Earth Sciences research field) were applied and compared.

Since bone degradation can occur at different scales, macroscopic, biomolecular, microscopic, ultramicroscopic and chemical, in this PhD thesis 63 human remains coming from five different burial sites of the Northern-Italy, four located in Milan and one in Travo (PC), and dated back from Late Roman age to contemporary one, were studied.

## **Chapter 2**

# **Materials and Methods**

### **2.1.1 - Bones coming from four known dating burial locations of Milan**

#### **2.1.1.1 - Site 1: Università Cattolica**

The first site (Population 1) is a necropolis located in the courtyard of the Università Cattolica del Sacro Cuore of Milan dated back to 3<sup>th</sup>-5<sup>th</sup> century AD. All the recovered skeletons comes from inhumations buried in ground, in single or multiple tombs (800 in total), dug between the 1996 and 1998 (SANNAZARO, 2001). Compared to the roman city, the cemetery was located outside the wall, in the north-west suburb, near the ancient Vercellina and Ticinese's gates (fig. 2.1a).

#### **2.1.1.2 - Site 2: Viale Sabotino**

The second site (Population 2) was discovered during the construction of a large underground car park in Milan in 2005-2006. It is a huge mass grave, containing the skeletal remains of two hundred and forty individuals. Based on the chronology of the adjacent Spanish walls and on ceramics, the mass burial was dated to 17<sup>th</sup> century AD. On the basis of the typology of the corpses deposited and

the chronology, archaeologists supposed that a plague outbreak might have been responsible for these deaths (MARSDEN & PAGANI, 2008) (fig. 2.1b).

### **2.1.1.3 - Site 3: Ca' Granda**

The third site (Population 3) is an ossuary discovered under the ground of Santa Maria Annunciata Church in the University of Milan. It is dated back to 15<sup>th</sup>-18<sup>th</sup> century AD, when the building was the greater hospital of the city, therefore the skeletons could belong to the patients died in the hospital during this period and buried inside the crypt (fig. 2.1c).

### **2.1.1.4 - Site 4: Cimitero Maggiore**

The last skeletons (Population 4) are unclaimed remnants of individuals died between the 1990 and the 1992, kept in coffin and exhumed after 15 years, when the skeletonization process was completed, in the Cimitero Maggiore of Milan. Thanks to an agreement between the municipality of Milan and LABANOF (Laboratory of Forensic Anthropology and Odontology, University of Milan), in accordance to the Police Mortuary Rules (Article 43 of law Decree 09/10/90 n. 285)<sup>1</sup>, unclaimed human remains can be used for educational and scientific remnants (fig. 2.1d).

### **2.1.1.5 - Samples**

For each site were selected 10 long bones, among femora and tibia, belonging to 10 adult individuals, equally divided in males and females, without pathological signs and subjected to the same taphonomic conditions.

---

<sup>1</sup> Article 43 of the law D.P.R. of September 10, 1990 n.285 of Italian Mortuary Police Regulations:

- 1.The health coordinator of the local health unity, by written request of the mortuary rooms director, can authorize the delivery to university of bones laid in the cemetery's communal charnel house.
- 2.Bones, listed on a standard acceptance report, are taken on responsibility of the mortuary room director, who will use them for didactic and study purposes.
- 3.In no other circumstance it is permitted to take away bones from cemeteries.
- 4.Human bones trading is forbidden.





Fig. 2.1 - a) Site 1: example of tomb recovered from the necropolis discovered in the Catholic University of Milan (3<sup>th</sup>-5<sup>th</sup> century AD) (SANNAZARO, 2001); b) Site 2: overview of the mass grave discovered in Viale Sabotino in Milan (17<sup>th</sup> century AD) (MARSDEN & PAGANI, 2008); c) Site 3: partial view of the human remains discovered in the ossuary under the ground of the Santa Maria Annunziata Church of the University of Milan (15<sup>th</sup>-18<sup>th</sup> century AD); d) Site 4: example of unclaimed human remains stored in the Cimitero Maggiore of Milan (1990-1992 AD).

## 2.1.2 - Bones coming from the Archaeological site of Travo (PC)

### 2.1.2.1 - Necropolis of S.Andrea

The archaeological excavation, conducted from 2005 to 2011 in Travo, Sant'Andrea (PC) area, put in light the remains of a necropolis and a settlement, for a total surface area of 545m<sup>2</sup>, dated back from 7<sup>th</sup> to 8<sup>th</sup> century AD.

The necropolis is east-west oriented, and 117 burials were dug up; among them, 19 tombs are earthy pits, 75 are earthy pits with a stone roof, and 23 have a stone structure and stone roof (fig. 2.2). All the bodies are east-west oriented in single tombs, with head west, and belong to adult and subadult individuals entombed in supine position. In few cases the tombs preserve the remains of several individuals in secondary laying.

No cultural materials were recovered near the skeletons, excepts for the individual of the tomb 40, an adult female that wore two *armille*, one for each wrist (CONVERSI & MEZZADRI, 2011).

In this study, 23 burials, with different typologies and containing only adult individuals, were selected and studied to understand the relationship between the conservation degree of human remains and the soils in which they were buried (tab. 2.1).

Tab. 2.1 - subdivision of the 23 studied tombs according to the burial type.

Burial type	Tombs
Earthy pit	T.39
Earthy pit with stone roof	T.1, T.15, T.17, T.18, T.19, T.28, T.32, T.35, T.49, T.50, T.55, T.56, T.60, T.73, T.99, T.100
Tomb with stone structure and stone roof	T.16, T.25, T.37, T.40, T.107, T.116



Fig. 2.2 – examples of: a) earthy pit (T.39); b) earthy pit with stone roof (T.35); c) grave with stone structure and stone roof (T.40) (Soprintendenza archeologica belle arti e paesaggio per le province di Parma e Piacenza).

To investigate the macroscopic tissue conservation were selected 14 skeletons coming for the tombs: T.16, 17, 18, 19, 28, 49, 50, 55, 56, 60, 73, 99, 100, 107; instead to perform histological analyses were chosen only long bones (either femora or tibiae) collected from the following tombs: T. 16, 17, 18, 19, 28, 37, 39, 40, 50, 55, 56, 60, 100, 116.

### 2.1.2.2 - Geology

The study area is located in the territory of Travo, in the Trebbia Valley, on the Western Appenines, at 170m above sea level, on the left bank of the Trebbia River.

As reported on Carta Geologica Italiana, paper's number 72 "Fiorenzuola d'Arda (scale 1:100.000), the area is characterized by sedimentary litotypes, made by debris, conglomerates, sandstones, siltstones, argillites, marls, limestones and jaspers. Igneous and metamorphic rocks are also frequently found. Travo is located where the litotypes of Luretta Valley merges, which is made by an alternation of sandstones and clays with marls and limestones, for a total thickness of 1600m. Val Luretta has a marine sedimentary origin, NO-SE orientated to Appennines. This formation is constituted by two lithostratigraphic unit: Poviago's Membro and Monteventano's Membro. The first was dated back from Upper Pliocene to Lower Eocene and was made by clays and sandstones, with a thick of 750m. The second one is dated back from Lower to Middle Eocene, and was made by marls, limestones and clays, and is 850m thick.

In the Trebbia Valley also the Montepiano's marls emerge, formed by sand and clay at the top and by clays on the base. These marls are dated back from Middle to Upper Eocene – Oligocene and are 80-100m thick.

Overlying the Montepiano's marls there are the Ranzano's sandstones, 80m thick and dated back from Upper to Lower Oligocene.

Moreover, as superficial deposits, in the valley can be recognized also fluvial materials derived by recent and present day alluvial deposits.

The first and the second ones are made by gravelly and sandy alluvial unweathered deposits, while the third one forms, at the present day, the gravelly and sandy riverbed of the Trebbia's river, which originates a big torrential valley perpendicular to Appennines (CREMASCHI, 1990).

### **2.1.2.3 - Geopedology**

The soils of the study area are mainly vertisols. Vertisolization processes are induced by shrinking and swelling properties of the parent material: during the wet season the smectite - montmorillonite swelling clays (i.e. rich in calcium and magnesium), can adsorb a large amount of water in the interlayer space, increasing their volume and inducing the typical phenomenon of slickensides; then, during the dry season, when the water evaporates, the clays reduce their volume and the contraction of soil aggregates break the formation vertical deep and wide cracks, in which, over time, by gravity effect, the organic material of the surface horizons can fall; finally, during the new wet season, the expansion of the swelling clays, can incorporate the organic material in the deepest horizons. Due to the vertical movements of the soil particles, the soil profile appears rather homogeneous (BRADY & WEIL, 1999; DUCHAUFOR, 1983; GIORDANO, 1999).

## **2.2 - Methods**

### **2.2.1 - Macroscopic analysis**

Forty long bones coming from forty different skeletons of the site number 1, 2, 3 and 4 of Milan, already washed and restored, were macroscopically evaluated with naked eye and through the use of stereomicroscope (Wild Heerbrugg Leitz M650), which is connected to a camera (Tiesselab) for the acquisition of images at different magnifications thanks to the software Belview.

Since in the taphonomic process weathering represents the response of the bone to its immediate environment, Behrensmeyer, in the 1978, defined six stages of bone weathering in subaerial/surface contexts, and suggested that bone weathering features might “give specific information concerning surface exposure of bone prior to burial and the time periods over which bones accumulated”. The research was performed on recent bone mammals in the Amboseli Basin in southern Kenya, and the bone weathering was defined as the decomposition and destruction of bones “as part of the normal process of nutrient recycling in and on soils.” Thus, weathering is continuous over time, involves mechanical and chemical changes, and occurs in surface and subsurface contexts. For Behrensmeyer, the six weathering stages are based on “easily observable criteria” and may be applied as descriptive comparison both in fossil both in recent bones. So, the weathering model can assist in understanding and reconstructing the *post mortem interval* (PMI), because the stages indicate the passage of time (HAGLUND & SORG, 1997).

As summarized in table 2.2, Behrensmeyer assigned a stage (from 0 to 5) in accordance to the general appearance of the remains and their state of preservation. Initially (stage 0) the bone surface shows no signs of cracking or flaking (fig. 2.3a); the bone is greasy, marrow cavities contain tissue, and there are muscle, ligament and skin still adherent to the bone tissue. During time, bones lack soft tissue, became fragile and easily broken by moving, the compact bone became fibrous and rough in texture, weathering penetrates the inner cavities, and appear crack and splinters (fig. 2.3b). In the last stage the originally bone shape is difficult to determine (stage 5) (BEHRENSMEYER, 1978).

Tab. 2.2 - Behrensmeyer’s classification of bone weathering (BEHRENSMEYER, 1978).

Stage	Description
0	No cracking or flaking; greasy; soft tissue present
1	Cracking parallel to fiber structure (longitudinal) in long bones
2	Flaking of outer surface, usually associated with cracks; flakes are long and thin with one edge attached to bone; crack edge angular; exfoliation started
3	Bone surface rough, fibrous texture; weathering only 1.0 to 1.5 mm deep; crack edges rounded
4	Bone surface coarse, rough, and fibrous; large and small splinters loosely attached; weathering penetrates to inner cavities; cracks open
5	Bone mechanically falling apart into pieces, very fragile

So, in accordance to Behrensmeyer’s stage some macroscopic parameters were evaluated in this study: general state of bone (complete or incomplete), cortical surface appearance (complete or incomplete), presence of fatty substance, skin, muscles, ligaments, spongy tissue, tissue in medullary cavity, cracking, flaking, color (for value, hue and chroma, according to Munsell® Color charts), bleaching and odor.



Fig. 2.3 - a) femur with a well preserved diaphysis: Behrensmeier's stage 0; b) femur with a badly preserved diaphysis: Behrensmeier's stage 4.

### 2.2.2 - Bone conservation after the recovery

The study was performed on fourteenth skeletons, not cleaned and restored, coming from the archeological site of Travo (PC), recovered only from earthy pits with stone roof: T.16 US 128, T.17 US 113, T.18 US 115, T.19 US 118, T.28 US 163, T.49 US 824, T.50 US 827, T.55 US 842, T.56 US 845, T.60 US 858, T.73 US 8100, T.99 US 8264, T.100 US 8245 and T.107 US 8272.

To investigate the skeletal record after the recovery, for every skeletal district available (divided in cranium, upper limbs, hands, ribs-sternum, vertebrae, pelvis, lower limbs and feet) were collected the following parameters, as listed in table 2.3.

Tab. 2.3 - parameters collected for each skeleton district.

Quantity	Solidity	Fragmentation
Scarce (0-30%)	Highly deteriorated (powder)	Highly fragmented (> 80%)
Partial (31-50%)	Deteriorated (broken)	Fragmented (79-20%)
Good (51-80%)	Fragile (brittle)	Whole (<20%)
Excellent (>81%)	Preserved	

### 2.2.3 - Biochemical analysis (Luminol test)

The luminol test is a non-expensive method for detecting blood traces. It is based on Luminol chemiluminescence (CL) reaction, as a predictive tool for the presence of haemoglobin and its

derivatives (also in traces) in bones, not visible to the naked eyes. Luminol reaction has been extensively studied for helping anthropologists in determining the time since death of the skeletal materials, thanks to its high sensitivity to reveal blood and blood-stains. In skeletal remains it was demonstrated that even low haemoglobin concentrations (between 1:100000 and 1:5000000) can make a detectable chemiluminescence reaction develop (RAMSTHALER *et alii* 2009).

The experiment was performed on 40 long bones coming from different individuals from Population 1, 2, 3 and 4. For each one was taken a small fragment of the anterior mid-shaft diaphysis of either femora or tibia, of 10x10 mm, using a multipurpose minitool (Dremel®). The bone sections were then powdered (weight of 50mg) with a grinder and stored in an Eppendorf® tube. The Luminol solution (Sigma-Aldrich®) was prepared according to WEBER (1966) and then the test was conducted in a darkened room. After, Luminol was added to the bone powder, the tube was gently shaken for few seconds and the response immediately recorded. The intensity of the response was graded in three categories, listed in table 2.4, according to the protocol described by CAPPELLA *et alii* (2015).

The reaction between hydrogen peroxide, sodium hydroxide and Luminol solution in the presence of iron catalyts produces a bluish chemiluminescence (CL), which intensity is proportional to the quantity of proteins containing Hb.

Tab. 2.4 - classification of the CL intensity according to CAPPELLA *et alii*, 2015.

Intensity	Description
-	No CL
+	Weak CL
++	Positive CL

In the figure 2.4 three examples of reaction intensities are shown.



Fig. 2.4 - different degree of chemiluminescence intensities produced by different amount of Hb preserved in bone powder.

## 2.2.4 - Microscopic analysis

### 2.2.4.1 - Histology

Histology is a relatively easily technique that allows to several degradation phenomena to become visible in a qualitative or semi-quantitative way. Furthermore, diagenetic changes can be localized within the bones, giving a more detailed picture of diagenesis. So, bones that looks similar macroscopically, can show wide variation in preservation status at histological scale (JANS *et alii*, 2002). The most common and rapid mechanism of bone deterioration is microbial attack. Some authors estimate that microbiological attack can be complete within 500 years *post mortem* (HEDGE, 2002), instead others demonstrated that histological changes of compact bone occurred at least five years after death (YOSHINO *et alii*, 1991), or as soon as three months (BELL *et alii*, 1996). A number of factors, such as temperature, time and environmental pH can influence the rate at which collagen and mineral phase are lost. Organisms from the burial environment penetrate the canal wall of buried bone and then attack the osteon tissue, producing an enzyme (collagenase) which digests bone collagen; the dissolution, as a result of microbial attack focuses in discrete zones of destruction, is known as microscopic focal destruction (MFD). Hackett suggests that bacteria are the major cause of MFD and identified three types classified as “linear longitudinal”, “lamellate” and “budded” according to their shape and size. The demineralized areas due to fungi are known as centrifugal (Wedl) tunnels (HACKETT, 1981).

In this research, histological analysis was performed on 40 clean long bones from Milan (10 for each site) and on 14 uncleaned long bones from Travo (PC).

In this case were selected 14 skeletons buried in tomb with different typologies: T.16 US 128, T.17 US 113, T.18 US 115, T.19 US 118, T.28 US 163, T.37 US 1316, T.39 US 1315, T.40 US1324, T.50 US 827, T.55 US842, T.56 US 845, T.60 US 858, T.100 US 8245, T.116 US 8325.

#### 2.2.4.1.1 - Optical light microscopy on calcified bone thin sections

Each long bone was cut, with a handsaw, transversely at mid-diaphysis to obtain semi-circular section of ca. 4mm thick, and then smoothed down through a grinding wheel, supporting abrasive discs of grainsize from 320 to 4400 (Struers Dap-7), to obtain flat semi-lunar shaped fragments that possessed



the whole cortical bone. After the mounting on glass with Pertex (Histolab Products AB), the samples were grinded again in order to be thin enough to be analyzed in transmitted light using a polarizing optical microscope (Zeiss Axio Scope A1 A Pol, equipped with Zeiss N-Achroplan), which is connected to a camera (True Chrome Hd II) for the acquisition of images at different magnifications using software Icapture 3.6.7. At histological scale the presence of alterations of the normal bone tissue were evaluated in transmitted and polarized light microscopy and classified according to the Oxford Histological Index (score 0-5) created by HEDGES (2002) (tab. 2.5). This classification evaluates the amount of destructive foci due to fungal and bacterial activities, and the percentage of preserved bone, i.e. osteon structure. According to Wedl, who for first described the microbial attack on bone tissue in 1864, the alteration removes the minerals and exposes the collagen simultaneously; subsequently, the remineralization appears as an area (focus) less translucent than the surrounding bone (HACKETT, 1981).

Tab. 2.5 - summary of the score proposed in the Oxford Histological Index (Hedges, 2002).

Index	% of unaltered bone	Description
0	< 5	No original feature identifiable, other than Haversian canals
1	< 15	Small areas of well preserve bone present
2	< 33	Clear lamellae structure preserved between foci
3	> 67	Clear preservation of some osteocyte lacunae
4	> 85	Minor amount of destructive foci
5	> 95	Very well preserved, indistinguishable from fresh bone

In the figures below (fig. 2.5 a, b) are shown two different conservation of bone, according to the OHI.

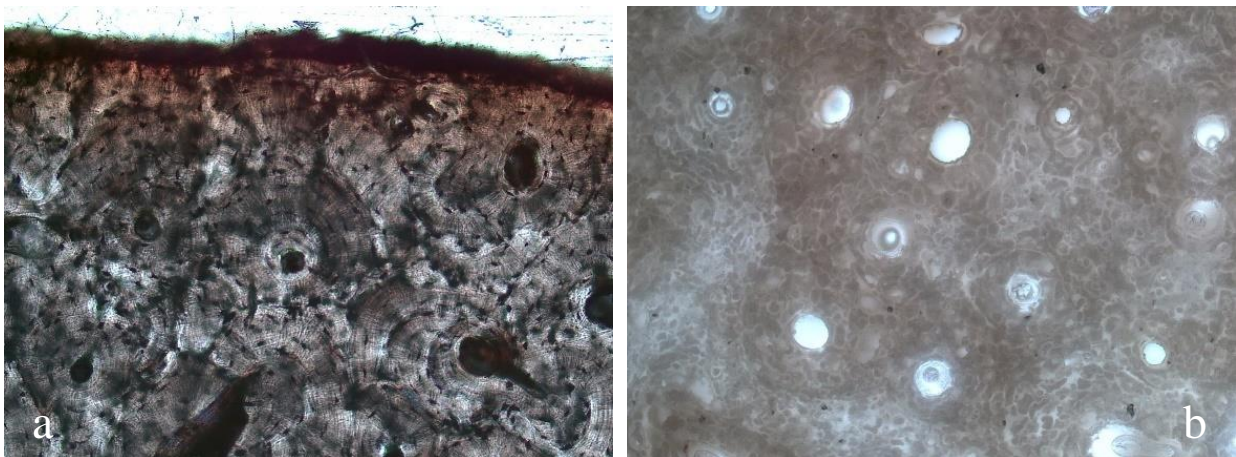


Fig. 2.5 - a) well preserved thin section of femur in transmitted light (10X): OHI score 5; b) badly preserved thin section of tibia in polarized light (10X): OHI score 0.

### **2.2.4.1.2 - Optical light microscopy on decalcified thin bone sections**

Decalcification is one of the most sensitive laboratory technique, which can be carried out by chemical acids (hydrochloric acid) to form soluble calcium or chelating agents (ethylenediaminetetracetic acid - EDTA) that bind to calcium ions.

In this work, the most common standard decalcification protocol was applied on 40 long bones coming from different individuals of Population 1, 2, 3 and 4. From each one was cut a cross section from the anterior mid-shaft diaphysis through a handsaw, approximately of 1 cm thick, which was then fixed in formalin (v/v, PH 7-7.6) for 24h, ratio 20:1 v/v and decalcified at room temperature in Decalc, 14% hydrochloric acid (Histo-Line Laboratories, Milan). Subsequently each section was rinsed in tap water for 24 hours, dehydrated in alcoholic scale, and embedded into paraffin. From each block, 5-microns section was cut and stained with Hematoxylin and Eosin (H&E). These stainings allow the appearance of detailed bone structures, since Eosin possess high affinity to basophilic components, as collagen fibres and lamellae, and exhibits them with a rosy-red stain, whereas Hematoxylin is acidophilic and stains violet the osteocyte nuclei in their lacunae (DE BOER *et alii*, 2012; MAAT *et alii*, 2001).

Since the lack of criteria in the evaluation of bone preservation on decalcified thin sections, a new histological index (DHI, Decalcified Histological Index) was created. This classification evaluates the percentage of organic components (mainly collagen fibers) stained rose/violet by H&E, compared to the degraded tissue (not stained), due to microscopic focal destruction.

Since collagen is one of the few birefringent biomolecules to transmit polarized light, depending on the quantity and orientation of collagen fibres (DIXON *et alii*, 2008), the degradation of structural collagen was also evaluate using the birefringence's appearance on bone thin sections in polarized light microscopy. In fact, any absence of light and dark banding indicates a loss of intact bone due to taphonomic degradation.

In the current work, the degree of birefringence was divided in high (fig. 2.6c), medium and low (fig. 2.6d) score, according to the intensity and diffusion observed on the all thin section. The presence of birefringence means that osteon anisotropy is preserved, on the contrary the absence of birefringence indicates that all the osteon structures are degraded.

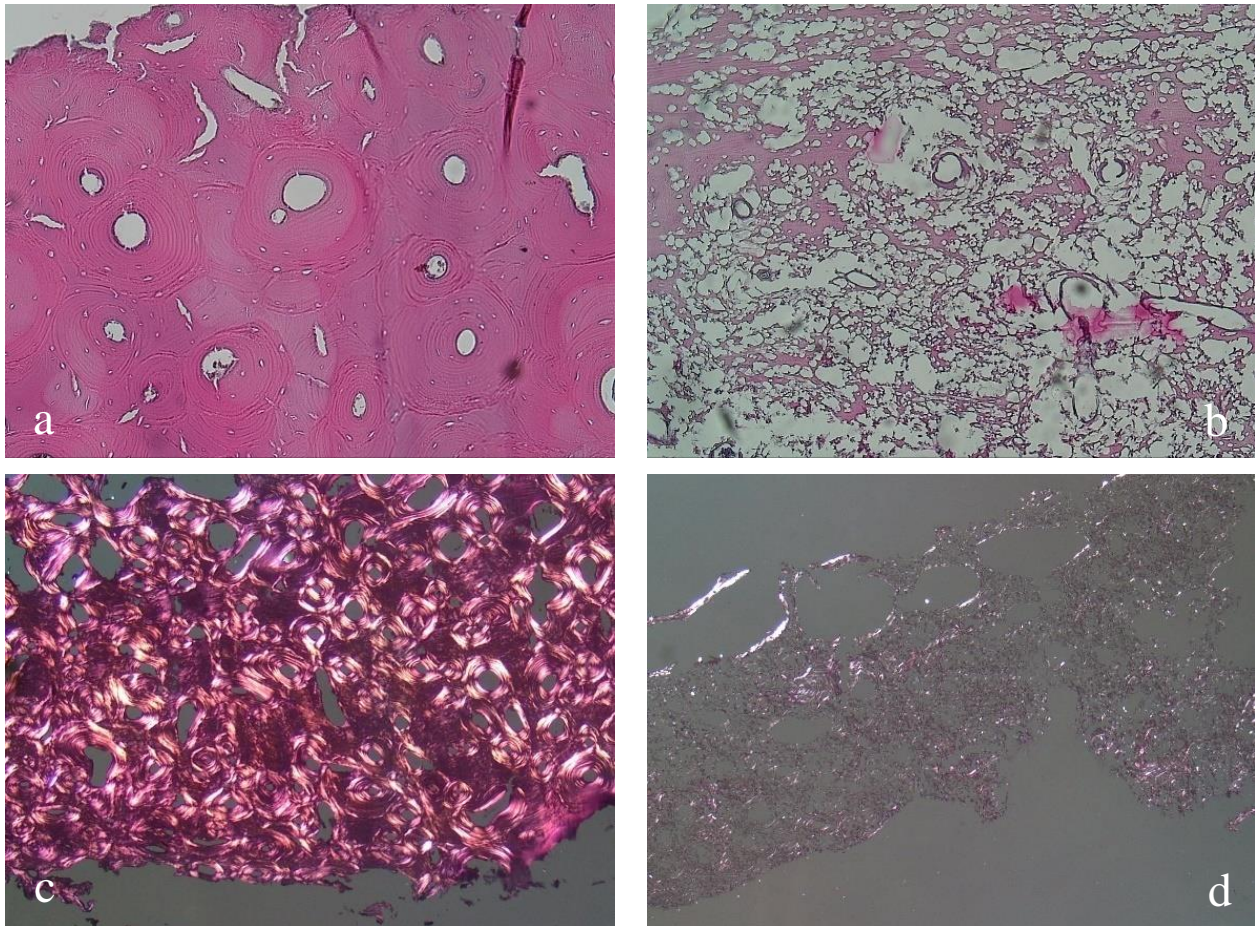


Fig. 2.6 - a) well preserved thin section of femur in transmitted light (10X): DHI score 3; b) badly preserved thin section of femur in transmitted light (10X): DHI score 1; c) high degree of birefringence in polarized light (2.5X); d) low degree of birefringence in polarized light (2.5X).

### 2.2.4.3 - Scanning electron microscopy with energy-dispersive X-ray spectroscopy EDS

The electron microscope is an instrument specifically developed to obtain high magnification images. It employs electron beams accelerated in the range  $10^2$ - $10^4$  eV, corresponding to wavelengths of the order of 0.123-0.012nm. The tool is commonly used both to produce images of surface topography, with gold coating, and to obtain chemical composition of the specimens with graphite coating, by means of the EDS spectrometer (ARTIOLI, 2010).

In this work, a Cambridge Stereoscan 360 with back-scattered detector (BSE), coupled with an energy-dispersive X-ray (EDS) spectrometer Oxford ISIS 300 for elemental analysis (expressed in metal oxide percentages), was used and the images were acquired with Oxford Link Pentafet software.

The SEM-EDS analyses were carried out on 40 bone sections coming from Milan and on 10 bone sections with their related grave soils (T.16, 17, 18, 19, 28, 50, 55, 56, 60, 100) from the necropolis of Travo (PC). To investigate the presence of exogenous oxides on the bone surface (principally due to contamination with the burial environment) and the histological appearance of the tissue (preserved or degraded by diagenetic agents over time) at high resolution, two different sections were employed for the 40 long bones from Milan: non-embedded and embedded in epoxy resin. For the 10 long bones from the archaeological site of Travo (PC) were prepared only non-embedded sections to detect the oxides present on the bone surface. For each bone, the grave soil adherent to the external cortical tissue were also collected and analyzed with SEM-EDS to establish the chemical composition, with the aim to find a possible relationship between bone and its burial context.

#### **2.2.4.3.1 - Preparation of non-embedded bone sections**

For the preparation of non-embedded bone sections from Milan (40) and Travo (10), was taken a cross sections of ca. 2.5x1cm, by means of Proxxon Micromot System saw, from the mid-shaft of femora and tibiae. The sections prepared were then fixed on slides with hot glue and then coated with graphite in the sputter coater Scancoat Six.

#### **2.2.4.3.2 - Preparation of embedded thin bone sections**

After cut through a handsaw, the forty bone sections, coming from Site 1, 2, 3 and 4 of Milan, were also embedded in Araldite, an epoxy resin made by Araldite-D and a harden HY956, in relationship of 10:1. The resin, at 70-80°C temperature, was pour slowly on the sample, arranged inside a container, and the consolidation was of 24H at temperature of 23-24°C. The specimens were then polished with a grinding wheel, equipped with an abrasive disc of carborundum, from 400 to 1000 grainsize, and cleaned with water. Finally, the bones were polished by means a diamond paste, thin 1 µm, and cleaned with water. For the SEM-EDS analysis the polished sections were coated with graphite in the sputter coater Scancoat Six.

### **2.2.4.3.3 - Grave soil samples preparation**

Using a double-sided adhesive tape on the bone surface, the soil particles have been sampled from 10 different long bones coming from the osteological material of Travo (PC). The adhesive tapes were mounted on the glass and then coated with graphite in the sputter coater Scancoat Six.

### **2.2.4.3.4 - Elaboration of quantitative data**

The chemical composition measured by EDS spectrometer of the 40 bone sections from Milan were elaborated in a multivariate statistical analysis by an Excel Add-In program named Multibase, developed by NumericalDynamics.com. With this software, the PCA (Principal Component Analysis) was applied to explain the variability of the samples among the different populations. Principal Component Analysis (PCA) attempts to simplify the distributions of samples and identify the underlying factors that explain the pattern of variable and sample correlations. When samples are assigned into some categories (or groups), the distributions of the categories will be shown with ellipses. Comparing sample scatter plot (Score) with variable one (Loadings), the significant variables which contribute sample distribution can be easily identified (NumericalDynamics.com).

### **2.2.4.3.5 - Elaboration of qualitative data**

The chemical composition measured by EDS spectrometer of 10 non-embedded bone sections and the related soil materials, sampled by means of adhesive tape, coming from Travo site, were classified and compared to verify a possible chemical exchange between them.

By means of BSE-SEM observations, the conservation degree of the bone tissue morphology was observed on 40 embedded sections from Milan. Each bone section was ideally divided in three zones: internal cortical border, central cortical and external cortical border, and for each one five parameters was evaluated (tab. 2.6): preserved osteons, degraded areas, remineralized zones, cracks influenced by bone structure or not.

Tab. 2.6 - parameters observed for bone tissue evaluation at SEM-EDS.

Parameter	Description
preserved osteons	all bone structures are recognized: lamellae, lacunae, Haversian canal, cement line
degraded areas	no bone structures are recognized due to the presence of fungal and bacterial action (Wedl and non-Wedl tunneling (HACKETT, 1981)); the bone also appears less dense, with increase of porosity (presence of holes)
remineralized zones	areas with redeposition of bone mineral (BELL, 1990)
cracks related to bone tissue	perpendicular short cracks at the contacts between osteons, small radial cracks around haversian canal, circumferential cracks outside the osteons (ROGOZ <i>et alii</i> , 2012)
cracks non-related to bone tissue	multidirectional cracks independent from bone histological structures (ROGOZ <i>et alii</i> , 2012)

In the figures below (figs. 2.7a, b) are shown two different degree of bone conservation, well and badly preserved, in BSE-SEM view.

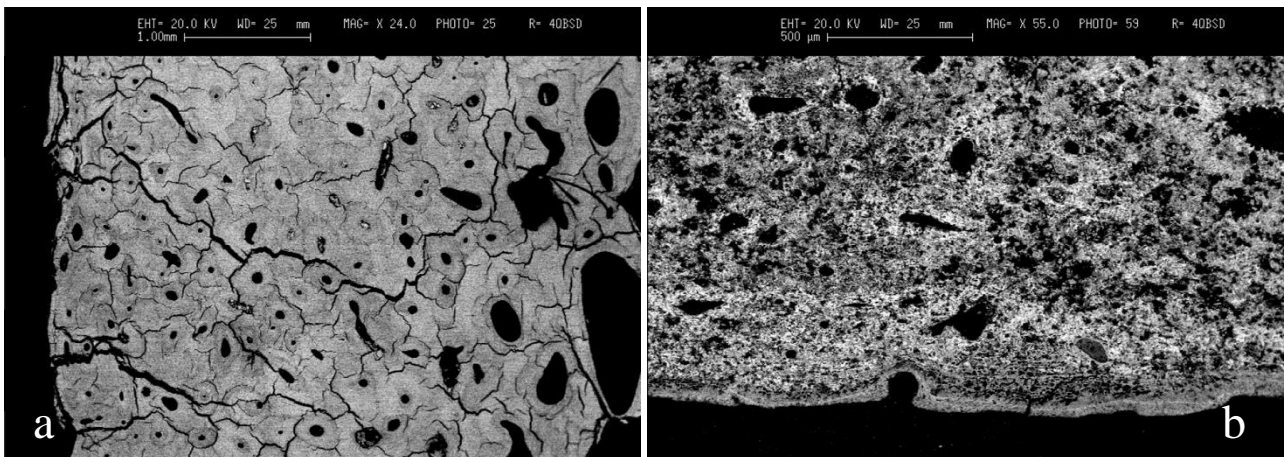


Fig. 2.7 - a) well preserved bone thin section at BSE-SEM: osteon structures are clearly defined and there are macro and microcracks inside the tissue; b) badly preserved bone thin section at BSE-SEM: no osteons are identifiable, and there are high electron-dense zone, bright color, where the bone tissue is remineralized.

## 2.2.5 - 3D micro-computed tomography

### 2.2.5.1 - Samples preparation

From the four sites of Milan, 24 long bones (either femora or tibiae) were chosen to perform 3D micro-computed tomography. For each site were collected 6 samples, the most representative of the whole population at macroscopic and histologic scale: samples 2, 3, 4, 5, 8, 10 of Population 1;

samples 1, 2, 3, 5, 8, 10 of Population 2; samples 3, 4, 5, 8, 9, 10 of Population 3; samples 1, 2, 4, 5, 7, 10 of Population 4.

For the analysis was employed for each bone a cross section of ca. 20 x 4 x 4 mm, taken from the anterior mid-shaft diaphysis, by a Proxxon Micromot System saw.

### **2.2.5.2 - Synchrotron radiation**

The experiments were performed at SYRMEP (Synchrotron Radiation for Medical Physics) beamline at the ELETTRA Synchrotron Facility in Trieste, Italy. The optics is based on a double-crystal Si (111) monochromator, which works in an energy range between 8keV and 35keV. The beamline provides at a distance of about 20m from the source, a monochromatic, laminar-section X-ray beam with a maximum area of 120x4mm<sup>2</sup>. The horizontal acceptance covered by the light-port of the front-end is 7mrad. In the withe beam configuration the X-ray beam from the ring is intercepted before the monochromator and absorption and phase contrast radiography and tomography are available in a dedicated end-station.

The micro-tomographic technique starts from the acquisition of a large number of radiographic projections of the sample, which is placed on a rotary table and positioned at different angular positions with respect to the radiation source. In this work, 1800-3000 projections for each tomographic scan were acquired over 360° with a white beam and at a source-detector distance of 12cm. A micrometric vertical and horizontal translation stage allows the positioning and the scanning of the sample with respect to the stationary beam and the rotational stage. The energy was set up to 27keV, thanks to the application of aluminum (1mm) and silicon (1.5mm) filters, and the exposure time was about 2s per projections. The resulting pixel size was 2.1µm.

The white beam mode is preferable to allow the sampling of a relative wide area (4mm) of the bone surface at higher resolution, with respect the monochromatic mode, avoiding the extraction of 1mm-sized chips based on a limited visual inspection. To perform the flat-fielding procedure, dark and flat images were acquired as well before and after the projections to take in account the degradation of the beam. Each dataset (projections, dark and flat images) is converted in the HDF file format (a hierarchical file format to manage large amounts of data) (DE CARLO *et alii*, 2014) and then managed by the STP (SYRMEP Tomo Project) (BRUN *et alii*, 2015), an in-house software suite developed by the beamline scientific staff, to perform the image reconstruction through the Filtered Back-Propagation (FBP) algorithm. A filter for ring removal (MUNCH *et alii*, 2009) was used to compensate the so-called ring artefacts. It uses a wavelet and Fourier mode decomposition and then applies a Gaussian function with a damping factor to remove, or at last reduce, rings. Since ring removal

algorithm “default” the data, we tried to find a good compromise between ring removal while preserving at the same time the physical information of each voxel.

### 2.2.5.3 - Imaging Analysis

For morphometric analysis were employed 3 imaging software: ImageJ, Blob 3D and Avizo, instead 3D rendering was created by Avizo (fig. 2.9) and VGStudio Max (fig.2.10).

Because all of these programs work on binary images, a preliminary imaging elaboration was required.

ImageJ Fiji (version 1.51e) is an open source processing program for multidimensional image data, developed by the National Institute of Health (U.S.A).

To the program was upload all the slices (fig. 2.8a) then converted in 8-bit grayscale. Subsequently the largest possible subvolume from the original data set was chosen to have more statistically meaningful data, named Volume of Interest (VOI) (fig. 2.8b). Due to the large size of the aggregate particles it is difficult to say how large a true representative elementary volume needs to be anyway the data showed an acceptable consistency by checking the porosity variation for each slice.

Once the subvolume was selected, after a brightness and contrast adjusting, in order to obtain a binary volume, where the voids were separated from the solid phases, a histogram- based global thresholding was applied to select the bone porosity in black and the mineralized tissue in the foreground in white. The black objects were counted and their total volume measured separately from the total volume stack by “Analyzed Particles” command. In the first case was measured the total porosity volume (BV) instead in the second one the bone total volume (TV).

Then the natural bone porosity, constituted by lacunae and canals, was counted and measured separately; lacunae and canals were automatically selected about their pixel size area into the “Analyzed Particle” command (lacunae was selected between 10-50pixels<sup>2</sup>, and canals >500pixels<sup>2</sup>). Also, remineralized areas of bone, principally due to diagenetic changes, was selected with a manual thresholding, counted and measured too. Then, the volumes of lacunae (LaV), canals (CaV) and remineralized areas (RV) were also calculated on the total stack.

For each measure detected, the following ratios were also calculated: total volume fraction (%BV/TV), canal volume fraction (%CaV/TV), lacunae volume fraction (%LaV/TV), remineralized tissue volume fraction (% RV/TV).



Once the binary volume was obtained, the 3D morphological characteristics of the voids, canals and lacunae, were determined using Blob3D, a custom-developed software written in IDL<sup>®</sup> language and based on the filtered backprojection algorithm. In Blob3D, voids can be separated automatically as single objects by a procedure based upon 3D eroding and dilating cycles. For each object, its volume, surface, aspect-ratio, and maximum axis orientation were measured. Volumes and surfaces were then used to calculate the sphere-normalized surface/volume ratio that gives a better idea of the surface complexity of the object than the simple surface-to-volume ratio. With this parameter a sphere, of whatever size, would have a value equal to 1, then the more irregular the object, the higher this parameter would be. So, the surface/volume ratios cited in this work have all been normalized with respect to a sphere of the same volume, for each object. Voids with aspect ratio equal of 0 were not considered for statistical measurements.

In order to describe and quantify the canals and lacunae in three dimension, morphological parameters were also taken by means of Avizo, a 3D software platform (version 9.2.0) for visualizing and manipulating data from computed tomography.

The binary volume previously created with ImageJ was upload in the program, and lacunae and canals were automatically separated and labeled with connected component function. For each label were carried out 3D length (maximum of the Feret diameter), 3D width (minimum of the Feret diameter), 3D Euler and anisotropy.

This procedure was repeated for each sample.

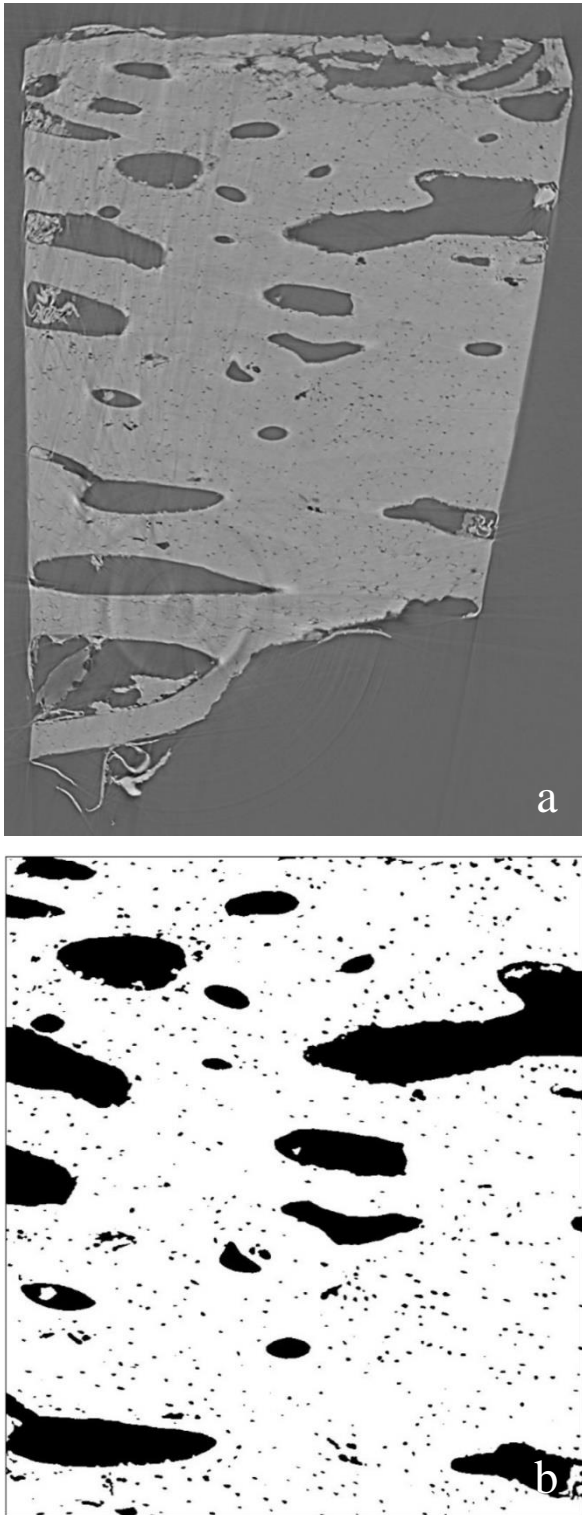


Fig. 2.8 - a) example of slice produced by synchrotron light source and reconstructed with STP software; b) selected area of slice converted in 8-bit grayscale after automatic thresholding; in black are highlighted the total porosity whereas in white the foreground bone tissue.

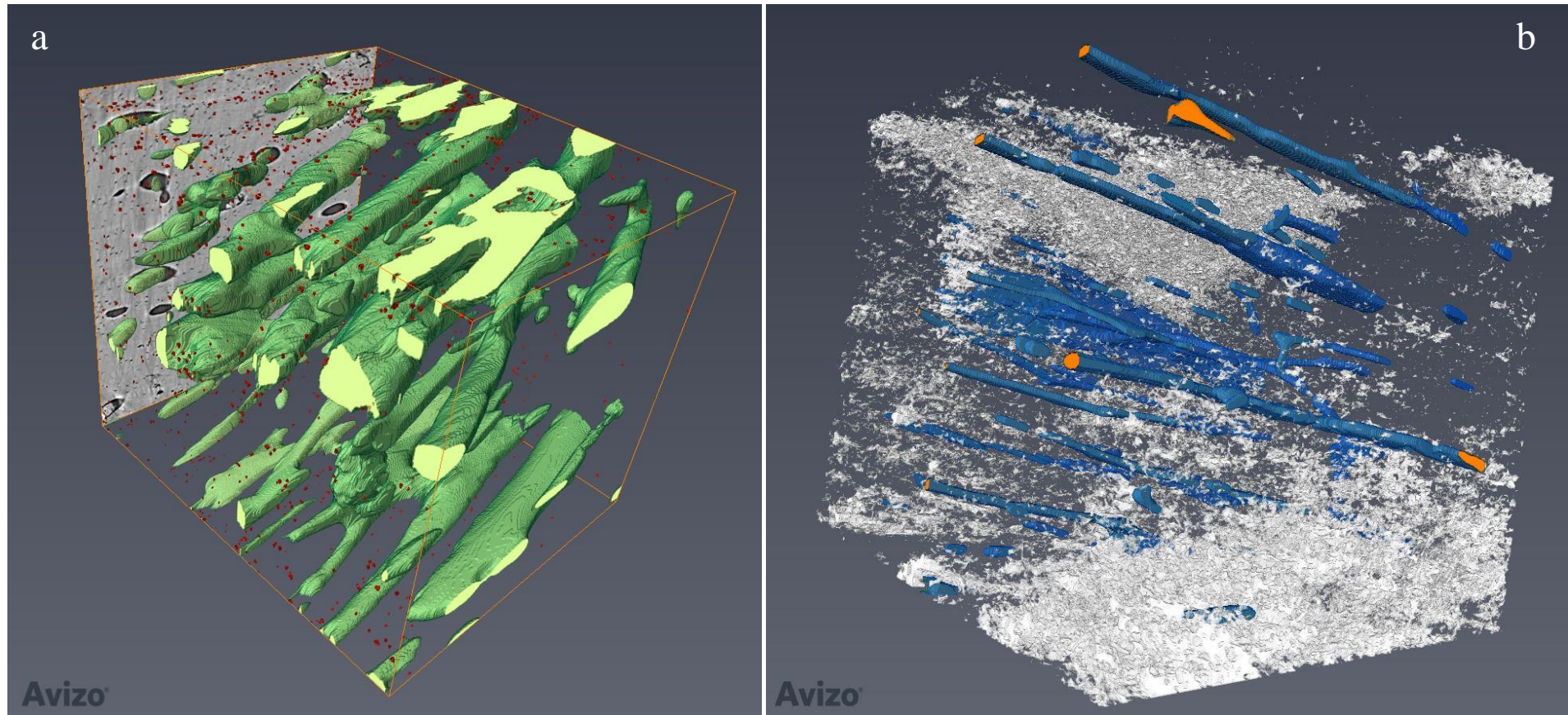


Fig. 2.9 - 3D rendering of VOI by Avizo. a) bounding box with inside canals (green) and lacunae (red) created by the slice stack; b) canals (blue) and remineralized areas (white) of bone tissue created from stack volume.

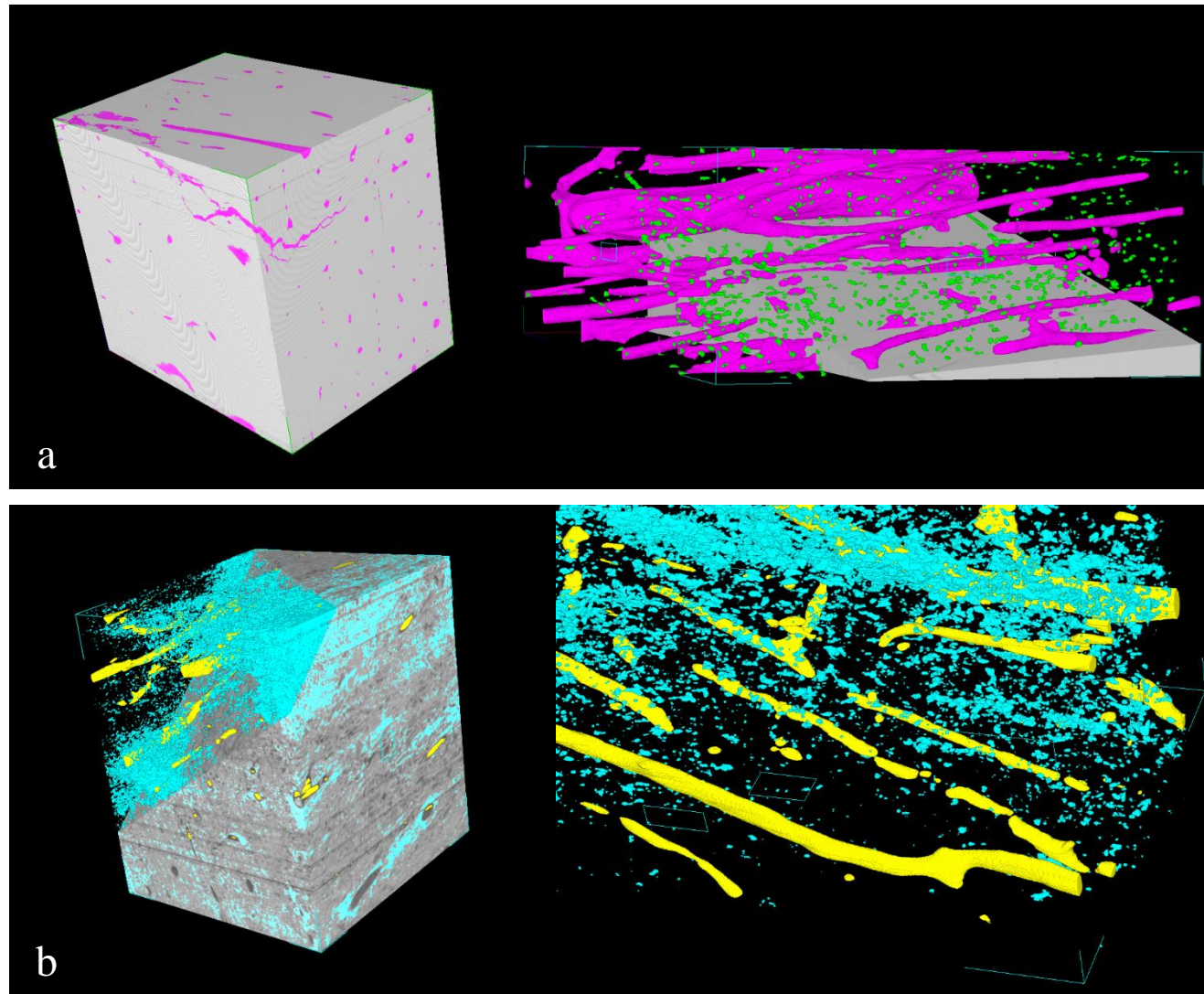


Fig. 2.10 - 3D rendering of selected bone volume by VGStudio Max; in the figure are shown the reconstructed volume bulk by slices and its detail where are highlighted; a) canals (violet) and lacunae (green), b) canals (yellow) and remineralized areas (light blue).

## **2.2.6 - Fourier transform infrared spectrometry (FT-IR) and micro-spectrometry (mFTIR)**

Fourier transform infrared spectrometry (FT-IR) and micro-spectrometry (mFTIR) were performed at the Department of Archaeology of Simon Fraser University (Burnaby) in Canada.

### **2.2.6.1 - Fourier transform infrared spectrometry (FT-IR)**

#### **2.2.6.1.1 - Whole bone sample preparation**

Ten specimens of bone populations 1, 2, 3 and 4 (40 samples in total) were analyzed by FT-IR. Approximately 4 mm thick cross section of the mid-diaphysis of each bone (either tibia or femora) was cut using a handsaw. The 4mm cross sections were powdered for 15 second using a multipurpose minitool (Dremel®).

#### **2.2.6.1.2 - Bone Acid Insoluble Fraction (AIF)**

To determine the composition of organic and mineral component of bones, seven selected specimens (samples 4 and 7 from Population 1; sample 6 from Population 2; sample 9 from Population 3; samples 5, 7, 10 from Population 4) were dissolved in a solution of 1N hydrochloric acid (HCl) following the procedure describe below: 0.300-0.500g aliquots of powdered material (see above) were weighted with a 0.000g detection limit Ohaus Explorer Pro precision scale and placed in a 15ml conical centrifuge tube. The weighted aliquots were treated with 10ml of 1N HCl for 12-24 hours at room temperature, and then, the content of each conical centrifuge tube was thoroughly mixed using a VWR Vortex Genie 2, and centrifuged at 3000 rpm for 2 minutes in an Eppendorf 5810 centrifuge. The acid solution supernatant was discarded and the pellet washed with 10 ml of distilled water by thoroughly mixing using a VWR Vortex. The distilled water suspension was centrifuged at 3000 rpm for 2 minutes. After centrifugation the supernatant was carefully discarded using a clean glass pipette. The washing process with distilled water was repeated two more times. The conical tubes with the washed 1N HCl insoluble fraction pellets were air-dried at 55° C for 72 hours in a VWR Oven Air 3650F. The dried pellets were weighted before further analysis (see below) using the Ohaus Explorer Pro precision scale.

### 2.2.6.1.3 - FT-IR Spectra collection

Whole bone powder and bone acid insoluble fraction were pulverized further with agate mortar and pestle to obtain representative ca. 4 micrograms of fine silt size particles. The 4 micrograms of finely pulverized bone samples were suspended in 5mg of IR grade potassium bromide (KBr) powder. The KBr-sample mixture was pressed into a clear 7mm diameter pellet using a Pike hand press and a 7mm die set. To avoid cross contamination, after each sample preparation mortar and pestle were washed with 1N hydrochloric acid (HCl) solution, rinsed with distilled water, wiped with clean Kimtech tissues, rinsed with anhydrous acetone and dried under a heat-lamp.

The bone powder KBr pellets were analyzed in transmission mode with a Thermo Scientific Nicolet iS5 transportable FT-IR spectrometer equipped with a transmission mode sampling chamber (model iD1). Absorption spectra in the 4000 to 400  $\text{cm}^{-1}$  wavenumber range were collected collecting 32 scans at a resolution of 4  $\text{cm}^{-1}$ . Two samples for each bone population were run in triplicate to quantify sample variability and instrumental error. Instrumental operation and spectra collection and analysis were conducted using Thermo-Nicolet Omnic (version 9) software.

### 2.2.6.1.4 - Spectral Analysis

Since, infrared incident radiation is absorbed by the sample at a particular wavelength, by means of this technique it is possible to carry out information on molecular bonds and their chemical environment.

The phosphate ion has four vibration frequencies: a symmetric stretch ( $\nu_1$ ), a double degenerate symmetric bend ( $\nu_2$ ), a triply degenerate asymmetric stretch ( $\nu_3$ ) and a triply degenerate asymmetric bend, ( $\nu_4$ ) (SANTOS & CLAYTON 1995).

Infrared spectrum of hydroxyapatite depends on the substitution mechanism of  $\text{CO}_3$  in the lattice structure. Crystals in which the carbonate replaces the  $\text{PO}_4$  (type B) has the major infrared  $\text{CO}_3$  band at  $871\text{cm}^{-1}$ , whereas HA in which carbonate replaces the OH (type A) has the major infrared  $\text{CO}_3$  band at  $878\text{cm}^{-1}$ . Also, a third band at  $866\text{cm}^{-1}$  correspond to a labile carbonate environment.

The carbonate ions are distorted into the lattice, so in the HA type B these ones are oriented parallel to the  $c$  axis, instead in the HA type A are perpendicular to the  $c$  axis.

Free  $\text{CO}_3$  ion has 3 modes of vibration too: a symmetric stretching vibration ( $\nu_1$ ), an out of plane vibration ( $\nu_2$ ), a doubly degenerate asymmetric stretch ( $\nu_3$ ) and a doubly degenerate bending mode ( $\nu_4$ ). Among these ones, the strongest IR peak in calcite is the  $\nu_3$  near  $1440\text{cm}^{-1}$ .

When OH group is substituted by F there is a more stronger IR band at  $603\text{cm}^{-1}$  respects to the  $567\text{cm}^{-1}$  band in the  $\nu_4\text{PO}_4$  domain (ARTIOLI, 2010).

Fluoridation also affects the  $\text{CO}_3$  vibrational frequencies (SANTOS & CLAYTON 1995).

To quantitatively inter-characterize the different samples and gain insights on diagenetic processes that may have occurred in the different burial conditions the following FT-IR spectral ratios were calculated. Their statistical variability was estimated from the values measured on samples run in duplicate (see above).

#### Amide I/ $\nu_3(\text{PO}_4)$ spectral ratio and weight % organic estimation

For each whole bone sample the FT-IR absorption intensity of Amide I band was measured at ca.  $1653\text{cm}^{-1}$  and the absorption intensity of the  $\nu_3(\text{PO}_4)$  band was measured at ca.  $1035\text{cm}^{-1}$ . Both bands intensities were measured from a baseline traced between  $2000\text{cm}^{-1}$  to  $800\text{cm}^{-1}$  wavenumbers. The Amide I /  $\nu_3(\text{PO}_4)$  spectral ratio was calculated by dividing the numerical values of the baseline corrected intensities.

For each bone sample, the weight percentage of organic component was estimated using the equation:

$$\text{Weight \% organic} = 11.06 \ln(\text{AmI}/\text{PO}_4) + 32.43 \quad \text{from TRUEMAN } et \text{ alii (2004)}$$

#### $\nu_2(\text{CO}_3)$ / $\nu_3(\text{PO}_4)$ spectral ratio

The  $\nu_2(\text{CO}_3)$  /  $\nu_3(\text{PO}_4)$  spectral ratio was calculated for each sample by dividing the absorption intensity value of the  $\nu_2(\text{CO}_3)$  absorption measured at ca.  $873\text{cm}^{-1}$  by the intensity value of the  $\nu_3(\text{PO}_4)$  absorption measured at ca.  $1035\text{cm}^{-1}$  both absorptions intensities were corrected using a baseline traced between  $2000\text{cm}^{-1}$  to  $800\text{cm}^{-1}$  wavenumbers.

#### Infrared splitting factor (IRSF) and mean bone mineral crystal length

To estimate the degree of recrystallization of the bone mineral (carbonate- hydroxyapatite) of each sample with respect to in vivo reference values (2.6) the calculation of the infrared splitting factor (IRSF) was measured according to WINER & BAR-YOSEF, (1990). The IRSF, a the crystallinity of hydroxyapatite, was calculated summing the peak intensities at  $\sim 604$  and  $\sim 590\text{cm}^{-1}$  and dividing by the intensity of the valley between them. The splitting factor was calculated using a baseline with a wavenumber from  $800\text{cm}^{-1}$  to  $445\text{cm}^{-1}$ .

The mean bone carbonate-hydroxyapatite crystallite length was estimated using the equation:

$$\text{Mean crystal length (nm)} = (\text{IRSF}-0.822)/0.048 \quad \text{from TRUEMAN } et \text{ alii (2008)}$$

### 2.2.6.2 - Fourier transform infrared micro-spectrometry (mFTIR)

The thin sections prepared according to the procedure shown at pp.24,25 of twelve selected samples (Population 1: samples 4, 7, 10; Population 2: samples 4, 5, 6; Population 3: samples 3, 9, 10; and Population 4: samples 5, 7, 10) were analyzed by mFTIR. Selected cross-section areas of each of the 12 samples were mapped in Reflection mode using a Thermo Scientific Nicolet iN10 MX FTIR imaging microscope. Each map was collected with MCT/B detector, in the 2000 to 450 $\text{cm}^{-1}$  wavenumbers range, with a 150x150 $\mu\text{m}$  spot size, 100x100 $\mu\text{m}$  step size, and 64 scans at a spectral resolution of 8 $\text{cm}^{-1}$  wavenumbers. Instrumental operation and spectra collection and analysis were performed using Thermo-Nicolet Omnic Picta software (fig. 2.11).

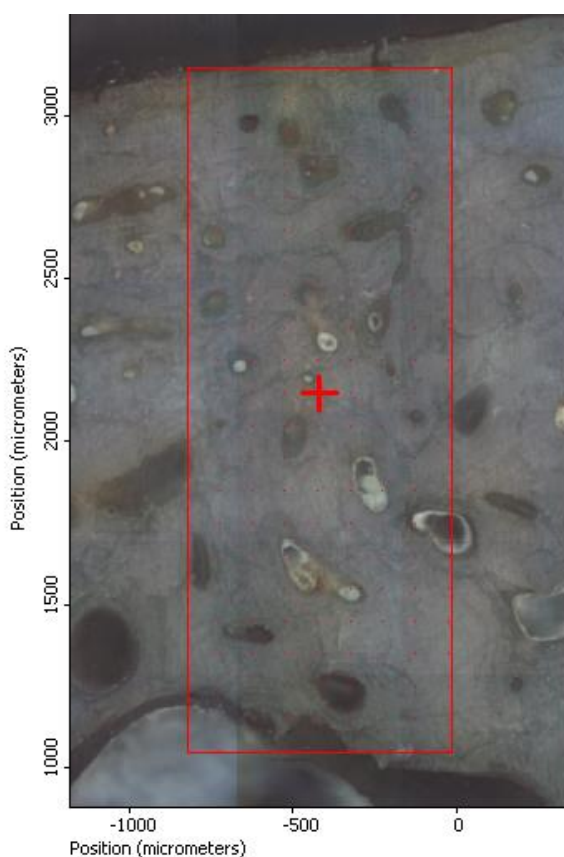


Fig. 2.11 - example of bone thin section with selected the analyzed area by mFTIR and the spots where the spectra were collected.



## 2.2.7 - Characterization of grave soil

In this research 23 grave soils were characterized by color, particle size, pH, organic carbon and organic matter, coming from the following tombs: T.1, T.15 US 199, T.16 US 201, T.17 US 203, T.18 US 205, T.19 US 207, T.25 US 240 e 253, T.28 US 243, T.35 US 250, T.37 US 1304, T.39 US 1315, T.40 US 1323, T.49 US 823, T.50 US 826, T.55 US 841, T.60 US 857, T.73 US 899, T.99 US 8242, T.100 US 8246, T.107 US 8271, T.116.

### 2.2.7.1 - Color

Soils have varied colors, ranging from gray to black, green, and yellowish to red or brown. Soil color reflects environmental conditions, soil forming processes, and other influences on the soil. It generally indicates the status of organic matter and moisture, drainage, and the state of oxidation and reduction. It may also indicate mineralogical composition of the soil such as presence of iron, manganese, and dark minerals. Humus-rich soils have dark gray to black coloration. Saturation of soil with moisture may also give darker colors. Well-drained soils have generally yellowish-red to brown color. Oxidized iron compounds give reddish color to soils (SSSA 2010). Iron compounds under impeded drainage in the subsoils give them green colors (gleying). Manganese compounds, if present in large quantities, may give a black color. Color does not affect the behavior of the soils, however. A soil may have a ground color (matrix color) different from mottle (discontinuous spotted streaks and small spots or blotches of contrasting color, usually red or yellow) colors. In describing soil color, both matrix and mottle colors are mentioned. The pattern may relate to the aeration or drainage of the soil. Gleyed colors (greenish) are low chroma matrix colors with or without mottles. If the soil is gleyed, it is likely to be reduced (due to prolonged moisture saturation) and wet for much of the year. Mottles occur in soils that undergo seasonal oxidation and reduction due to fluctuating groundwater. Colors vary in their purity, lightness or darkness, and intensity. Munsell color charts are used to provide standard descriptions and names of soil color. Soil color is expressed by the color notations: hue, chroma, and value. Hue denotes the specific color or purity of color (red, orange, yellow, green, blue, indigo, violet). Value refers to the lightness or darkness of the color, ranging from 0 (most dark) to 10 (most light). Chroma is the light intensity which range from 0 (least intense) to 10 (most intense). The color notations are given in the order: hue, value, and chroma. For example, 10YR 6/4 is a light yellowish-brown soil color; 10YR is the hue, 6 is the value, and 4 is the chroma. Soil color varies with soil moisture; therefore, the state of soil moisture is to be mentioned when soil color is recorded (e.g., 10YR 6/4 dry, light yellowish-brown). Soil color is influenced by several

actors, including mineralogical composition, organic matter content, soil moisture, soil development, and climate (OSMAN, 2013).

All samples have undergone a series of laboratory pretreatments before being subjected to the subsequent analysis. They were dried, weighed and sieved with a sieve with a square mesh of 2 mm, to separate the coarse fraction (retained in the sieve) from the fine earth. The coarse fraction was then thoroughly washed and weighed. Its weight was then expressed as a ratio to the total weight of the sample. The fine earth was used instead to perform all subsequent chemical, mineralogical and physical analyses (AVERY & BASCOMB, 1974; GALE & HOARE, 1991; MINISTERO PER LE POLITICHE AGRICOLE, 1999).

### **2.2.7.2 - Particle size distribution**

The particle size distribution of a soil is the distribution of its mineral particles into size classes; it is a fundamental property on which depend many other chemical and physical properties of soils, and its determination is the basis of a correct classification of a soil (MINISTERO PER LE POLITICHE AGRICOLE, 1999). Knowing the particle size, it is then possible to derive the texture of the sample, i.e. the proportion of the constituents of the earth end of the soil, grouped into size classes (MCRAE, 1991).

For particle size analysis it was used the fine earth fraction in quantities of about 100g. The portion to be subjected to analysis was obtained by one or more subsequent quartering, so arranged that the sub-sample was representative of the original sample. The obtained fraction was weighed and then pre-treated with hydrogen peroxide (H<sub>2</sub>O<sub>2</sub>, 130 volumes) in order to destroy organic matter, which, by favoring aggregate formation, interferes with the analysis.

Each sample was then analyzed using two distinct methodologies applied to different granulometric fractions: the distribution of sand (particles of diameter varying between 2mm and 63µm) was determined by sieving, the distribution of silt (particles of diameter varying 63 and 2µm) was determined by the Casagrande aerometer method (AVERY & BASCOMB, 1974; GALE & HOARE, 1991); the amount of clay was deduced by subtracting the sands and silts to the initial weight of the sample. Sand sieving was conducted on both wet and dry samples, using a column of 10 mesh sieves with decreasing values (1400, 1000, 710, 500, 355, 250, 180, 125, 90 and 63µm). For the wet sieving it was used a stirrer under a constant stream of water to favor particle passage through the sieve; for dry

sieving was used an intermittent mechanical stirrer, operated for 20 minutes. The sieves were then weighed in order to obtain the amount of sand fraction for every class.

The fraction of the sample passing through the 63 $\mu$ m sieve was collected in water tanks and left to settle for at least 24 hours; the volume of water has been progressively reduced by siphoning to obtain a total volume smaller than 1000ml. The material thus obtained was analyzed by aerometry with the method of the Casagrande aerometer, into columns of 2l volume after treatment with calgon (i.e. 3g of sodium hexametaphosphate for each column). The aerometric analysis exploits Stokes law according to which settling velocity of a particle is proportional to its size. Density of the suspension thus tends to decrease with the passage of time and its variation depends on the size of the particles contained in the column. The measurement of density and temperature at standard intervals over 24 hours allows therefore to establish the amount of silt present in the sample.

The data obtained by sieving and aerometry are then unified into frequency cumulative curves that allow an effective visualization of the distribution of the constituents of the soil into dimensional classes.

However, for some tombs the particle size distribution were not possible due to the scarce material: T.1, T.15 US 199, T.25, T.35 US 250, T.37 US 1304, T.39, T.40 US 1323, T.11 US 8246, T.116

### **2.2.7.3 - pH**

The pH was determined in water, using the sample sieved to 2mm. For each sample 10g of soil were added to 25ml of solution (proportion soil/solution of 1/2.5); the suspension was placed on a shaker for twenty minutes and then left to stand for 24 hours. The pH measurement was carried out through the use of a dual point calibration automatic tester.

### **2.2.7.4 - Organic carbon**

Organic carbon determination was obtained through the standard method by WALKLEY & BLACK (1934), which uses the reduction of potassium dichromate  $K_2Cr_2O_7$  excess by organic matter and the subsequent determination of the remaining  $K_2Cr_2O_7$  by oxide-reductive titration iron with a solution of iron ammonium sulphate. The quantity of sample subjected to testing was always particularly low (approximately 0.250g), given the high quantity of organic carbon content in the soils studied (the amount of sample must be such as to ensure that, at the end of the reaction, at least 3ml of  $K_2Cr_2O_7$  remain in excess). The procedure is as follows:

1. the organic matter is oxidized with 10ml of  $K_2Cr_2O_7$  and 20ml of sulfuric acid ( $H_2SO_4$ ). It is left to react inside a covered flask for 30 minutes.
2. 200ml of water are added thus stopping the reaction. Then 5ml of  $H_3PO_4$  acid and 0.5ml of acid 4-diphenilaminsulphonate sodium ( $C_{12}H_{10}NaNO_3$ ) are added.
3. The excess dichromate is titrated by the solution of ferric ammonium sulphate (Mohr salts)  $Fe(NH_4)_2(SO_4)_2 \times 6H_2O$ . The titration is carried out on a magnetic stirrer.

The organic carbon content is expressed in g/kg without decimals; to obtain the corresponding value of organic matter starting from the organic carbon content was used a multiplication factor equal to 1.724 (ASTORI *et alii*, 1994; MINISTERO PER LE POLITICHE AGRICOLE, 1999).

### **2.2.7.5 - Calcium carbonate equivalent**

Calcium carbonate equivalent was chemically performed using a Dietrich–Fruhling calcimeter; the method is based on the measurement of the  $CO_2$  volume developed by acid reacting with the sample, which is proportional of carbonate concentration.

## **Chapter 3**

# **Results**

### **3.1 - Macroscopic analysis**

The macroscopic analysis shows, in general, a good state of preservation for contemporary (Population 4) and archaeological samples (populations 1-3).

The bones collected from Population 4 are all complete, on the contrary those from Population 3 are lacking of one or both epiphyses. Population 1 and 2 show complete bones in 5 and 4 cases respectively. Spongy tissue is exposed in all samples coming from Population 1, 2 and 3, and in 8 bones from Population 4.

The cortical surface is complete on 7 samples of Population 1, on 4 samples of Population 2 and on 7 samples of Population 4. All the samples coming from Population 3 have an incomplete cortical surface (10 samples).

Skin, muscles, ligaments, fatty substance, tissue in medullar cavity and odour are absent in all specimens.

Bleaching is present on 5 samples of Population 3, instead for the others is absent.

Longitudinal cracking were observed on 3 samples of Population 1, on 7 samples of Population 2, and only in 1 samples for both Population 3 and 4.

Flaking is present on 3 specimens of Population 1, on 5 specimens of Population 3, and on 2 specimens of both Populations 2 and 4 (Appendix 1).

As show in table below (tab. 3.1), in general all samples have a low (stage 0-1) or medium (stage 2-3) weathering stage, except for one bone of Population 2, that has a bad conservation (stage 4).

Tab. 3.1 - summary of the macroscopic results based on the classification proposed by Behrensmeyer. For each population is indicated the number of samples that belong to the stage.

Stage	Population 1	Population 2	Population 3	Population 4
0	6	0	6	4
1	2	4	0	3
2	2	2	2	3
3	0	3	2	0
4	0	1	0	0
5	0	0	0	0

In all populations the most popular colors detected on bone shafts are brown (7.5YR) and yellow (10Y), with different tonalities, from light to dark. Population 3 and 4 have more black bones (Black, 2/1 10YR, and Very Dark Brown, 2/2 10YR) than Population 1 and 2 that show more yellow (10YR 8/6) and pale brown bones (6/3 10YR). Regards the other colors was observed: grey color (8/2 2.5Y and 4/2 2.5YR) on 2 samples, one from Population 3 and one from Population 4; white color (8/1 10YR and 8/2 7.5YR) on 2 samples, one from Population 1 and one from Population 2; red color (4/3 10YR and 3/4 10YR) on 3 samples, two from Population 2 and 1 from Population 4, and orange color (8/4 10YR and 7/4 10YR) on 3 samples only from Population 3, as shown in table 3.2.

Tab. 3.2 - summary of the colors detected on bones.

Color	Population 1	Population 2	Population 3	Population 4
Black	0	1	5	5
Brown	9	7	7	9
Gray	0	0	1	1
Yellow	6	5	4	4
White	1	1	0	0
Red	0	2	0	1
Orange	0	0	3	0

### 3.2 - Preservation degree of buried human skeletons

Macroscopic preservation of the 14 buried human remains from Travo (PC) shows that regards the bone quantity, 10 skeletons have a high degree of recovering, with a score between 31-87.5%. A good

conservation was seen in all samples, with a score between 7-56%. Partial and scarce conservation are present in 13 and 10 skeletons, with a score between 6-43% and 6-56% respectively.

No skeletons are highly deteriorated; in general the bones are preserved or fragile in all skeletons, between 12.5-75% in the first case and between 19-71% in the second case. In 8 skeletons the bones are deteriorated with a score between 6-56%.

Whole bones are present in 13 skeletons with a percentage between 19-63%; fragmented bones have a score between 12-69%, and highly fragmented bones were detected with a score between 6-69%.

All the skeletal districts were recovered for each tomb analyzed, except for the tomb 99, where the individual were dug up without the cranium, and for the tomb 73 where the individual has not the right hand.

In the table below (tab. 3.3) are shown the number of individuals with a high degree of conservation, regards the quantity, solidity and fragmentation.

Tab. 3.3 - skeletal conservation according to bone quantity, solidity and fragmentation.

Tomb	Skeletal conservation										
	% Quantity				% Solidity				% Fragmentation		
	Scarce	Partial	Good	Excellent	Highly deteriorated	Deteriorated	Fragile	Preserved	Highly fragmented	Fragmented	Whole
T.16 US 128	0	25	44	31	0	0	38	62	6	50	44
T.17 US 113	6	19	25	50	0	19	19	62	6	31	63
T.18 US 115	12.5	37.5	19	31	0	0	50	50	19	62	19
T.19 US 118	0	6	56	38	0	12	69	19	12.5	50	37.5
T.28 US 163	6	6	25	63	0	0	25	75	13	56	31
T.49 US 824	25	31	44	0	0	56	25	19	69	12	19
T.50 US 827	0	6	38	56	0	6	31	63	6	38	56
T.55 US 842	12.5	6	12.5	69	0	0	50	50	0	37.5	62.5
T.56 US 845	6	12.5	12.5	69	0	6	56	38	6	50	44
T.60 US 858	0	0	12.5	87.5	0	0	56	44	0	50	50
T.73 US 8100	31	25	44	0	0	12.5	62.5	25	31	69	0
T.99 UUSS 8241,8264	28.5	43	28.5	0	0	0	71	29	50	21	29
T.100 US 8245	56	13	25	6	0	25	62.5	12.5	19	44	37
T.107 US 8272	53	40	7	0	0	13	67	20	33	40	27

Upper limbs, lower limbs, and feet have an excellent-good quantity in the 85% of cases; hands and feet in general are well preserved and whole between 71-85% and 71-76% of cases respectively.

Pelvis was recovered in 76% of cases with an excellent-good conservation about quantity, however it appears deteriorated and fragmented in all the 14 tombs (100%).

Cranium, ribs and sternum were not recovered wholes in all tombs (tab. 3.4).

Tab. 3.4 - number of skeletons with a high degree of conservation for each bone district listed.

<b>Bone district</b>	<b>Quantity (excellent-good)</b>	<b>Solidity (preserved)</b>	<b>Fragmentation (whole)</b>
Cranium	7	1	0
Ribs-sternum	8	1	0
Vertebrae	5	3	3
Upper limbs	12	6	5
Hands	6	10	11
Pelvis	11	0	0
Lower limbs	12	5	6
Feet	12	12	10

All the individuals recovered did not show residues of soft tissue, and clothes or ornaments were not recovered.

### 3.2 - Biochemical analysis

The Luminol test was negative or weak positive in all samples with a PMI >50 years (Populations 1-3). However, a 20% of recent bones (Population 4) had a negative chemiluminescence, as shown in table 3.5. A very strong positive was recorded only on contemporary bones coming from Population 4 (7).

Tab. 3.5 - results of Luminol test according to the chemiluminescence intensity proposed. For each population are indicated the number of samples.

<b>score</b>	<b>Population 1</b>	<b>Population 2</b>	<b>Population 3</b>	<b>Population 4</b>
-	7	9	7	2
+	3	1	3	1
++	0	0	0	7



### 3.3 - Microscopic analysis in optical light

Calcified histology of bones from Milan showed in general a high (OHI score 4-5) osteonic conservation (80%) in Population 4, whereas archaeological bones (populations 1-3) showed a high OHI only in 30% of samples (tab. 3.6).

Tab. 3.6 - results of microscopic analysis of calcified thin sections based on the Oxford Histological Index. For each population are indicated the number of samples that belong to the index.

score	Population 1	Population 2	Population 3	Population 4
0-1	4	10	0	0
2-3	5	0	2	4
4-5	1	0	8	6

Decalcified thin sections show a bad state of preservation in 60% of samples of Population 1 and 2, instead no bad samples are present in Population 3.

In 80% of sample of Population 3 the score is high (score 3), as for the bones of Population 4 (60%); on the contrary the more ancient populations (1 and 2) show no or few samples well preserved.

All the results of the decalcified analysis are reported in the table below (tab. 3.7).

Tab. 3.7 - results of microscopic analysis of decalcified thin sections based on the Decalcified Histological Index. For each population are indicated the number of samples that belong to the index.

score	Population 1	Population 2	Population 3	Population 4
1	8	6	0	0
2	2	2	1	1
3	0	2	9	9

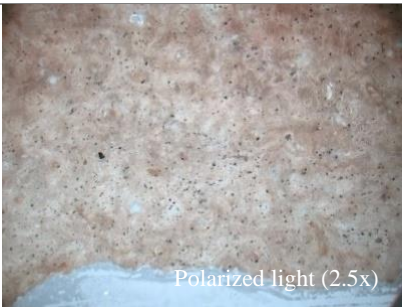

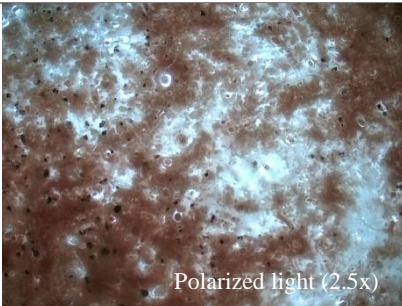

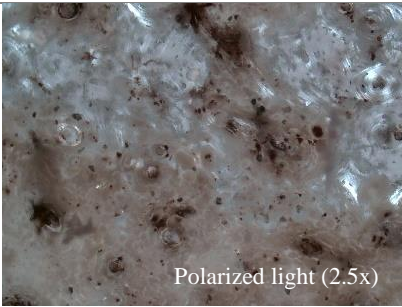

On calcified thin sections the intensity of birefringence was very low and the evaluation was not performed. Whereas on decalcified thin bone sections the birefringence is preserved in 100% of samples, with different degree of appearance. In particular, a high degree was observed on all specimens of Population 4 and on 9 sample of Population 3, instead in Population 2 and 3 a high birefringence is present on 4 and 1 specimens respectively (tab. 3.8).

Tab. 3.8 - results of birefringence degree of decalcified thin sections.

Degree of Birefringence	Population 1	Population 2	Population 3	Population 4
Absent	0	0	0	0
Low	4	1	0	0
Medium	5	5	1	0
High	1	4	9	10

Histological results of bones coming from Travo show a bad degree of preservation for many samples (8 tombs), instead only 3 thin sections show a high OHI between 3-4, as shown in tab. 3.9.

Tab. 3.9 - results of histological analysis.

OHI	sample		
0-1	T.16 US 128, T.18 US 115, T.19 US 118, T.28 US 163, T.50 US 827, T.39 US 1315, T.100 US 8245		
2-3	T.55 US 842, T.40 US 1324, T.37 US 1316, T.60 US 858, T.116 US 8325		
4-5	T.56 US 845, T.17 US 113		

### **3.4 - Chemical and morphological analyses performed by scanning electron microscopy coupled with energy-dispersive X-ray spectroscopy (SEM-EDS)**

In this section, the results carried out from the 40 bones of Milan regards the quantitative chemical analysis and the qualitative morphological analysis performed on non-embedded and embedded sections will be shown first. Then, the results concerning the bone sections and the grave soils, from the 10 tombs of Travo, will be presented.

#### **3.4.1 - SEM-EDS results of bone sections from Milan**

By means of energy dispersive X-ray spectrometer (EDS) the chemical compositions of the 40 non-embedded bone sections have been determined. Human bone is principally made by carbonate-hydroxyapatite,  $\text{Ca}(\text{PO}_4\text{CO}_3)_3\text{OH}$ , however chemical exchanges and substitution during diagenesis can be occur. In this study the following oxides were detected:  $\text{Na}_2\text{O}$ ,  $\text{Cl}_2\text{O}$ ,  $\text{MgO}$ ,  $\text{Al}_2\text{O}_3$ ,  $\text{SiO}_2$ ,  $\text{P}_2\text{O}_5$ ,  $\text{SO}_3$ ,  $\text{K}_2\text{O}$ ,  $\text{CaO}$ ,  $\text{TiO}_2$ ,  $\text{MnO}$ ,  $\text{FeO}$ ,  $\text{SnO}_2$ ,  $\text{BaO}$ ,  $\text{Cr}_2\text{O}_3$ ,  $\text{CuO}$ ,  $\text{PbO}$ ,  $\text{Bi}_2\text{O}_3$ ,  $\text{Sb}_2\text{O}_3$ ,  $\text{La}_2\text{O}_3$ ,  $\text{Ce}_2\text{O}_3$ ,  $\text{Nd}_2\text{O}_3$ ,  $\text{ZnO}$ ,  $\text{NiO}$ ,  $\text{SrO}$ ,  $\text{CoO}$ ,  $\text{ThO}$ ,  $\text{Ag}_2\text{O}$ ,  $\text{Au}_2\text{O}_3$ ,  $\text{ZrO}_2$ ,  $\text{P}_2\text{O}_5$ .

However, some oxides were not found in all populations but only on single bones:  $\text{ZrO}_2$ ,  $\text{Au}_2\text{O}_3$  and  $\text{Sb}_2\text{O}_3$  were identified on one sample of Population 1;  $\text{CoO}$ ,  $\text{ThO}$  and  $\text{Ag}_2\text{O}$  were detected on one sample of Population 2.

Also,  $\text{SrO}$  was found in all populations excepts in Population 1,  $\text{SnO}_2$  was observed in Population 1 and 4 but not in Population 2 and 3,  $\text{Na}_2\text{O}$ ,  $\text{SrO}$ ,  $\text{ZnO}$  were found in all population excepts in Population 2;  $\text{Bi}_2\text{O}_3$  and rare earth elements ( $\text{La}_2\text{O}_3$ ,  $\text{Ce}_2\text{O}_3$ ,  $\text{Nd}_2\text{O}_3$ ) were detected in Population 1 and 4 but not in Population 3 and 4.

$\text{FeO}$  is much abundant in all populations, because was detected on all 10 samples of Population 1, on 9 samples of Population 4 and on 8 samples of Population 2 and 3. Also  $\text{ZnO}$  was often detected, i.e. on 9 samples of Population 1, on 6 samples of Population 3 and on 5 samples of Population 2 and 4. In the table 3.10 the oxide occurrences per sample are reported, instead the percentages of each oxide per sample are reported in Appendix 3.

Tab. 3.10 - number of samples on which were collected the oxides.

Oxide	Population 1	Population 2	Population 3	Population 4
Na <sub>2</sub> O	7	2	5	6
MgO	7	2	5	5
Al <sub>2</sub> O <sub>3</sub>	7	2	5	6
SiO <sub>2</sub>	7	2	5	5
SO <sub>3</sub>	7	6	5	7
Cl <sub>2</sub> O	1	4	1	5
K <sub>2</sub> O	5	4	6	6
CaO	6	2	4	4
P <sub>2</sub> O <sub>5</sub>	6	2	4	4
FeO	10	9	9	9
CuO	6	2	5	5
ZnO	7	5	7	5
PbO	5	2	3	2
BaO	5	5	3	5
TiO <sub>2</sub>	7	6	5	5
Cr <sub>2</sub> O <sub>3</sub>	5	3	3	2
MnO	6	5	4	4
NiO	4	4	4	1
SnO <sub>2</sub>	2	0	1	1
SrO	0	0	1	1
ZrO <sub>2</sub>	1	0	0	0
Bi <sub>2</sub> O <sub>3</sub>	1	1	0	0
Sb <sub>2</sub> O <sub>3</sub>	0	0	0	0
Au <sub>2</sub> O <sub>3</sub>	1	0	0	0
Ag <sub>2</sub> O	0	1	0	1
ThO	0	1	0	0
CoO	0	1	0	0
La <sub>2</sub> O <sub>3</sub> , Ce <sub>2</sub> O <sub>3</sub> , Nd <sub>2</sub> O <sub>3</sub>	0	1	0	0

To elaborate the high variability of the data collected by EDS analysis, the oxides detected in all populations were organized in a table to perform statistical analysis. For every analysis listed, numbered in progressive order, were reported the percentage of the following oxides: Na<sub>2</sub>O, MgO, Al<sub>2</sub>O<sub>3</sub>, SiO<sub>2</sub>, P<sub>2</sub>O<sub>5</sub>, SO<sub>3</sub>, K<sub>2</sub>O, CaO, TiO<sub>2</sub>, MnO, FeO, SnO<sub>2</sub>, Cr<sub>2</sub>O<sub>3</sub>, CuO, PbO, Bi<sub>2</sub>O<sub>3</sub>, La<sub>2</sub>O<sub>3</sub>, Ce<sub>2</sub>O<sub>3</sub>, Nd<sub>2</sub>O<sub>3</sub>, ZnO, NiO, SrO, CoO, P<sub>2</sub>O<sub>5</sub> (Appendix 3).

With the purpose to explain the variability of each oxide in every population, a statistical analysis was performed by means of the Principal Component Analysis (PCA): the oxides were uploaded in the program as variables, and the analyses as samples. In the resulting statistical graph (fig. 3.1) the analyses performed from the same population were gathered in an elliptic shape colored green for Population 1, grey for Population 2, violet for Population 3 and red for Population 4.

As shown in fig. 3.1 the analyses appear homogeneously distributed along the PC2 and PC3 axes, ranging from -3.21 to 2.648 and from -3.28 to 2.825 values respectively, in all the bone samples, irrespective of population. The values along PC1 axis are close to 0 in all analyses, ranging from -0.210 to 0.829, excepts for tow ones, which have a PC1 value of -12.71 and -2.18 in Population 2 and 3 respectively. The standard deviation for each axis is ca.  $\pm 1.72$  for PC1, ca.  $\pm 1.39$  for PC2 and ca.  $\pm 1.49$  for PC3.

Regards the oxides variability, they appear close to 0 in PC2 axis, ranging from -0.21 to 0.12, excepts for  $\text{SiO}_2$  and  $\text{Al}_2\text{O}_3$  that show the lower values, equal of -0.40 and -0.38 respectively, whereas CaO and  $\text{P}_2\text{O}_5$  have the higher ones, equal of 0.51 and 0.50 respectively.

Along the PC3 axis the oxides are homogeneously distributed, ranging from -0.47 to 0.35, instead for PC1 axis the values are all close in the range between 0.0089 and 0.19, excepts for the rare earth elements which assumes a value of -0.56.

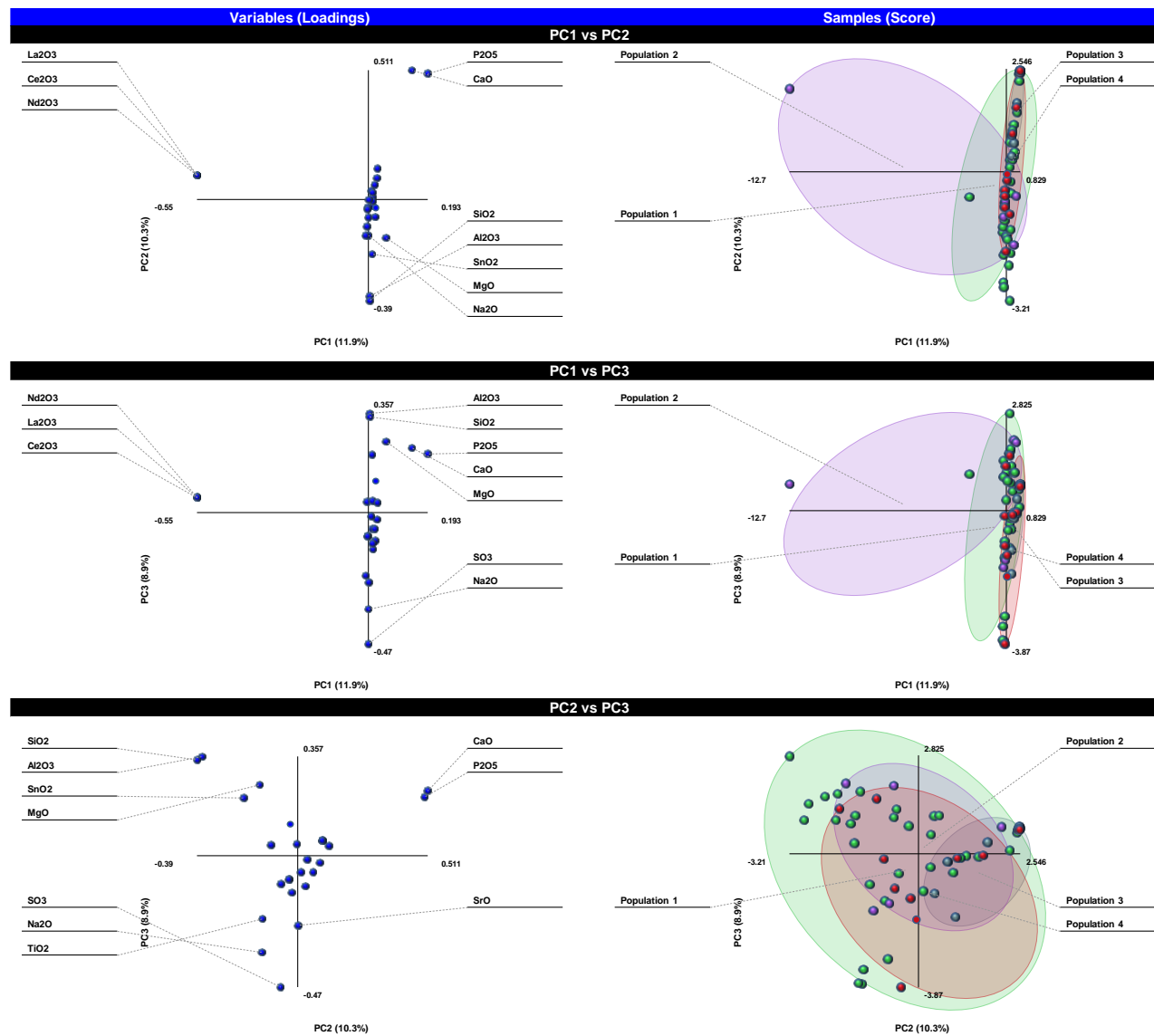


Fig. 3.1 - statistical graphs results by PCA analysis, on the left are shown the variables (oxides) and on the right the samples (populations).

Subsequently, with the aim to understand which elements could be responsible of the variability of the samples in the different populations, the PCA was applied on the transposed table, uploading the analyses as variables and the oxides as samples. To reduce the complexity level of the output, the oxides were subdivided in groups, based on their possible source, according to the literature: related to decomposition process, from soil contamination, from contamination with blade saw during the sample preparation, and due to the type of burial (metal coffin) (tab. 3.11).

Tab. 3.11 - oxides divided in accordance to their probable origin.

Oxides	Origin
MgO, P <sub>2</sub> O <sub>5</sub> , SO <sub>3</sub> , CaO	Decomposition
Al <sub>2</sub> O <sub>3</sub> , SiO <sub>3</sub> , TiO <sub>2</sub> , MnO	Soil
FeO, Cr <sub>2</sub> O <sub>3</sub>	Saw
CuO, PbO, ZnO	Burial

The statistical graph in figure 3.2 reports the oxides with the same origin assembled in an elliptic shape colored green for Decomposition, grey for Soil, violet for Saw and red for Burial, and the variability of each analysis performed.

Regards the Decomposition, the oxides are heterogeneous distributed along the PC1 axis, with values from -3.04 to 11.25, instead are closer along the PC2 and PC3 axis, where range from -3.55 to -0.29 and from -1.08 to -0.45 respectively.

Soil oxides range from -3.26 to -1.13 on PC1 axis, and from -2.72 to 0.94 on PC3 axis; the high variability is observed on PC2 axis, where the 5 values range from -1.03 to 10.46.

The two oxides of the Saw group have values close to 0 on PC1 and PC2 axes, where range from -3.17 to 1.74 and from -0.94 to 1.89 respectively, instead on PC3 axis the values are between -0.73 and 9.93.

Finally, the oxides related to the Burial context are close to each other on the all PCA axes, and range from -2.85 to -2.82 on PC1 axis, from -1.51 to -0.79 on PC2 axis and from -1.07 to -0.66 on PC3 axis. In this case, the standard deviation is ca. 0.017 for PC1, instead for PC2 and 3 is 0.36 and 0.21 respectively. For the other groups (Decomposition, Soil and Saw) the standard deviation has a mean of  $\pm 3.5$  for each axis.

The analyses plotted show a homogeneous distribution along the 3 axes in all populations: for Population 1 the values on PC1 axis range from -0.061 to 0.20, instead on PC2 axis range from -0.12

to 0.26 and on PC3 range from -0.095 to 0.30; for Population 2 the values are between -0.033 and 0.18 on PC1 axis, between -0.085 and 0.22 on PC2 axis and between -0.10 and 0.11 on PC3 axis; for Population 3 the values ranging from 0.076 to 0.18 on PC1 axis, from -0.0022 to -0.12 on PC2 axis and from -0.050 to 0.28 on PC3; finally for Population 4 the values range from -0.018 to 0.19 for PC1 axis, from -0.11 to 0.24 for PC2 axis and from -0.10 to 0.31 for PC3 axis.



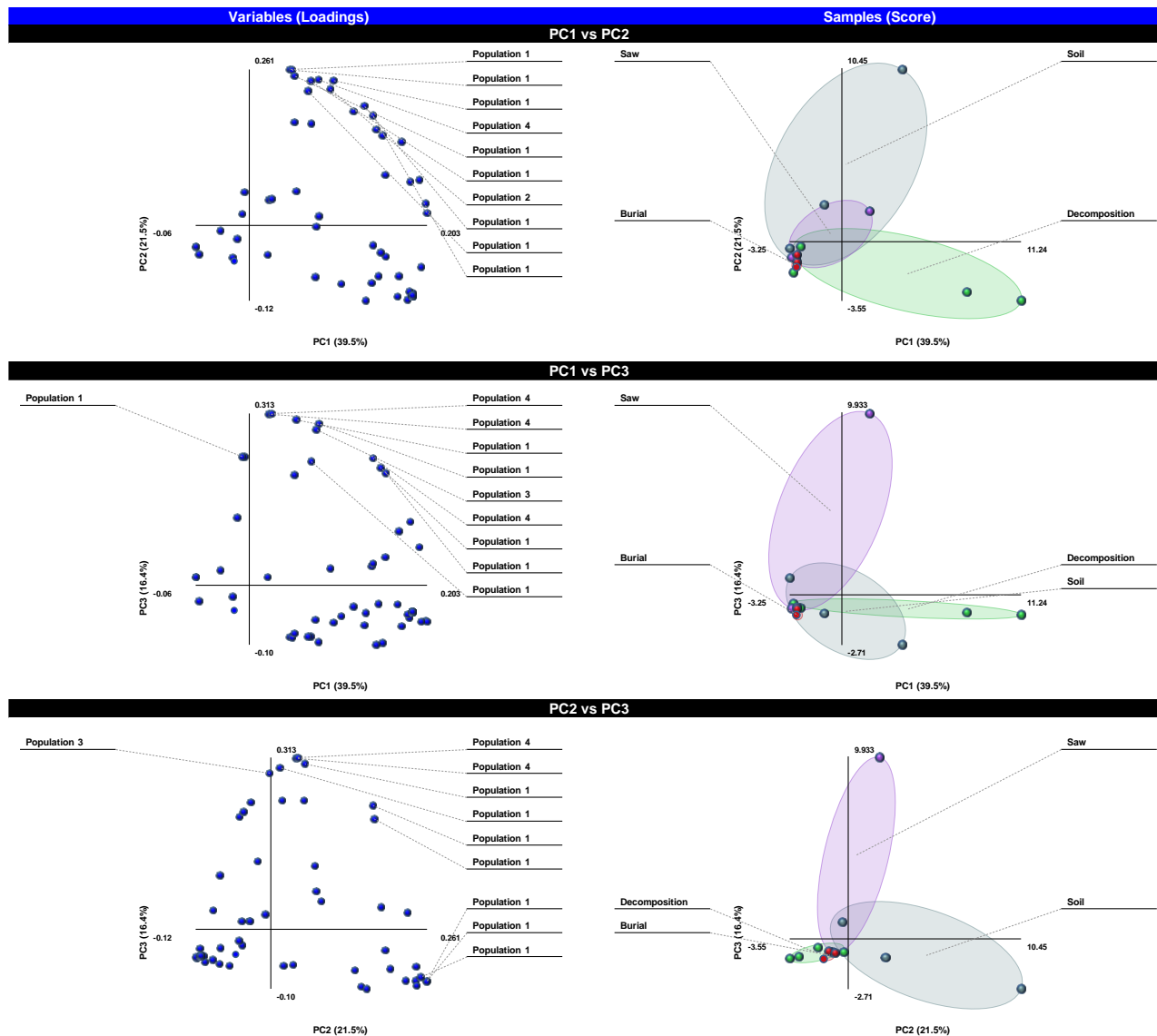


Fig. 3.2 - statistical graphs results by transposed PCA analysis, on the left are shown the variables (populations) and on the right the samples (oxides collected by their probable origin: Decomposition, Soil, Saw, Burial).

By SEM-EDS analyses, the composition of some minerals were also estimate using DEER *et alii* 1966 (Appendix 4).

In the table below (tab. 3.9) are reported all the minerals identified.

Tab. 3.9 - the table reports the mineral detected for each population on the thin sections studied.

Population	Minerals
1	K-feldspar, barite, ilmenite, pyrite, zircon, albite, quartz, clay
2	barite, potassium chloride, rutile, quartz
3	barite, rutile, pyrite, chlorite
4	K-feldspar, barite, ilmenite

However, some minerals are present only in single samples, for example: albite, zircon and clay were detected only on single bones from Population 1, instead chlorite was recovered only on one sample of Population 3.

Also in this case, the statistical PCA model was applied, uploading as variables the minerals and as samples the analyses. The results as graphically plotted in figure 3.3.

Mineral analyses are not grouped on the three axes, among the populations. For Population 1 along the PC1 axis the values range from -1.71 to 2.68, instead on PC2 and PC3 axes range from -1.58 to 1.51 and from -1.19 to 0.36 respectively. For Population 2 the values range from -1.63 to 1.30, from -1.58 to 1.22 and from -0.19 to 3.29 on PC1, 2 and 3 axes respectively. In Population 3 the values on PC1, PC2 and PC3 range from -2.82 to 1.30, from 0.87 to 3.05 and from -0.51 to 3.29 respectively. Finally, Population 4 shows values between -1.09 and 0.88 for PC1 axis, between -1.58 and -0.38 for PC2 and between 0.43 and 0.37 for PC3.

Furthermore, the oxide values are not close to each other, but show the same variability among the axes: for PC1 the values range from -0.37 to 0.54, for PC2 range from -0.35 to 0.51 and for PC3 range from -0.45 to 0.53. The standard deviation is ca.  $\pm 0.31$  for all axes.

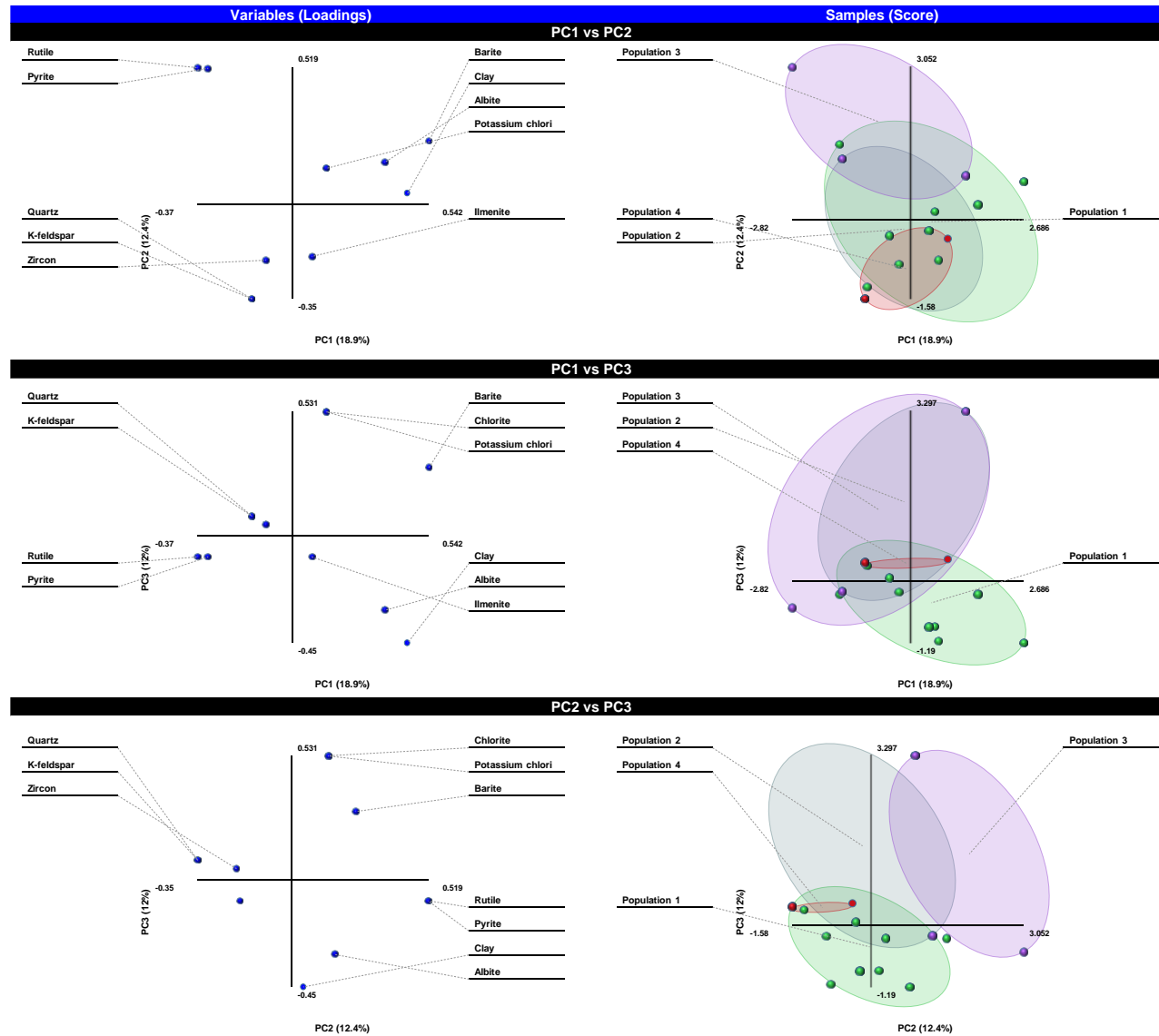


Fig. 3.3 - statistical graphs resulting by PCA analysis employed on mineral elements detected by the analysis for each population: on the left are shown the variables (minerals) and on the right the samples (populations).

In the table below (tab. 3.10) are summarized the results obtained by morphological analysis of embedded thin bone sections. For each parameter observed is reported the number of bones on which was detected.

Tab. 3.10 - for each population is reported the number of thin sections having: preserved osteons, degraded areas, remineralized zones, and cracks related or not to bone structure, according to the bone area on which were observed.

<b>Parameter observed</b>	<b>Bone position</b>	<b>Population 1</b>	<b>Population 2</b>	<b>Population 3</b>	<b>Population 4</b>
preserved osteons	internal cortical border	2	7	8	10
	central cortical	5	6	10	10
	external cortical border	2	7	9	10
degraded areas	internal cortical border	10	7	7	0
	central cortical	10	6	4	0
	external cortical border	10	10	8	2
remineralized zones	internal cortical border	10	7	6	1
	central cortical	10	6	5	1
	external cortical border	10	8	7	2
cracks related to bone structure	internal cortical border	4	8	9	9
	central cortical	4	8	8	9
	external cortical border	3	8	9	9
cracks not related to bone structure	internal cortical border	9	9	10	10
	central cortical	9	9	9	10
	external cortical border	10	9	10	10

In Population 1 preserved osteons were seen in central cortical bone in 50% of cases, instead on borders the percentage is low; degraded areas were recorded on the total section for all bones examined, as the remineralized areas (100%). Cracks related to bone structure are present only on 30-40% of sections, on the contrary, which ones not related are on 90-100% of samples.

For Population 2 preserved osteons were found in 60-70% of cases, as the degraded areas, except on the external cortical border, where were observed in 100% of samples. Remineralized zones are

homogeneously distributed on the total sections, from 60 to 80% of samples. Cracks related and not related to bone structure are detected in 80 and 90% of specimens respectively.

Population 3 shows preserved osteons in 80-100% of samples, instead degraded areas are more frequent on internal and external borders (70-80%), except for central cortical, where were observed in 40% of samples. Remineralized zones were detected in 60-70% on internal and external borders respectively, and in 50% on central cortical. Cracks related and not related to bone structure were detected in 80-90% of sections in the first case and in 90-100% in the second one.

In Population 4 all thin sections show preserved osteons (100%), non-degraded areas were seen in 20% of cases, only on external cortical border. Remineralized zones were detected in few cases, 10-20% of samples, particularly on external cortical border. Cracks related and not related to bone structure were detected in 90 and 100% of bones respectively.

Among the cracks not related to bone structure are frequent which ones that run from external to internal border, found in 30%, 40%, 80% and 90% for Population 1,2,3 and 4 respectively (Appendix 5).

### 3.4.2 - SEM-EDS results of bone sections and grave soils from Travo (PC)

The oxides and minerals detected by SEM-EDS analysis on the 10 bones from the necropolis of Travo (PC) are shown in table 3.11:

Tab. 3.11 – oxides and minerals detected on bone sections from Travo.

<b>Tomb</b>	<b>Oxide</b>	<b>Mineral</b>
T.16 US 128	exogenous and endogenous manganese oxide	/
T.17 US 113	barium sulfate	zircon
T.28 US 163	endogenous manganese oxide	ilmenite
T.50 US 827	exogenous manganese oxide, iron oxide, rare earth elements	/
T.55 US 842	exogenous manganese oxide, iron oxide	zircon
T.56 US 845	exogenous and endogenous manganese oxide, barium sulfate, iron oxide	/
T.60 US 858	exogenous manganese oxide	zircon

On the bones coming from T.16 US 128, 17 US 113, 56 US 845 were also detected traces of clay.

The bone section of T.18 US 115, T.19 US 118, T.100 US 8245 are completely clean.

The SEM-EDS analysis performed on gravel soils carried out the following results (table 3.12):

Tab. 3.12 - oxides and minerals detected into the grave soils from Travo.

<b>Tomb</b>	<b>Oxide</b>	<b>Mineral</b>
T.16 US 201	iron oxide, manganese oxide, calcium phosphate	ilmenite
T.17 US 203	iron oxide, rare earth elements, titanium oxide, calcium phosphate	ilmenite, chlorite, zircon
T.28 US 205	iron oxide, quartz, titanium oxide, mica, calcium phosphate	/
T.19 US 207	iron oxide, manganese oxide, calcium phosphate	mica, ilmenite
T.28 US 243	iron oxide, titanite, sulfur oxide, calcium phosphate	ilmenite, chlorite
T.50 US 826	iron oxide, potassium oxide, calcium phosphate	zircon, quartz
T.55 US 841	manganese oxide, nickel oxide, calcium phosphate	ilmenite, chlorite
T.56 US 844	iron oxide, titanium oxide, rare earth elements, calcium phosphate	zircon, chlorite,
T.60 US 857	iron oxide, titanium oxide, manganese oxide, rare earth elements, chrome oxide, calcium phosphate	ilmenite, zircon, chlorite
T.100 US 8246	iron oxide, titanium oxide, thorium oxide, rare earth elements, calcium phosphate	zircon

In all grave soils analyzed were detected clay.

A large amount of coccolith was detected into the grave soil of the tombs: 18, 28, 56, 100.

Also, one foraminifera was observed into the tomb 28.

### 3.5 - Computed tomography imaging

In the table below (tab. 3.13) are summarized the principal results of the morphometric analysis, carried out by the tomography (reconstructed in 3D view, with a spatial resolution around the micrometer) obtained with synchrotron light source, of the 24 bone cross sections coming from the four burial locations of the Milan area (tab. 3.13).

Tab. 3.13 - summary of the results obtained by tomographic analysis for each population. For every morphometric parameter was reported: the minimum and the maximum value detected and the related mean calculated with its standard deviation.

Morphometric parameter	Population 1	Population 2	Population 3	Population 4
% Total bone porosity	6.7-16.3 (11.5 ± 3.13)	2.8-23.9 (15.3 ± 8.26)	2.7-19.6 (10.1 ± 6.47)	7.3-26.2 (16.8 ± 6.36)
% Canals porosity	0.8-8.5 (3.6 ± 2.9)	1.2-18.7 (5.8 ± 6.8)	1.4-5.0 (3.2 ± 1.7)	3.6-25.5 (15.0 ± 7.2)
% Lacunae porosity	/	0.3-1.7 (0.3±0.6)	0.4-1.2 (0.8±0.6)	0.4-12.6 (0.9 ± 0.6)
% Remineralized areas	3.7-10.4 (8.3 ± 4.3)	3.6-10.8 (5.2 ± 4.7)	0.8-3.0 (0.6 ± 1.2)	3.6
Canals volume (µm <sup>3</sup> )	0.6-27.4 (6.7 ± 10.3)	1.1-15.7 (3.8 ± 5.8)	1.1-4.5 (2 ± 1.3)	4.5-28.8 (15.6 ± 9.8)
Lacunae volume (µm <sup>3</sup> )	/	1e <sup>-03</sup> -4.6e <sup>-04</sup> (7.6e <sup>-04</sup> ± 4.2e <sup>-04</sup> )	2.5e <sup>-04</sup> -7.5e <sup>-04</sup> (5.04e <sup>-04</sup> ± 2.16e <sup>-04</sup> )	4.3e <sup>-04</sup> -1.1e <sup>-03</sup> (7.6e <sup>-04</sup> ± 3.1e <sup>-04</sup> )
Canals surface (µm <sup>2</sup> )	81.1-903.6 (303.2 ± 309)	108.9-568 (221.7 ± 172.3)	109.4-304 (172.6 ± 75.9)	330.7-1021.2 (659.8 ± 279)
Lacunae surface (µm <sup>2</sup> )	/	0.4-0.8 (0.6 ± 0.2)	0.2-0.6 (0.4 ± 0.1)	0.3-1 (0.6 ± 0.2)
Canals surface/ canals volume	114.4-166.4 (134.6 ± 20.5)	79.7-181.1 (134.3 ± 32.6)	102.9-165.5 (133.2 ± 22.3)	87.7-154.1 (103.6 ± 25.3)
Lacunae surface/ lacunae volume	/	915.2-1030.5 (972.9 ± 81.5)	953-1097.4 (1022.4 ± 58)	886-1023.9 (949.2 ± 54.7)
3D canals length (µm)	518.2-1020.3 (753.7 ± 226.6)	424.3-1253.3 (740.1 ± 276)	676-950.7 (801.2 ± 108.8)	652.7-1364.8 (907.9 ± 247.9)
3D canals width (µm)	70.8-177.9 (110.6 ± 48)	79.5-211.1 (112.1 ± 49.2)	71.9-129.9 (105.5 ± 19.7)	102.2-222.4 (150.5 ± 40.4)
3D lacunae length (µm)	/	1.8-2.6 (2.2 ± 0.5)	2.1-3.4 (2.7 ± 0.5)	1.3-3.1 (2.2 ± 0.6)
3D lacunae width (µm)	/	0.1-0.3 (0.2 ± 0.1)	0.2-0.3 (0.2 ± 0.03)	0.1-0.3 (0.2 ± 0.06)

The Euler number of canals has an average value of 0.96 for Population 1, of 0.95 for Population 2, of 0.88 for Population 3 and of 0.19 for Population 4. No connectivity was observed among the lacunae in all samples.

Bone anisotropy has the same average value of ca. 0.9 in all populations.

### 3.6 - Organic and mineral fraction by FT-IR analysis

In this section the results obtained by Fourier transform infrared spectrometry (FT-IR) and Fourier transform infrared micro-spectrometry (mFTIR) are presented.

The FT-IR transmission analysis performed on bone powders provided information on the preservation state of the mineral and the organic phase of the bone populations analyzed. In particular the absorptions of collagen ( $\nu_1$ Amide I), phosphate ( $\nu_3$ PO<sub>4</sub> and  $\nu_4$ PO<sub>4</sub>) and carbonate ( $\nu_2$ CO<sub>3</sub>) and their relative intensities have been analyzed in detail (Appendix 7, 8) and given in table 3. 14.

Tab. 3.14 – summary of the results obtained by calculation of the ratios  $\nu_1$ AmI/  $\nu_3$ PO<sub>4</sub>,  $\nu_2$ CO<sub>3</sub>/ $\nu_3$ PO<sub>4</sub> and IRSF of every populations with transmission IR spectrometer. For each ratio are reported the minimum, maximum and average value detected, and the related standard deviation (st.dev.). Regards the  $\nu_1$ AmI/ $\nu_3$ PO<sub>4</sub> ratio the sample variability is ca. 8% for Population 1, 9% for Population 2, 14% for Population 3 and 7% for Population 4;  $\nu_2$ CO<sub>3</sub>/ $\nu_3$ PO<sub>4</sub> ratio has a sample variability of 8% 6% 7% 4% for Population 1, 2, 3 and 4 respectively; the sample variability for IRSF is ca. 2% for Population 1, 1% for Population 2, 3% for Population 3 and 2% for Population 4.

Population		$\nu_1$ AmI/ $\nu_3$ PO <sub>4</sub> ratio	$\nu_2$ CO <sub>3</sub> / $\nu_3$ PO <sub>4</sub> ratio	IRSF
1	min. value	0.21	0.26	2.61
	max. value	0.41	0.49	3.62
	mean	0.29	0.36	2.89
	st.dev.	0.06	0.07	0.28
2	min. value	0.25	0.32	2.61
	max. value	0.69	0.52	3.01
	mean	0.36	0.39	2.83
	st.dev.	0.14	0.06	0.11
3	min. value	0.28	0.29	2.53
	max. value	0.71	0.58	3.02
	mean	0.48	0.40	2.85
	st.dev.	0.17	0.11	0.16
4	min. value	0.42	0.32	2.52
	max. value	1.04	0.73	2.98
	mean	0.73	0.52	2.72
	st.dev.	0.18	0.12	0.14



The FT-IR spectra Population 4 samples show relatively high  $\nu_1$ Amide I absorptions if compared to  $\nu_3$ PO<sub>4</sub> absorptions with an average value of 0.73 for the  $\nu_1$ Amide I/ $\nu_3$ PO<sub>4</sub> absorption ratio. The average value of the  $\nu_1$ Amide I/ $\nu_3$ PO<sub>4</sub> absorption ratio is directly proportional to the amount of collagen contained in the bone tissue and not surprisingly this ratio progressively decreases with the increasing age of the population analyzed. The oldest population (Population 1) has the lowest ratio, with an average value of 0.29. On the other hand the variability of the  $\nu_1$ AmI/ $\nu_3$ PO<sub>4</sub> decreases with the age of the analyzed population as shown by the standard deviation that is 0.06 for Population 1 and 0.18 for Population 4

The  $\nu_1$ Amide I/  $\nu_3$ PO<sub>4</sub> absorption ratio was used to estimate the weight percentage of collagen using the formula provided in TRUEMAN *et alii* (2004). The calculated collagen weight percentage decreases from Population 4 to Population 1, ranging from 28.65 to 18.37 weight percent. TRUEMAN *et alii* (2004) reported a weight percentage of organic material in fresh bones of ca.30%. Thus in this study the estimated collagen loss is equal to 11.6%, 9.3%, 5.7% and 1% for Population 1, 2, 3 and 4 respectively.

The variability of CO<sub>3</sub> content in the bone tissues of the different populations is evaluated by the calculating the  $\nu_2$ CO<sub>3</sub>/ $\nu_3$ PO<sub>4</sub> ratio. This ratio is lowest in average in the samples of Population 1, with an average of 0.36, and progressively increases for Population 2, 3 and 4, reaching an average value of 0.52 in Population 4. Standard deviation has similar values for Population 1 and 2, 0.07 and 0.06 respectively, instead Population 4 shows the higher one, 0.52.

Infrared splitting factor (IRSF – WEINER & BAR-YOSEF, 1990) provides an assessment of crystallinity of bone mineral (carbonate-hydroxyapatite). The crystallinity index of fresh bone mineral is very low and provides IRSF values of ca. 2.6 to 2.8. The higher the crystallinity of the mineral phase the higher value of the IRSF. The average IRSF values for Population 2 and 3 is 2.83 and 2.85 respectively. For Population 1 and Population 4 the average values are respectively of 2.89 and 2.72. These data show positive correlation between age of the population and bone mineral crystallinity. The standard deviation of the measured IRSF values is similar for Population 1, 2 and 3 (0.11, 0.16, 0.14) while for Population 4 has the higher value of 0.28.

The mean crystal length of bone carbonate-hydroxyapatite was estimated using the IRSF value according to the equation given in TRUEMAN *et alii* (2008). The estimated mean mean crystal length of bone carbonate-hydroxyapatite shows an increase from Population 4 to 1, ranged from 39.51 to 43.12 nm. These values indicate a slight bone mineral recrystallization among the population that appear to be positively linked to the relative older age of the populations.

Traces of quartz were detected by FT-IR in the bone powders of samples 4 and 8 from Population 1 and sample 4 from Population 2 indicating that fine sediments adheres to the bone surface or penetrated in the cracks of these specimens.

The preliminary results of the mFTIR chemical map analysis performed on 12 thin cross sections show that bone material is homogeneously composed across the sections analyzed.

Four samples showed peculiar distributions. In Sample 4 of Population 4 the Amide I absorption (collagen) at the edges of the cross section is below detection limit suggesting that locally collagen is highly degraded or diminished (fig. 3.4a).

Similarly, in Sample 6 of Population 2 Amide I absorptions are below detection limits on the external and internal cortical surfaces while is detected spottily in a few areas in the center of the section not degraded by microbial action (fig. 3.4b). Sample 3 of Population 3 has few traces of collagen preserved on internal border, while sample 10 of Population 4 (modern) appears to have typical Amide I absorption homogeneously distributed across the all section (fig. 3.4c).

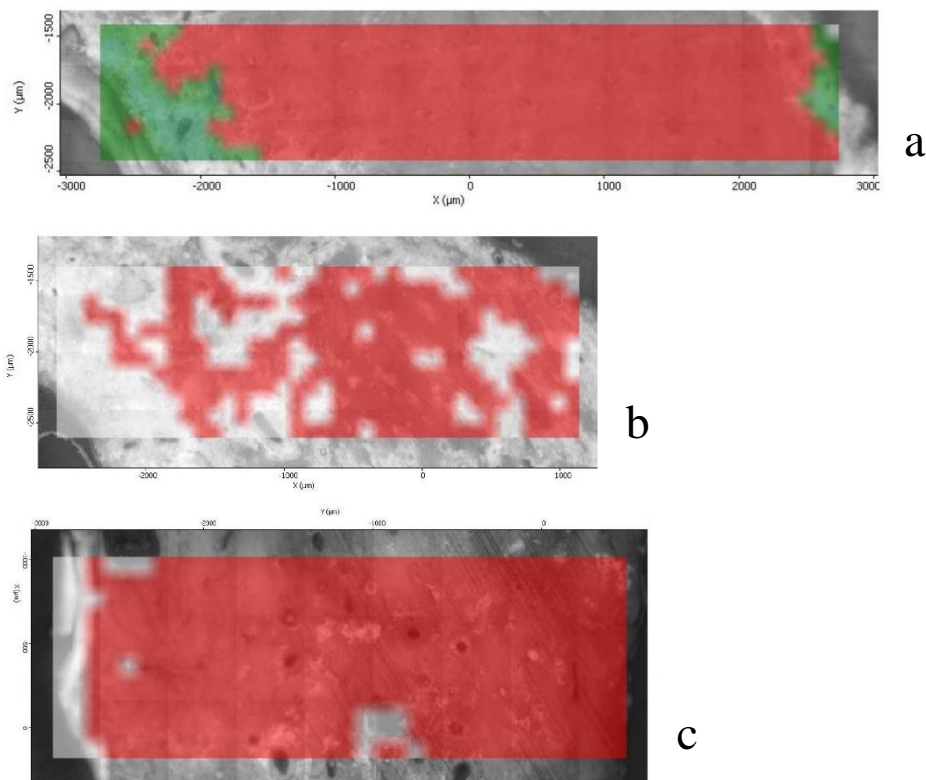


Fig. 3.4 - a) badly preserved collagen on the thin section edges (sample 3 of Population 3); b) preserved collagen only in few areas of the section (sample 6 of Population 2); c) thin section with best preserved collagen (sample 9 of Population 3).

### 3.7 - Grave soil analyses

Regards the color, all 23 grave soils have the same color: 5/3 10 YR.

Particle size distribution shows that, out of 13 grave soils analyzed, gravel was detected between 1-40%, sand between 12-35%, silt between 20-49% and clay between 19-46% (fig.3.4a). A high content of gravel was detected only in one tomb, T.107 (40%), while it is ranging between 1% and 9%, excepts for tomb 73 and 56, whose gravel content increases to 11% and 14% respectively. As regards the sand, in all samples the content varies between 12% and 22%, however in tomb 60 the sand increases to 35% (fig. 3.5a).

Cumulative curves (fig. 3.5b) show a constant increase in frequency towards the finest fractions in all tombs: silt ranging between 36% and 49%, excepts in T.107, where rises to 20%, and clay is from 26% to 46%, decreasing to 19% only in T.107.

The pH is neutral-basic for all 23 tombs, because the values ranging from 7.38 to 8.04, with an average value of 7.85 (tab. 3.15).

The organic carbon content of the 23 studied tombs is ranging between 0.32 g/Kg to 18.09 g/Kg, with an average value of 11.89 g/Kg. Only in one tomb, the T.19, was detected a value of 0.32 g/Kg (fig. 3.6a).

The equivalent of calcium carbonate is ranging between a minimum value of 2.79% and maximum value of 13.21 %, with an average value of 7.28 % (fig. 3.6b).

Tab. 3.15 - results obtained by grave soil analyses from the 23 tombs of the necropolis of Travo (PC). For T.1, 15, 25, 35, 37, 39, 40, 116 the particle size distribution was not performed due to the scarce material available.

Tomb	Particle Size Distribution				pH	Organic Carbon (g/Kg)	Calcium Carbonate Equivalent (%CaCO <sub>3</sub> )
	Gravel	Sand	Silt	Clay			
T.1	/	/	/	/	7.87	17.11	3.04
T.15 US 199	/	/	/	/	7.74	11.16	5.76
T.16 US 201	2%	12%	40%	46%	7.63	15.71	4.82
T.17 US 203	3%	16%	46%	35%	7.38	3.02	5.48
T.18 US 205	1%	17%	39%	43%	7.71	13.79	8.27
T.19 US 207	3%	13%	49%	35%	7.88	0.32	5.93
T.25 US 240	/	/	/	/	7.63	15.70	6.93
T.25 US 253	/	/	/	/	7.59	9.34	7.93
T.28 US 243	9%	20%	35%	36%	7.73	11.60	7.90
T.35 US 250	/	/	/	/	7.61	10.82	10.98
T.37 US 1304	/	/	/	/	7.68	11.50	12.15
T.39 US 1315	/	/	/	/	7.42	12.98	2.79
T.40 US 1323	/	/	/	/	7.92	12.44	5.81
T.49 US 823	4%	13%	46%	37%	7.97	12.22	7.66
T.50 US 826	7%	15%	45%	33%	8.04	9.21	9.07
T.55 US 841	9%	17%	37%	36%	7.87	12.74	7.85
T.56 US 844	14%	13%	38%	35%	7.89	11.75	6.05
T.60 US 857	3%	35%	36%	26%	7.92	14.88	8.51
T.73 US 899	11%	17%	42%	30%	7.9	11.19	9.13
T.99 US 8242	3%	22%	41%	34%	7.75	18.09	9.19
T.100 US8246	/	/	/	/	7.92	13.86	3.81
T.107 US 8271	40%	21%	20%	19%	7.9	11.96	13.21
T.116 US 8324, 8342	/	/	/	/	7.85	11.96	4.53

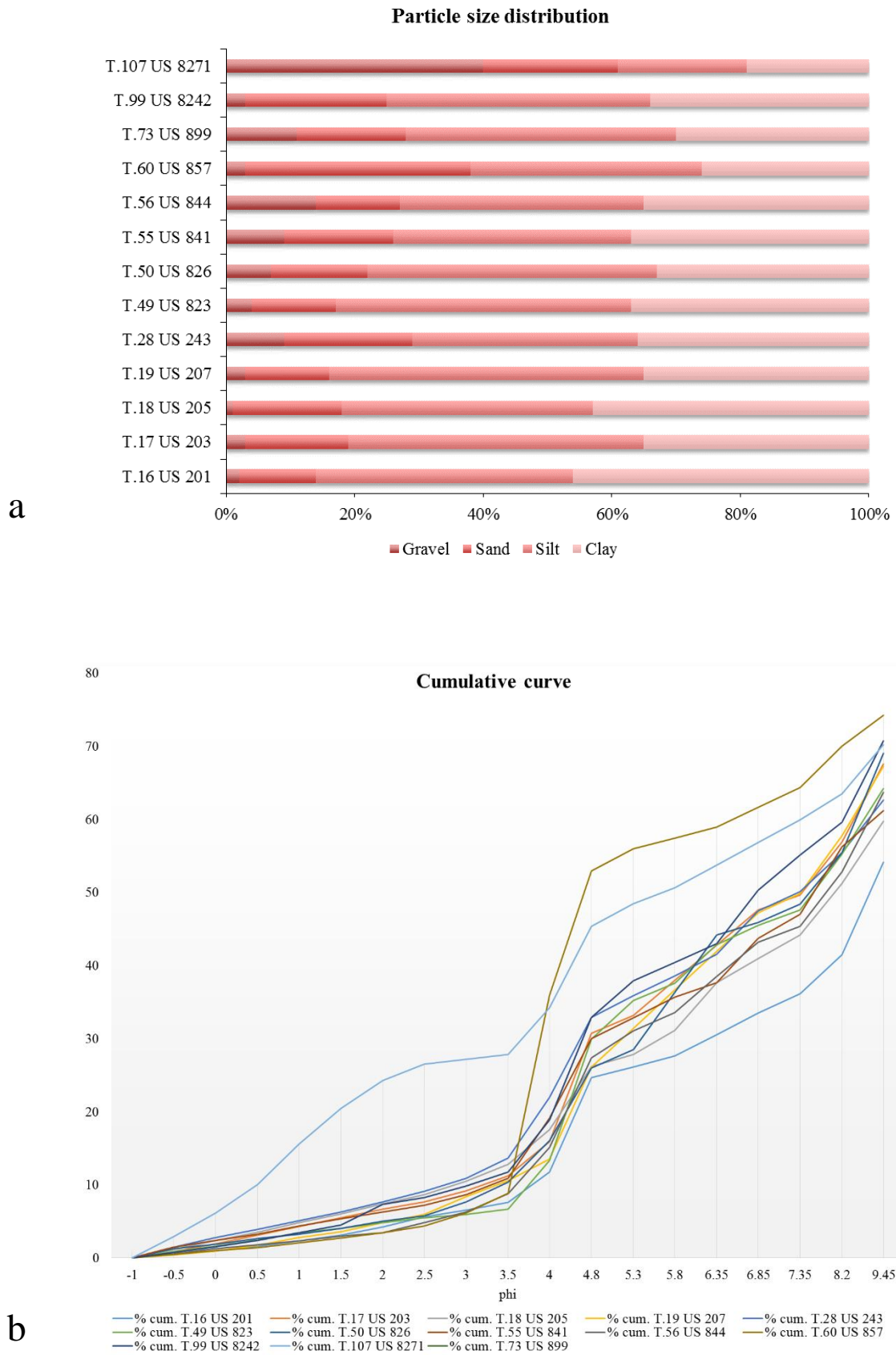
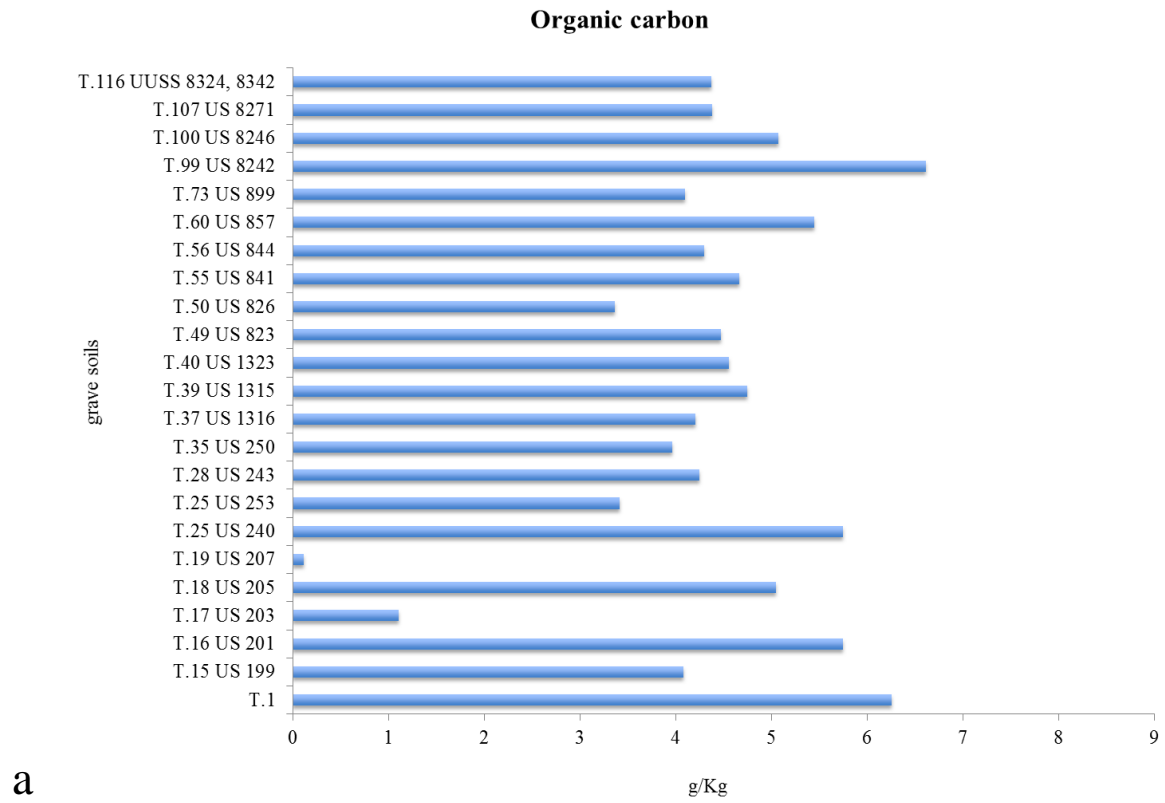
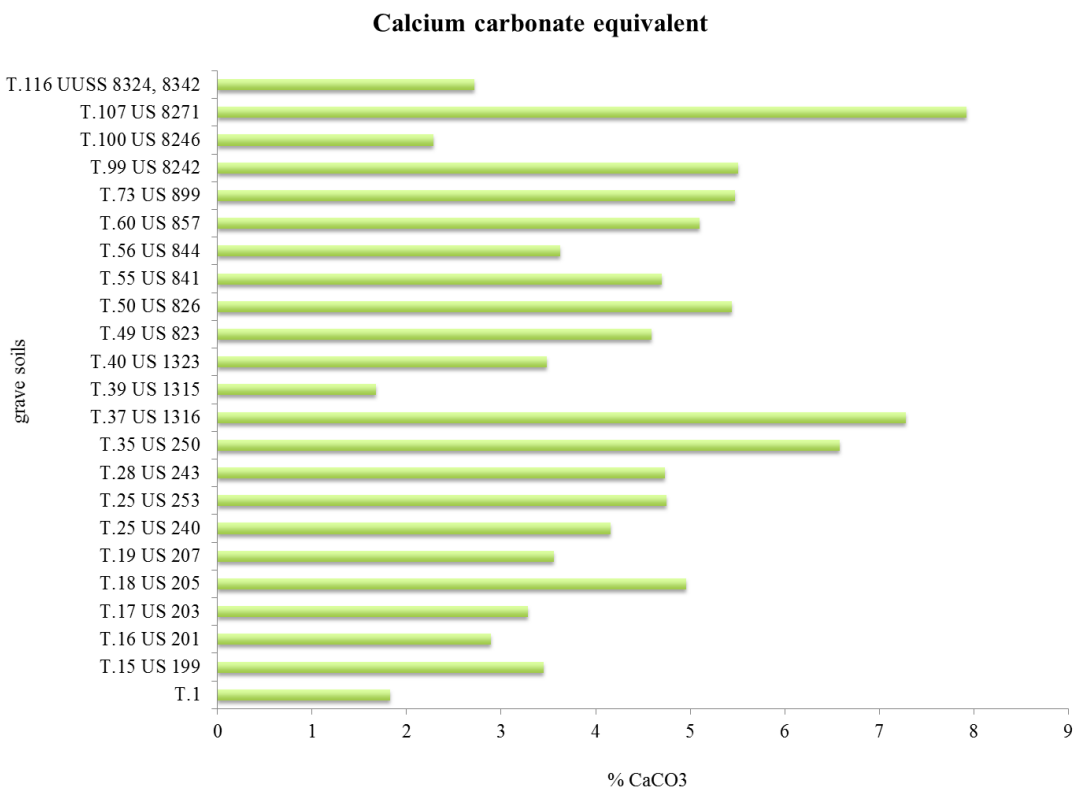


Fig. 3.5 - a) results of particle size distribution: for each tomb are reported the percentage of gravel, sand, silt and clay; b) comparison of cumulative curves of fine size particles (sand and silt).



a



b

Fig. 3.6 - a) results of organic carbon present in each grave soil; b) percentage of calcium carbonate equivalent detected in each grave soil.

## Chapter 4

# Discussions

In this PhD thesis different analytical techniques were applied on 40 long bones (either femora or tibiae) coming from four different known dating burial locations of the Milan area (from Late Roman age to contemporary one), to compare how the mineral and organic components degrade in the tissues over time.

Also, 23 skeletons from different burial typologies of the archaeological site of Travo (dated back from 7<sup>th</sup> to 8<sup>th</sup> century AD) were selected to investigate how the environmental conditions, principally due to soil composition, influenced the bone tissue preservation.

For this purpose, traditional anthropological methods, such as macroscopy, biochemistry and histology, were employed and compared to analytical techniques derived from the Earth Science field. In particular, scanning electron microscope (SEM) coupled with an energy-dispersive X-ray spectrometer (EDS), 3D micro-computed tomography and infrared spectroscopy were applied to understand if bone conservation may be different according to the scale at which one examines it.

To better understand the degradation process of bones, it could be useful the evaluation of the time since death (PMI), the reconstruction of the burial environment or the prediction of biological tests applicability. For these reasons, it is fundamental to verify how, when and in which components the bones degrade. For example, is a well preserved bone surface a predictor of the survival of the histological component? Or does a negative biological test necessarily mean that the collagen in the bone has all gone?

Very few comparative studies exist in literature, so our study has a multiple aim: to investigate the preservation of the organic and inorganic bone components, to test the accuracy and precision of the

conventional methods already employed and to evaluate how the new unconventional techniques can help the research in this field.

In the first section, the results carried out by different analytical techniques performed on 40 dated bones coming from 3 archaeological and one contemporary sites of Milan will be presented. Macroscopic, microscopic, biochemical, 3D micro-computed tomography and infrared analyses were employed and compared to investigate a possible relationship between the bone tissue appearance and the time since death.

Subsequently, the results obtained by bone and grave soil analyses from the archaeological site of Travo (PC) will be discussed, to find a possible correlation between the bone conservation and the environment in which they were buried.

## **4.1 - Bone tissue conservation in archaeological and contemporary human remains from Milan: the role of degradation of organic and mineral phases**

### **4.1.1 - Macroscopic scale**

Our research was performed on 40 human long bones, either femora or tibiae, and for each one a macroscopic evaluation of the diaphysis was done in accordance to the six weathering stage of the Behrensmeyer's classification. Each evaluation was performed with naked eye and through the use of stereomicroscope.

At macroscopic scale, all bones studied have a good state of preservation in 60-70% of cases: the diaphyses are whole, except for few cases where one or both epiphyses are lacking; few bones show bleaching (only from Population 3); cracking and flaking are diffusely present in all populations; skin, muscles, ligaments, fatty substance, tissue in medullary cavity and odour are absent in all specimens. So, these results prove that these parameters examined are not useful to distinguish among bones with archaeological, historical or contemporary chronology. Behrensmeyer's classification has not also intermediate stages, and between them there are large morphological modifications, as consequence in this study most of the bones examined do not fit completely with the proposed weathering stages, but are attributable to ideal intermediate stages. Furthermore, Behrensmeyer doesn't propose a classification in which a bone can be dry and without any *post mortem* modification at the same time,



because the method evaluates the degree of bone alteration from death, when the soft tissues are still adherent to the bones.

Regards the colour, bones coming from Population 1 and 2 appear light, with pale brown and yellow colours, instead bones coming from Population 3 and 4 are dark, with black and very strong brown colours. In few cases grey, white, red and orange colours were detected on bones. Fresh bone has a yellowish-white or yellowish-brown color due to the retention of lipids and other fluids, but after death many taphonomic and environmental conditions can cause a myriad of color changes, in particular due to soil composition where the human remains were laid. Soils rich in sodium salts, carbonates, silt or quartz grains can produce a light coloration; whereas soils with high levels of organic matter (humus), as well as magnetite ( $\text{Fe}_3\text{O}_4$ ), cause a dark black or brown coloration; well-drained soils and oxidizing conditions (iron-bearing) can also produce a bright red coloration of bones (HAGLUND & SORG, 1997). In our research it seems that bones buried directly in ground, coming from a necropolis (Population 1) and a mass grave (Population 2), have the same light yellow color maybe due to dry soil condition, rich in quartz, detected on these bones by SEM-EDS, and fine-particles. Whereas, most of the bones buried in crypt (Population 3) and coffin (Population 4) appear dark; in this case, maybe burial condition could have preserved the human remains from weathering agents, delaying the decomposition process and/or producing a stagnation of body's putrefactive fluids. Also, a soil rich in organic substance could have caused a dark coloration. In both cases the soil quantity with the bones came in contact, is less than which one of the bones buried directly in ground. For Population 3 the soil was only used to prevent the gases diffusion from crypt towards the church, instead for Population 4 the soil could be penetrated into the coffins from the grave site.

Furthermore, some bones appear white (as slightly bleached); in our cases a white coloration could be due to adipocere remnants, detected sometimes near to articulated skeletons in the crypts and on the bottom of the coffins, and not to fire or sun as reported in literature (HAGLUND & SORG, 1997; POKINES & SYMES, 2014), because these phenomena are not documented for the sites examined.

Since macroscopic appearance cannot be considered discriminating among bones with different chronologies and sites, more invasive analyses are required.

### 4.1.2 - Biochemical scale

Luminol test is widely employed in medico-legal field to determine the *post mortem interval* (PMI), i.e. the time elapsed between the death and the discovery of the corpse or skeletal remains.

In this research 50mg of 40 human long bones were pulverized and reacted with Luminol solution, hydrogen peroxide and sodium hydroxide. The intensity of chemiluminescence developed was classified according to CAPPELLA *et alii* (2015).

Our results show that Luminol test was negative in 70% of ancient samples (populations 1-3), and in 20% of contemporary ones (Population 4), according to the literature. Many studies performed this tool in forensic practice, in particular Introna, who saw that the CL's intensity increased with decreasing PMI. Bones with a PMI ranging between 10 and 15 years showed a clear positive CL reaction in 80% of cases, whereas samples with a higher PMI (from 25 to 35 years) showed a weak positive CL in 33% of cases; on bones with a PMI over 80 years the CL was totally missing. So, in the study of Introna, it appears that false negatives detected were 37% (INTRONA *et alii*, 1999), on the contrary, Ramsthaler highlighted the presence of CL reaction in samples with a PMI over 80 years, with a percentage of false positives equal of 7.5%, thus reported less false negatives around 15% (RAMSTHALER *et alii*, 2009, RAMSTHALER *et alii*, 2011).

So, the test functionality could be challenged since both in the ancient population both in the more recent one, was observed a weak positive reaction for some samples, as shown in table below (tab.4.1). Only the recent samples have shown a strong positivity to the test, although some bones were unreacted.

Tab. 4.1 - false positives and negatives detected by Luminol test in each population.

<b>Results</b>	<b>Population 1</b>	<b>Population 2</b>	<b>Population 3</b>	<b>Population 4</b>
False positive	3	1	3	0
False negative	0	0	0	2
True positive	0	0	0	8
True negative	7	9	7	0

The different rates of false positive and false negative results could be related to the type of bone employed for the analysis: in fact, only cortical tissue (i.e. femur) has been examined up to now. Therefore, with the aim of investigating the influence that different bone types may exert on the response to Luminol test, was analyzed three different specimens (femoral diaphysis, vertebra and cranial vault), collected from ten exhumed skeletons (Population 4) with early PMIs (20 years). The overall results showed different responses, depending on the type of bone and on the integrity of the samples. So, Luminol test should be used with caution on bones, because can react differently on different bone districts or on non-intact bones. Also, negative results could be due to taphonomic

alterations, since the exposition to environmental agents might result in Hb loss (CAUDULLO *et alii*, 2016).

### 4.1.3 - Microscopic scale in transmitted and polarized light

In this work, 40 calcified thin sections and 40 decalcified thin sections were prepared from 40 long bone diaphyses, either femora or tibiae, and observed in transmitted and polarized light, to investigate a possible correlation between their histological conservation and the sample ages or burial contexts.

For each calcified thin sections was evaluated the preserved bone and the tissue degradation, due to fungal or bacterial action (MFD), according to the Oxford Histological Index.

Calcified histological microscopy showed in general a high osteonic conservation (fig.5.1b) in contemporary (60%) bones (Population 4), whereas archaeological bones (Population 1-3) showed a high OHI only in 30% of samples. In this case, all osteon structures are recognized: haversian canals, lacunae and lamellae.

The 47% of archaeological samples have a bad preserved tissue: only the haversian canals are detected, fragments of lamellae can be observed but in general the tissue appears eaten by fungal and bacterial action (fig. 5.1a). Out of total, the state of preservation observed in thin sections appears to be time dependent, but if we consider the single bones, some false positives (20%) were detected among the archaeological samples. However, in most ancient population (Population 1), dated back to Late Roman age, false positive were not observed, according to the literature, that estimates a complete histological degradation within 500 years *post mortem* (HEDGE, 2002). Whereas for Population 2, dated back to 17<sup>th</sup> century AD, the percentage of false positives is 10%, increasing to 50% for Population 3, dated back between 15<sup>th</sup> and 18<sup>th</sup> century AD. As consequence, it seems that bone histology was also influenced by burial context, and not only by age. The bones coming from Population 1 and 2 were buried in ground, so the direct contact with soil for more time could have caused a more diffuse deterioration by microbial attack. On the contrary, bones belonging to Population 3 were maybe preserved from microorganisms alteration, thanks to the local condition of the crypt that might have slowed the bone decomposition, because were detected adipocere remnants adherent to some remains.

Some recent bones have few traces of tissue deterioration, as expected by literature, where the bone degradation occurs as soon as 3 months (BELL *et alii*, 1996).

Decalcified bones were stained in Hematoxylin and Eosin to evaluate the organic component preservation.

For this purpose, a new Decalcified Histological Index (DHI) was created to evaluate the survival of collagen via H&E.

A well collagen preservation was observed on 37% of archaeological samples and on 90% of contemporary ones. On the contrary, a badly preservation (DHI 1) was detected on 47% of archaeological samples, instead no contemporary bones show deteriorated tissue. In the first case, all tissue is stained rose/violet and the few gaps observed are the natural holes related to haversian canals or lacunae (fig. 5.1f), in the second case, only osteon fragments are detected and the numerous gaps present are the degraded areas eaten by microbial attack (fig.5.1d).

When evaluating survival of the collagen component of bone via H&E, we noticed a slight amelioration in conservation, which may indicate that if the structure of the calcified matrix is degraded, the respective connective tissue component may be better preserved. In fact, calcified archaeological sections show a high OHI (4-5) in 30% of samples, but in the decalcified sections the percentage rises to 37. In contemporary bones the collagen preservation is the same in both calcified and decalcified samples. The good state of preservation observed in thin sections appears not to be time dependent; particularly, for some authors, collagen degrades in an insoluble product, unaffected by time. The decalcified section maintains their lamellar patterning, so histological analysis of decalcified sections can be applied on archaeological as well as recent bones (STOUT & TEITELBAUM, 1976). However, keep in mind that micromorphological appearances vary considerably not only within the same bone and within the individual bones, but also within skeletons from the same archaeological site (GARLAND, 1989). Since decalcified thin section allows a better reading of the organic matrix, the natural properties of the osteon structure can be easily recognized, particularly in this study, the different orientation of successive lamellae were observed in polarized light microscopy. Polarized light microscopy allows observing the orientation of successive lamellae in the osteon structure. Collagen fibres and mineral crystallites have a spiral arrangement alternatively clockwise and counter-clockwise, with an angle that vary between 0°-90° with the osteon axis. Transverse oriented lamellae, perpendicular to long axis, are better able to resist compressive forces, on the contrary, longitudinal lamellae, parallel to the long axis, are better able to resist tensile forces (ASCENZI *et alii*, 2003). In polarized light collagen fibres and mineral crystallites oriented transversely appear bright, instead collagen fibres and mineral crystallites oriented longitudinally appear dark. As a result, a “Maltese cross” effect appears on the osteon structure, because the analyser and polarizer filter transmission axes lie outside the vibration plane of light passing through lamellae at these positions (BROMAGE *et alii*, 2003). Thus proving that the birefringence signal depends on the degree of collagen fibres organization.

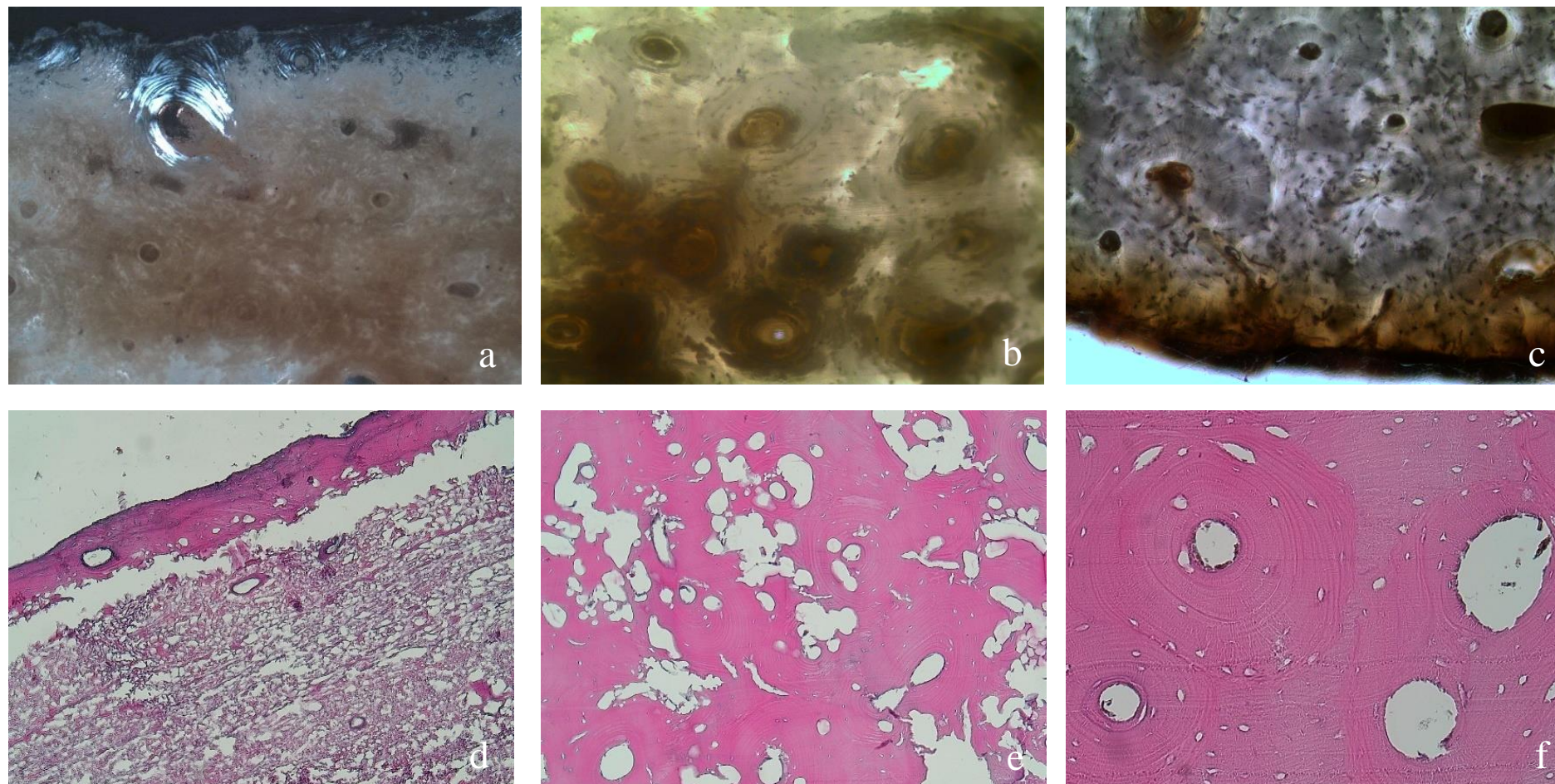


Fig. 4.1 - a) Low OHI score: no original bone tissue is preserved, only the haversian canal are recognized. Bone samples: 14 archaeological and 0 contemporary (polarized light view, 10x); b) Medium OHI score: some osteon structure are identified, however a lot of areas appear destroyed by microbiological action. Bone samples: 7 archaeological and 4 contemporary (transmitted light view, 10x); c) High OHI score: all osteon structure, lacunae and canals are identified. Bone samples: 9 archaeological and 6 contemporary (polarized light view, 10x); d) Low DHI score: low percent of organic component colored rose/violet by H&E. Bone samples: 14 archaeological and 0 contemporary (transmitted light view, 2.5x); e) Medium DHI score: few unstained areas destroyed by tunneling. Bone samples: 5 archaeological and 1 contemporary (transmitted light view, 10x); f) High DHI score: with H&E are well identified the osteon structure and lacunae. Bone samples: 11 archaeological and 9 contemporary (transmitted light view, 20x).

In our research birefringence was observed in all specimens. It is well preserved in all samples coming from Population 4 and in 90% of samples of Population 3, instead in Population 1 and 2 a high birefringence was detected on 1 and 4 specimens respectively. These results are in agreement with those observed by transmitted light microscopy on decalcified sections (DHI).

The causes could be due to decalcification process, which dissolves the hydroxyapatite crystals, but preserves the physical bone characteristics, because dense fibrous connective tissue remain cohesive. Also, the section thickness of calcified sections might have impeded the transmission of polarized light throughout the samples, because the sections were not cut by a microtome, so the resulting thickness is more than 5 $\mu$ m.

These results show that, to evaluate the merely presence of taphonomical insults, due to age and/or burial context, not often visible at macroscopic appearance, the standard preparation of calcified thin sections can provide enough information. However, to investigate the bone structure, decalcified thin sections need to be done, because allow a better reading of the bone tissue. Since on archaeological thin sections as well as on recent ones the osteons maintain their lamellar patterning, decalcified histological analysis can be applied in both these fields.

So, the choosing of a technique and/or processing method must be given according to the type of information being carried out; whether is necessary, for a diagnostic purpose, to differentiate mineralized bone from organic matrix or if morphometric measurements are required, it may be necessary to retain the mineral content by producing calcified sections. On the contrary, for evaluating the degree of diagenetic changes, and/or to identify the orientation of collagen fibers on intact or altered bones it essential to apply a decalcification protocol.

In summary histological evaluation cannot be considered predictive of *post mortem interval*, although they can be useful to discriminate in general recent (PMI<50years) from ancient bones (PMI>500 years). In fact, burial context can also influence the bone conservation.

Since light microscopy is not able to investigate the ultrastructure and chemical compounds of the bone tissue, scanning electron microscopy, couple with energy dispersive spectrometer (SEM-EDS), was employed to obtain high magnification images.

#### **4.1.4 - Quantitative and qualitative analyses by SEM-EDS**

With scanning electron microscopy (SEM), coupled with an energy-dispersive X-ray spectrometer (EDS), the alterations of organic and mineral phases of bone tissue were observed at high resolution.

In particular, with EDS spectrometer, the presence of exogenous oxides included in the bone pores or structures can be detected. By BSE-SEM, less or more electron-density zones, due to demineralization or hyper-mineralization of the tissue, were also distinguished on bone.

In this study was investigated the relationship between the oxide inclusions and the preservation degree at histological scale of 40 human skeletal remains, compared to the time since death (PMI) and the burial environments in which they were recovered. For each bone, two thin sections were prepared, non-embedded and embedded in epoxy resin, to test which one was able to detect the better information regards the oxides included in the tissue, and the bone alterations due to diagenetic process at ultramicroscopic scale.

Regards the typology and quantity of oxides identified, some differences were observed among the sites. In Population 1, the most ancient, were detected more spots of analyses (20) than others: 5 for Population 2, 7 for Population 3 and 3 for Population 4. This phenomenon could be related both to the age of the samples both to the different burial typology, because the most ancient bones (Population 1) were buried in soil and exposed to diagenetic agents for more time than contemporary ones (Population 4) buried in coffins.

However, all archaeological skeletons came from the same soil condition of Milan, even if the typology of burial was different. In Population 1 the bodies were buried in single tombs in ground, instead in Population 2 and 3 were stored together into a mass grave and a crypt respectively.

PCA results are not clustered, using oxides as variables and analyses as samples, so similarity among analyses were not observed.

Similar not clustered results were carried out using the probable origin of oxides (Decomposition, Burial, Saw, Soil), because a high variability within samples of the same population and within different populations exists. On the basis of these results, was not possible to discern which oxides are more characteristic of one population than another, because for each site specific oxides were not detected to discriminate the different environment (ground, crypt, coffin) in which the bones were buried.

The minerals identified do not also discern the samples regards the time since death and the burial context. On all samples were observed the same minerals, excepts in few cases; for example, albite, zircon, and clay minerals were detected only in Population 1 and chlorite in Population 3. So, minerals cannot be employed as indicator of burial context or to quantify the time since death of human bones, because of high variability observed within the samples coming from the same population.

About the morphological results, in general was observed a high histological modification of bone tissue on archaeological sections (Population 1-3), instead recent ones (Population 4) do not show MFD and remineralization, and all osteon structures are well defined.

However, not all the bones coming from the same population have similar degree of histological alteration. Within the same site, a discrete variability of degradation/conservation of bone tissue (fig. 4.1a) was observed, probably the causes are not due to the time since death or burial context, but are related to an intrinsic composition of bones and/or local factors. In general, the more altered zones are concentrated at the external and internal borders, on the contrary preserved osteons are frequently observed on the central cortical bone (fig. 4.2b). Archaeological bones have both Wedl and non-Wedl tunneling, the second one (fig. 4.2c) recognized by a network of pores and/or thin channels with hypermineralized zones (Müller *et alii*, 2011). Areas with change of density can be observed in BSE images; zones of bone tissue with markedly decreased density appear less electron-dense (dark color), frequently with holes in the matrix, instead remineralized zones, where the bone mineral was removed and then redeposited in the same bone matrix, appear high electron-dense (bright color) (fig. 4.2d). In this study, hypermineralized zones are only related to MFD in 100% of samples coming from the most ancient population (Population 1), instead for Population 2 and 3 remineralized zones can be detected also in non-altered tissue by fungal or bacterial actions (fig. 4.2e). All bones are cracked, particularly the more recent ones (Population 4); in this case the fractures are numerous, more extended and widespread from external to internal borders in 90% of samples (fig. 4.2f). Similar results (80%) were found for Population 3, instead for Population 2 and 1 the percentage decreases to 40 and 30% respectively. Probably the bone conservation influenced the cracks development, indeed the well-preserved bones coming from Population 4 have more cracks not related to bone histology, produced during the sample preparation, and not by diagenesis. Recent bones were probably more resistant to environmental forces than ancient ones, which were subjected to a demineralization and delamination of collagen fibers due to several taphonomic factors that acted for long time. In these cases, except for Population 3, that shows similar results to Population 4, cracks not related to bone histology were detected with a low percentage than cracks influenced by bone structure (JANS *et alii*, 2002, MÜLLER *et alii*, 2011). The bones coming from Population 3 have, in fact, a medium-high degree of preservation, probably due to the burial context, because most of the skeletons recovered in the crypt had adipocere formation adherent to the bones. Adipocere is a substance formed from the fatty tissues by bacterial action in warm, wet, and usually anaerobic environments (TURNER-WALKER, 2012). The low temperature and the high moisture of the crypt could have preserved the skeleton from the *post mortem* degradation.



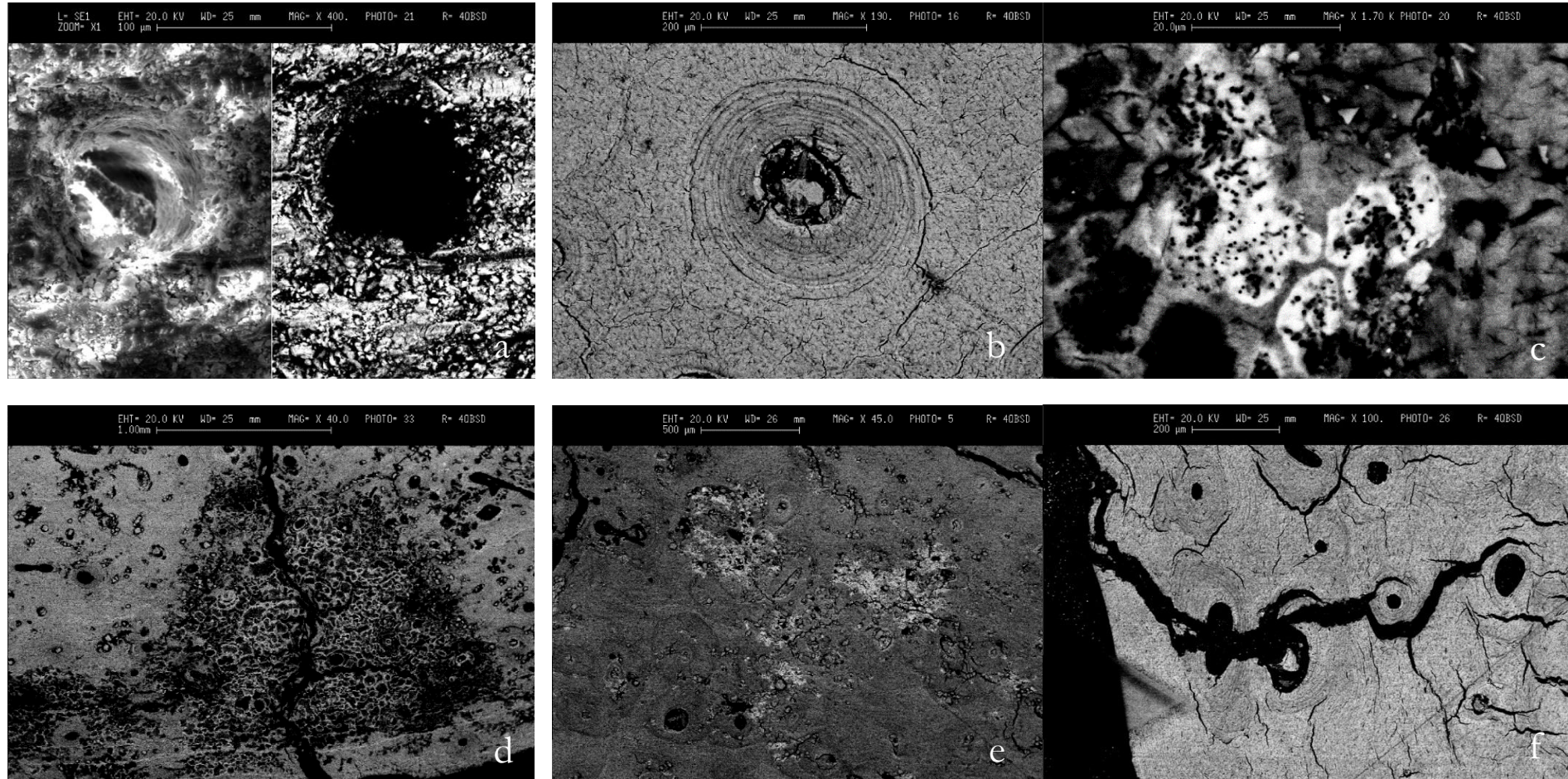


Fig. 4.2- a) example of degraded osteon; no original bone structure are identified because of tunneling; b) example of well preserved osteon in BSE view; c) detail of non-Wedl tunneling by bacterial action observed in BSE image of bone tissue section; d) hypermineralized zones (bright grey color) on bone tissue in BSE images related to the MFD borders; e) hypermineralized zones (bright grey color) on bone tissue in BSE images detected inside the non-altered tissue; f) examples of big cracks not influenced by bone structure in BSE view, probably due to sample preparation.

### 4.1.5 - 3D $\mu$ CT (bone porosity)

In this research, 3D micro-computed tomography was employed to study the human cortical bone porosity, because it contributes to the overall mechanical properties of bones. So understanding how bone porosity changes (or not) from modern bones throughout the taphonomic history of ancient bones is an important factor in understanding and describing diagenetic trajectories (HEDGE, 2002). However, natural intracortical vascular porosity associated with bone blood vessels changes during life, because the network of porous canals depends on the continuous bone remodeling, influenced by individual growth, drugs assumption, sex hormones, pathologies etc. Therefore, the bone conditions at death can predict as a bone interacts with the burial environment and how will survive in the fossil record. When studying modern or ancient human skeletons, the preservation degree of bones can affect what information is available from the tissue.

Out of 24 long bones examined, total bone porosity (BV) has similar values for Population 2 and 4, with a mean on total volume of 15.3% and 16.8% respectively, decreasing for Population 1, 12%, and 3, 10.1%. In a fresh bone the porosity fraction ranging from 2-28% (BOUSSON *et alii*, 2001), and is principally due to natural canals porosity, for ca. 0.8%, and lacunae porosity, for ca. 1.5% (DONG & GUO, 2004), instead, for *post mortem* bones, diagenetic phenomena can alter the tissue, producing fractures, collagen delamination and minerals lacking, thus increasing the porosity.

Population 2 has 5.8% of canals porosity and 0.3% of lacunae porosity, instead Population 4 has 15% of canals porosity and 0.9% of lacunae porosity. For Population 3 the canals porosity is 3.2% and the lacunae porosity is 0.8%, instead for Population 1 canals porosity is 3.6% (fig. 4.3). So, the percentage of bone porosity related to degraded tissue decreases from Population 2, 9.2%, Population 1, 8.4%, and Population 3, 6.1%, to Population 4, 0.9%. If we compare the sample ages, the most recent bones (Population 4) have the lowest degree of degraded tissue, than archaeological ones (population 1-3). Within these samples the percentage of degraded tissue increases from Population 3 to 2 and 1, despite Population 2 and 3, have the same age, dated back between 15<sup>th</sup>-18<sup>th</sup> century AD. By these results seems that, not only the age had a role on bone porosity but also local burial environment could have influenced the bone tissue preservation.

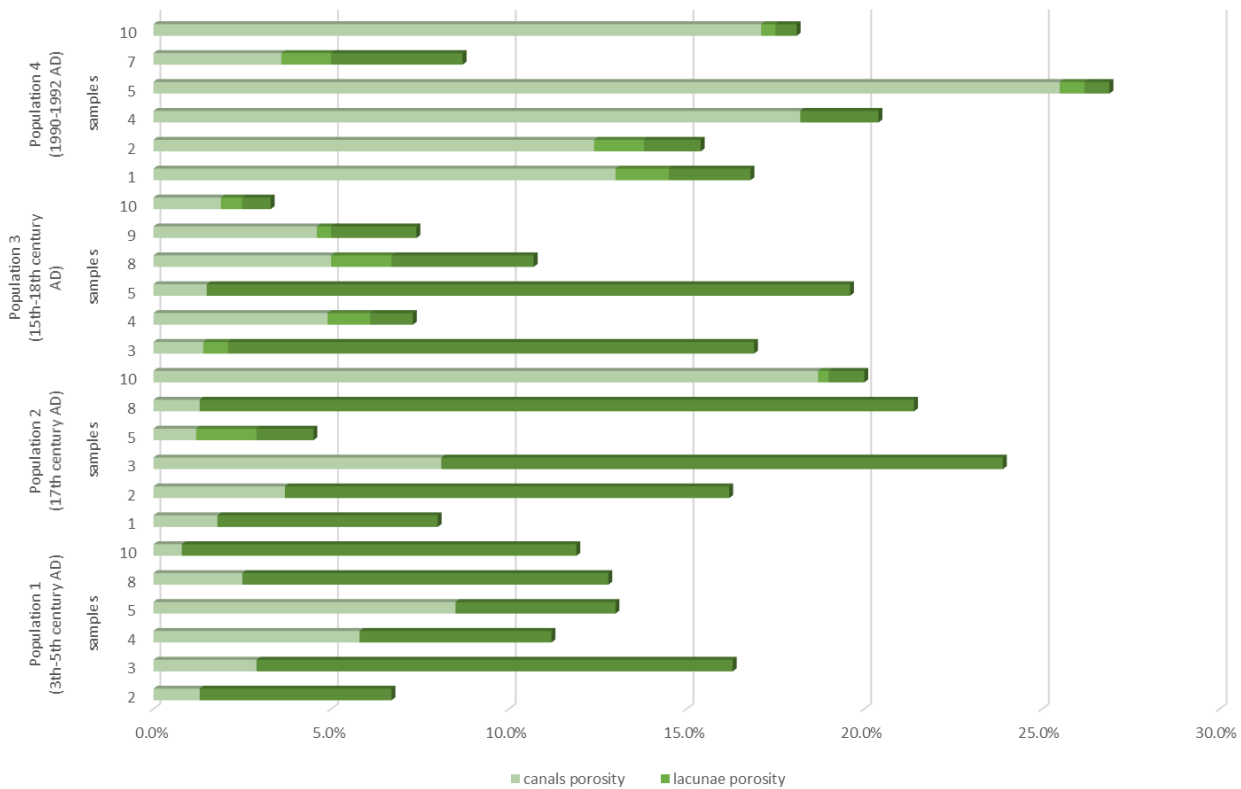


Fig. 4.3 - percentage of total bone porosity for every sample; with different tonalities are highlighted the percentages of canals and lacunae porosities out of the total detected per bone.

Remineralized areas, as more bright tissue zones, were detected in all samples of Population 1, 2 and 3, and in one specimen of Population 4. The percentage of remineralized tissue on total volume decreases from Population 1 to 3, ranging from 8.3 to 0.6. This phenomenon could be related to the sample age, because the most ancient bones, dated back to 3<sup>th</sup>-5<sup>th</sup> century AD (coming from Population 1), have a more high degree of remineralization than the samples of 15<sup>th</sup>-18<sup>th</sup> century AD (Population 2 and 3). Only one sample of contemporary age (Population 4) shows remineralization, equal of 3.6%, instead the other bones have not diagenetic alterations.

Regards natural bone porosity, recent samples (Population 4) have the higher average canals volume, with a value of  $15.6\mu\text{m}^3$ , than archaeological ones (Populations 1-3). If compared canals of archaeological bones among them, the most ancient samples have a high average volume of  $6.7\mu\text{m}^3$ , which are followed by samples of Population 3,  $3.8\mu\text{m}^3$ , and 2,  $2\mu\text{m}^3$ . The ratio of canals surface/canals volume has the same average value for Population 1, 2, 3, between 133-134, instead for Population 4 is less, 103, meaning that recent bones have a more regular canals surface than ancient ones.

Volume size could have been influenced by canals length and width. In fact, as observed in fig. 4.4, the bones with a big volume have also a big canals size, calculated by the ratio of 3Dwidth/3Dlength, whereas bones with a low volume show less length and width sizes. In this cases bone diagenesis could have degraded the tissue, fragmenting the canals length and reducing their widths. So, age could have played a fundamental role on bone taphonomy, because the archaeological bones have a low canals volume and size ratio than contemporary ones, since the tissue was exposed to environmental degraded agents for more time. However, the high variability among archaeological samples could mean that local environmental burial conditions might have been responsible to different canals preservation observed into the bones examined. As further evidence of canals fragmentation in archaeological bones, is the increase of Euler number, from Population 4 (0.19) to 1 (0.96), due to a reduction of canals connectivity over time (FELDKAMP *et alii*, 1989).

If compared the average canals size to its shape, all bones show similar oval flat canals, with an average value of aspect ratio between 1.0-1.9 (the aspect ratio is equal to 1 for a sphere).

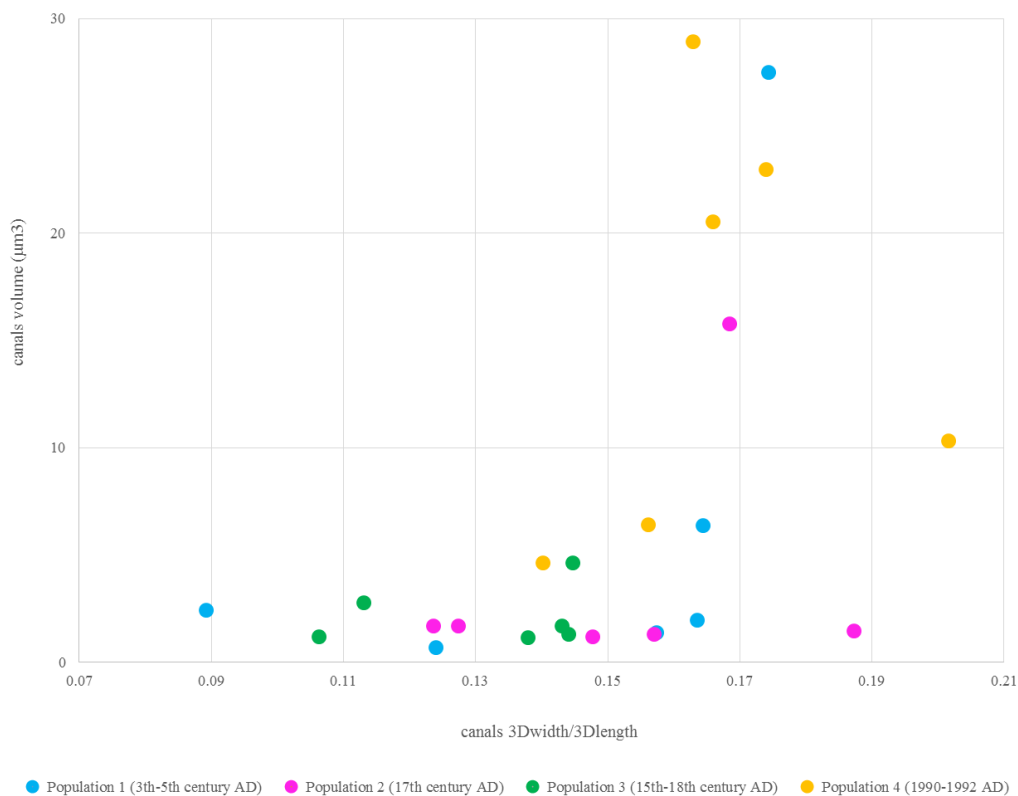


Fig. 4.4 – plot of canals volume and 3dwidth/3d length detected in the 24 bones examined.

Lacunae volume has the same average value of  $7.6e^{-04}\mu\text{m}^3$  for the samples coming from Population 2 and 4, which decreases to  $5e^{-04}\mu\text{m}^3$  for Population 3. Lacunae surface is the same for Population 2 and 4, equal of  $0.6\mu\text{m}^2$ , instead for Population 3 decreases,  $0.4\mu\text{m}^2$ .

Lacunae length and width have similar average values, ranging between 1.3-3.4 $\mu\text{m}$  and 0.1-0.3 $\mu\text{m}$  respectively, and an aspect ratio that ranges between 7.1-8.6 in all samples. The high surface/volume ratio observed for bone lacunae from Population 3 (equal of 1022) could be due to a more irregular shape, if compared to which one detected in the samples coming from Population 2 and 4 (973 and 949 respectively). Generally, a high aspect ratio means that lacunae morphology is vertically elongated.

Unfortunately, bone lacunae were counted and measured by imaging programs only on 2 specimens from Population 2, 3 specimens from Population 3 and 5 specimens from Population 4. From Population 1 we were not able to detect any traces of lacunae. The causes could be due to the tissue alteration, maybe promoted by age, burial environment, water and microbiological actions, which destroyed and/or covered the natural bone structures.

However, it needs to keep in mind that scan quality is potentially impacted by numerous factors including resolution, magnification, noise, artifact, and post-acquisition processing. In particular, automated measurement of porosity requires an imaging elaboration user-dependent, so the selection of cortical bone porosity might have been underestimated because some bone pixels were misclassified as the background. So our results could be influenced by thresholding (CHAPPARD *et alii*, 2006).

In the current study, no increase of bone anisotropy was observed in the samples with a high percentage of porosity, because, although the Population 4 has the higher average value of porosity, its value is the same in all sites. Generally, anisotropy reflects the mechanical properties of cortical bone, so an increase of bone porosity could result in an increase of anisotropy.

#### **4.1.6 – Qualitative and semi-quantitative analyses of organic and mineral matter by FT-IR spectroscopy**

The mineral phase of bone and teeth is carbonate-hydroxyapatite (CHA)  $[\text{Ca}(\text{PO}_4\text{CO}_3)_3\text{OH}]$ . In addition, bone tissue is composed by water and organic matrix, principally made by fibrous protein collagen (Amide I). CHA, collagen and water are intimately associated into a common building block, the mineralized collagen fibril, organized into high-ordered structure.

In living people sex, age, illness and drugs are the principal factors that influence the mechanical tissue properties, mostly strength and resistance (ARTIOLI, 2010).

After death, bone tissue is often unstable and subjected to diagenetic changes, depending on the environmental conditions where the human remains were laid, as well as loss of organic material,

increase in crystallinity, alteration of porosity and in trace element composition (TRUEMAN *et alii*, 2004).

Degradation of collagen fibres is intimately associated to alteration of mineral components, about structural and chemical compositions. Mineral recrystallization can be promoted by heating and fossilization processes, causing crystal growth and a more ordered lattice structure. Dissolution removes minerals, which may then reprecipitate. This phenomenon requires flowing water, tempered climate, presence of organic compound and a neutral-alkaline environment. The chemical conditions under which bone carbonated-hydroxyapatite can recrystallize into authigenic apatite, the so-called recrystallization window, are restricted and lie in a narrow alkaline pH range, and generally bones are likely to be best preserved only in sediments in which the pH of the pore solution is above 8.1. The recrystallization process together with the precipitation of additional apatite will result in a general increase in crystallinity of the bone mineral phase. Below pH 7.5, the original bone mineral will rapidly dissolve and will be totally replaced by authigenic apatite (BERNA *et alii*, 2004).

The more frequent substitutions of carbonate-hydroxyapatite are from monovalent anions like fluorine, which promote the formation of francolite  $[\text{Ca}(\text{PO}_4, \text{CO}_3)_3\text{F}]$ , by replacing OH group. Other important elements such as Mg, Si, Ba, Na, Cl, U, Sr, and REE (Rare Earth Elements) can be absorbed from the environment, altering the original crystal structure and chemical composition (ARTIOLI, 2010).

Archaeological bones are frequently altered over time; CHA crystals are thermodynamically unstable due to their plate shape and small dimension, so *post mortem* they tend to undergo recrystallization to achieve thermodynamic equilibrium as rod shaped larger size (BERNA *et alii*, 2004).

Numerous analytical technique can be employed to characterize the state of bone preservation.

In this section will discuss the results obtained by infrared analysis performed on 40 bone powders and 12 thin sections of archaeological and contemporary skeletons recovered from 4 different burial contexts in Milan (Italy).

For infrared analysis was employed a transmission IR spectrometer on bone powders and a Fourier transform infrared imaging microscope on thin sections at the Simon Fraser University (Burnaby), in Canada. Each bone was taken from mid-shaft diaphysis of femora and tibia of human remains dated back from Late Roman age to contemporary one.

Infrared spectroscopy is the most useful technique widely employed to characterize bone preservation, because it requires a low amount of material (ca. 1mg), is fast and not too expensive, and is able to carried out qualitative and semi-quantitative information about water, mineral and

organic phases of bone. Substitution of carbonate, fluorine, hydroxyl and hydrogen phosphate can be also recognized and measured by specific IR absorbance band.

The crystallinity index, named IRSF or infrared splitting factor (WEINER & BAR-YOSEF, 1990), of carbonate-hydroxyapatite was also calculated, which represents the atomic order/disorder of mineral and organic matter. So, it is related to mineral crystal size and shape, and to the preservation degree of inorganic component. The higher is the diagenetic transformation of the bone mineral, the higher the crystallinity of the bone mineral, the higher is the IRSF, pristine bone has IRSF values of 2.5-2.6. IRSF was determined summing the peak intensities of  $\nu_4\text{PO}_4$  at  $\sim 604$  and  $\sim 565\text{cm}^{-1}$  and dividing by the intensity of the valley at ca.  $590\text{cm}^{-1}$  between them (WEINER & BAR-YOSEF, 1990).

According to TRUEMAN *et alii*, 2004 in this work the presence of endogenous  $\text{CO}_3$  was detected at  $\sim 873\text{ cm}^{-1}$  intensity peak, whereas authigenic calcite has the carbonate absorbance at  $\sim 712\text{cm}^{-1}$ . Phosphate content was measured at the intensity band  $\sim 1035\text{cm}^{-1}$  ( $\nu_3\text{PO}_4$ ), instead Amide I was observed at  $\sim 1653\text{cm}^{-1}$ .

The results obtained by calculation of  $\nu_1\text{AmI}/\nu_3\text{PO}_4$  ratio show a decrease of the Amide I content from Population 4, the recent, to Population 1, the most ancient, which average values range from 0.73 to 0.29. So, the percentage of collagen weight, calculated by the equation of TRUEMAN *et alii*, 2004, ranging from 28.65 to 18.37. According to TRUEMAN *et alii* (2004) the intensities of  $\nu_1\text{AmI}/\nu_3\text{PO}_4$  ratio ranges from 0.8 in a fresh bone to 0.2 in an ancient one, with an equivalent percentage of organic material of  $\sim 30\text{wt}$  and  $\sim 15\text{wt}$  respectively. Since fresh bone has ca.30% of organic matter, Population 3 and 4, with a percentage of 23.59 and 28.65 respectively, were subjected to a minimal collagen degradation ( $\sim 3.5\%$ ), whereas the bones coming from Population 1 and 2, with a percentage of 18.37 and 20.61, undergo a serious collagen delamination during time ( $\sim 10\%$ ).

However, needs to keep in mind that the bones employed come from four different burial environments, so the collagen conservation could be also linked to diagenetic factors related to the four local contexts. The most ancient bones were buried in ground, and come from individuals laid in single tombs. The bones dated to 17<sup>th</sup> century AD come from a mass grave, where the plague victims were buried together in ground and maybe covered with lime. The bones dated between 15<sup>th</sup>-18<sup>th</sup> century AD belong to an ossuary, discovered under a church, where the skeletons partially or completely decomposed were stored, maybe taken from the near hospital's cemetery. Also in this case, the human remains were mixed with soil and maybe covered with lime. The recent bones belong to individuals buried in wood coffin.

Regards the IRSF, the higher average value of crystallization was detected for the samples from Population 1, 2.89, which is followed by Population 3, 2.85, and Population 2, 2.83. The samples of

Population 4 have the lesser average value of IRSF, 2.72. Because Population 2 and 3 have similar values and similar chronologies, it may be hypothesized that the infrared splitting factor detected among the 4 sites could be related to age, because between the most ancient samples and the most recent ones the difference of average value is high. Furthermore, as collagen conservation, local taphonomic conditions could have also influenced the crystallinity degree. Among the bones buried directly in ground that belong to Site 1 and 2, a necropolis and a mass grave respectively, were detected the higher values of IRSF in which samples where were observed traces of exogenous minerals. In fact, the samples 4 and 8 from Population 1 with an IRSF of 3.6 and 3.0 and the sample 9 of Population 2 with an ISRF of 3.0 are the only bones with traces of quartz into the tissue. As reported in literature, the IRSF could be also associated to the presence of exogenous minerals in the bone tissue (NIELSEN-MARSH & HEDGES, 2000).

Since Population 2 and 3 have similar average values of IRSF, we can hypothesize that both were subjected to similar taphonomic conditions, deriving from a burial context where the human remains were mixed together to each other and with soil and lime. However, due to the lack of exogenous minerals in the samples coming from the Site 3, the soil environment was maybe different.

A high IRSF value could be also associated with a neutral-alkaline environment. Unfortunately, no grave soils were available for this work. However, we may suppose that Site 1 and 3 could have had a more alkaline burial condition than the other sites; for Site 3 residues of adipocere were also recovered on bones, which formation is generally promoted in the presence of a  $\text{pH} > 7$ .

According to TRUEMAN *et alii* (2004) a splitting factor of ca. 2.8 or less is typical of fresh bones, and it may increase *post mortem* to 4.5–5.0. A value more than 7.0 is typical of bone heated to a calcined state (STINER *et alii*, 2001). However how this happens is not well understood.

At the infrared splitting factor is related the mean crystal length of the bone mineral, which was calculated using the formula proposed by TRUEMAN *et alii*, 2008. As IRSF, the greater average length was detected among the samples from Population 1, 43.12nm; a similar average value was observed for the samples coming from Population 3, 42.15nm, which is followed by Population 2 and 4 with an average length of 41.86 and 36.51nm respectively.

Bone's carbonated-hydroxyapatite crystals *in vivo* are plate-shaped and extremely small, with average dimensions of ca.  $40 \times 25 \times 2-4$ nm and a very large specific surface area of about  $240 \text{m}^2/\text{g}$  (BERNA *et alii*, 2004). As reported in literature a higher spitting factor value correspond to a larger and/or more ordered crystals in bone. An increase in mean crystal length may be also due to a growth of crystals, linked to a recrystallization process, or to the loss of smaller crystals from the tissue (or both). For some researchers the *post mortem* alterations of bone crystal size are closely related to decomposition of the collagen matrix, in fact, as the organic matrix is broken down, bone crystallites



increase in size. So, in this research the archaeological samples with a mean crystal length  $>40\text{nm}$  were slightly altered diagenetically, in fact in fossil bones the mean crystal length can rise to  $50\text{nm}$  (BERNA *et alii*, 2004).

$v_2\text{CO}_3/v_3\text{PO}_4$  ratio shows a progressive decrease of the amount of endogenous  $\text{CO}_3$  from Population 4 (contemporary) to Population 1 (dated back to Late Roman age), with an average value that ranges from 0.52 to 0.36. Standard deviation is almost the same for the samples that belong to the first and second population, 0.07 and 0.06, and for the samples of the third and the fourth one, 0.11 and 0.12. By these results seems that endogenous carbonate content was maybe lost over time, because it decreases from the contemporary samples to the ancient ones. The carbonate loss could be due to a spontaneous transformation of carbonate-hydroxyapatite in hydroxyapatite, a more thermodynamically stable form (NIELSEN-MARSH & HEDGES, 2000).

So, ancient bones underwent diagenetic processes for more time, which had an effect on carbonate preservation into the mineral tissue. However, the time since death was not the only taphonomic factor responsible for the *post mortem* carbonate conservation, because burial conditions could have had a role on carbonate conservation. Population 2 and 3, that show similar average values of  $\text{CO}_3/\text{PO}_4$  ratio (0.39 and 0.40 respectively), have not only the same chronology but maybe were also subjected to the same burial condition. The bones coming from Population 2 are dated back to 17<sup>th</sup> century AD, instead which ones coming from Population 3 are dated back between 15<sup>th</sup> and 18<sup>th</sup> century AD and belong to a mass grave and an ossuary respectively. As assumed by archaeologists, to prevent eventually bad smell, gas diffusion, infection and other unpleasant consequences produced by putrefaction processes, both burials were maybe covered by lime. In this work, no authigenic calcite was observed in all samples, since no peaks were detected at  $\sim 712\text{cm}^{-1}$  wavenumber. As observed in literature, archaeological bones tend to have exogenous  $\text{CO}_3$ , usually deposited as  $\text{CaCO}_3$  within cracks and pore spaces of the bone, so bones containing calcite often have much higher C/P values, but is not our case.

If correlated the amount of Amide I and the IRSF values among the samples of the four populations, an inverse correlation, as expected, can be observed between them; if crystallinity increases the Amide I IR relative intensity decreases, this correlation is particularly strong among the recent samples ( $R^2=0.77$ ). The same trend can be also seen for the samples of Population 3 ( $R^2=0.76$ ), instead the bones from Population 1 and 2 show a less correlation between the two parameters ( $R^2=0.45$ ,  $R^2=0.57$ ) (fig. 4.4).

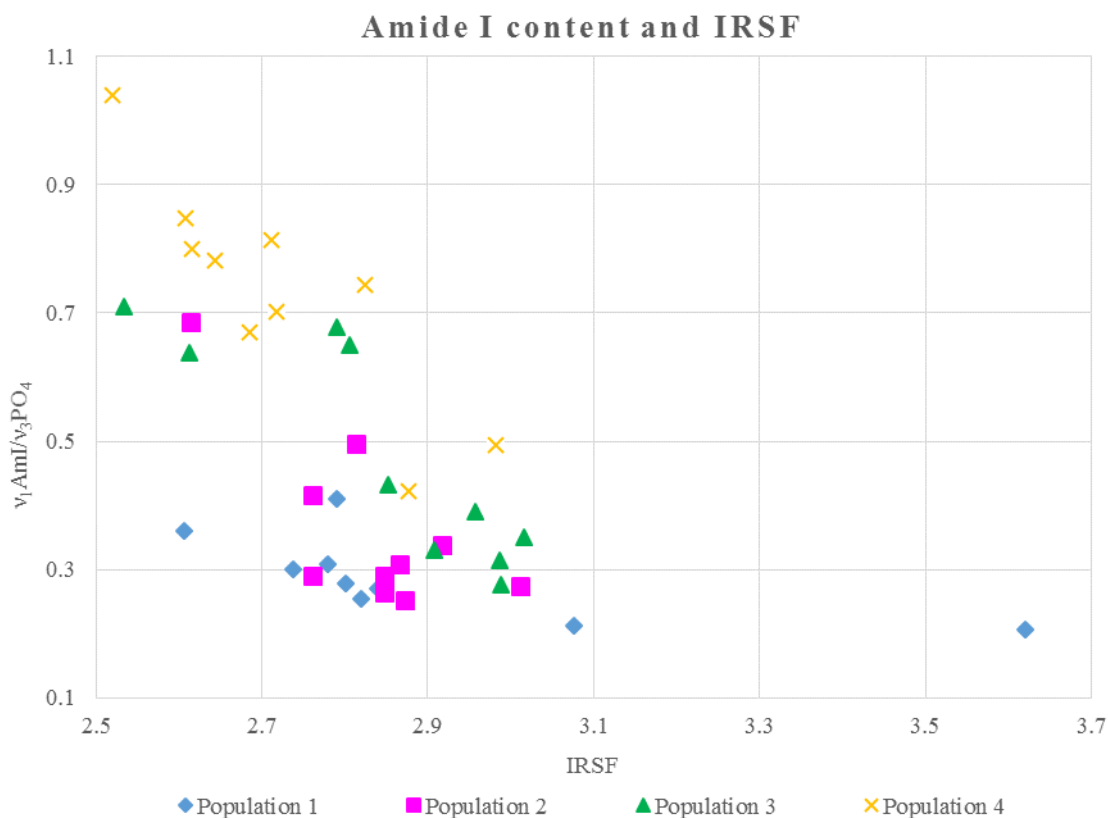


Fig. 4.4 – Relationship between crystallinity index (IRSF) and Amide I content detected by the samples of the four populations; the standard error for each value is ca.2%.

According to WEINER & WAGNER (1998) carbonate-hydroxyapatite morphology is plate-shaped with and hexagonal crystal symmetry, totally controlled by the biological environment of growth. This thin shape confers to the CHA crystals a high specific surface area-volume ratio that makes these ones thermodynamically unstable. Carbonate-hydroxyapatite crystals are regularly distributed at intervals of 600-700Å along the length of collagen fibrils, filling the gaps between molecules. Once collagen is removed, during bone diagenesis, the CHA crystals can become closer and fuse together, increasing their length and width. Furthermore, a dissolution of the thinner crystals can promote a reprecipitation of the CHA toward a more stable form (ARTIOLI, 2010).

On the contrary, the amount of carbonate into the bone tissue appears more correlated to IRSF in all samples. There is an inverse relationship between the CO<sub>3</sub> content and the crystallinity index, because at high levels of carbonate correspond less values of IRSF as shown in figure 4.5.

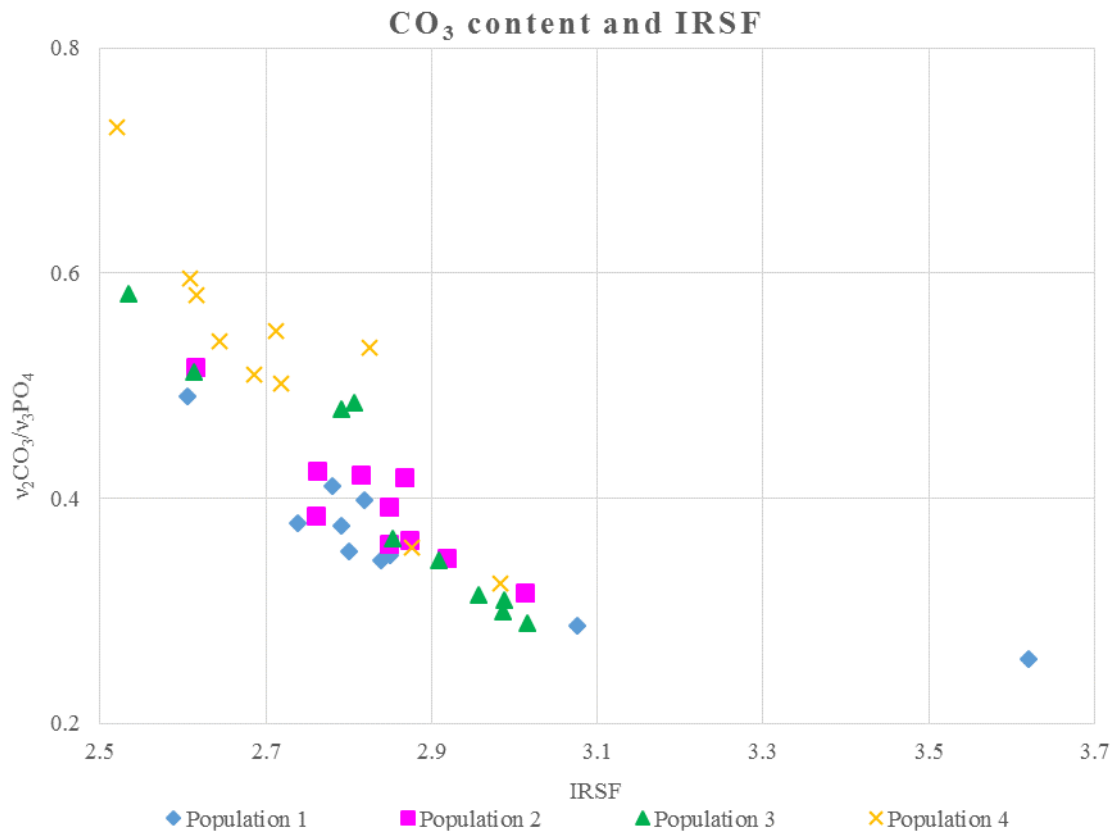


Fig. 4.5 - Relationship between crystallinity index (IRSF) and CO<sub>3</sub> content measured from the samples of the four populations; the standard error for each value is ca.2%.

Except for Population 2, where  $R^2$  is 0.57, the other three populations have a  $R^2$  between 0.70-0.85. As observed in literature, if IRSF increases the carbonate content decreases (STINER *et alii*, 2001). Hydroxyapatite crystals with high levels of carbonate are thermodynamically unstable, and tend to be dissolved during bone diagenesis, than ones without carbonate in the apatite structure. After death bone minerals spontaneously evolve to a more stable crystal lattices (like hydroxyapatite) over time. So, crystallinity index appears to negatively correlate more strongly to carbonate content, than Amide I.

FTIR mapping has been particularly useful to understand the distribution of preserved collagen and thus infer on mechanism of collagen degradation. In fact, Amide I absorption distribution analysis, mapped using mFTIR, shows that collagen seems to start degrading from internal and external cortical surfaces. In some samples of the oldest population it appears that degradation penetrated diffusely also in the internal areas.

## **4.2 - How human remains and grave soil interact? The case study of archaeological site of S. Andrea, Travo (PC)**

Since bone conservation can be influenced in different way by soil composition, in this research was compared the skeletal preservation of some individuals recovered from the necropolis of Travo (PC), dated back from 7<sup>th</sup> to 8<sup>th</sup> century AD, to soil composition.

Macroscopic bone conservation shows that, out of 14 tombs dug in ground analyzed, all skeletal districts are recovered (cranium, upper and lower limbs, vertebrae, ribs-sternum, pelvis, hand and feet), excepts for the tomb 99 and 73, lacking of cranium and right hand respectively.

Regards the quantity, the 36% of skeletons are excellent preserved; good, partial and scarce quantity are present in 28%, 19% and 17% of cases. The most preserved districts are upper and lower limbs, feet and pelvis, recovered in 12 and 11 tombs on 14. The most poorly preserved district is the column, recovered only in 5 skeletons on 14.

Regards the solidity, the 49% of skeletons are fragile, the 41% are preserved, instead the percentage of deteriorated ones is low, 11%. The most preserved bone districts are feet and hands, recovered in 12 and 10 tombs respectively, whereas cranium, ribs and sternum have a high degree of deterioration. The 43% of skeletons are fragmented, and the 37% are whole; highly fragmented bones were observed only in 19% of tombs. The most whole districts are hands and feet, recovered in 11 and 10 tombs on 14 respectively, instead cranium, ribs, sternum and pelvis have never been found whole.

Despite many bones were recovered in fragmented state, after restoration the biological profile was performed on every skeleton, about sex, age, racial, stature and pathologies.

Thanks to the well preservation of lower long bones, histological and chemical analyses were also performed.

Microscopic evaluation shows that out of 14 thin bone sections prepared, 7 have a low histological degree (OHI 0-1), 5 have a medium conservation (OHI 2-3) and only 2 have a high preservation (OHI 4-5).

No differences were observed about the tomb type: the three individuals laid in tombs with a stone structure and a stone roof (T.37, 40 and 116) have the same medium conservation of those recovered in earthy pits (T.55 and 60). From earthy pits coming also the only two individuals with a

high histological degree (T.17, 56), instead the bones recovered into the other 8 tombs are badly preserved (T.16, 18, 19, 28, 39, 50, 100).

Since no differences were observed at skeletal record within different tomb types, grave soil analyses were performed for every tomb to investigate a possible correlation among them for color, particle size distribution, pH, organic carbon and calcium carbonate. Furthermore, grave soil analyses were employed to understand if exists a relationship between the soil properties and the skeletal conservation.

However, if compared these results to previous studies conducted in this area, some discrepancies appear. In fact, in 2002 two trenches were opened near the N-O of the necropolis (10m long, 2m deep and 2m width) to investigate the soil stratigraphy. The soil profile shows that the most superficial horizons (0-0.80m) have an average content of sand, silt and clay of 7.5%, 32.5% and 12.5% respectively. The deeper horizons (>80cm) show an increase of sand compared to silt and clay; in this case the ratio between coarse and fine fraction is 50:50, compared to 10:90 ratio of the most superficial horizons (PESCIO, 2006-2007).

The content of sand, silt and clay of superficial horizons (within 0.80m) is in agreement to the results obtained by grainsize analyses of burial soil of this work. However, no gravels were detected in the previous study, instead in the burial soils a well content was detected, ranging between 1% and 40%. However, only one sample (T.107) has a percentage of gravel equal of 40%, because the other ones have a percentage between 1% and 14%.

The high content of gravel in tomb 107 could be due to the presence of a stone structure and stone roof; even if the tomb 16 has the same structure, but the value of gravel is low (2%). All other tombs are in earthy pits with stone roof.

From these results can be assumed that anthropic activities, probably to dig the tombs, could have altered the natural composition of the fine soil fraction. In fact, more coarse material may have been selected to consolidate the ground of the tomb walls and floors, particularly for tomb 107. Furthermore, some particles of stone roofs and lithic structures could be fallen inside the tomb.

On the basis of particle size and gravel morphology, coarse materials were maybe taken from another site, near the Trebbia's riverside, since the trenches dug near the necropolis do not show the same soil composition.

In addition, in this work we hypothesized that gravels may have been used to drain the tombs, because soils rich in clay and silt cause water stagnation (HAGLUND & SORG, 1997).

Regards the organic carbon, the average value is 11.89g/Kg in grave soils and, if compared to the results obtained from the previously mentioned trenches studied, it appears higher, because both superficial both deep horizons have an average value of ca. 5g/Kg.

On the contrary, as to concern the percentage of calcium carbonate concentration, the tombs analyzed show an average value of 7.28%, instead trenches have a higher average value of ca.15% for superficial layers and ca. 12% for deep ones.

Both these discrepancies could be explained by the decomposition process that affected the bodies laid in ground. Body decay maybe favored the organic matter enrichment in soil, particularly thanks to fungal and bacterial action, which consequently produced a decrease of carbonate calcium in the tombs (HAGLUND & SORG, 1997). However, the pH values registered in all tombs are neutral-alkaline, therefore even a small quantity of  $\text{CaCO}_3$  probably neutralized the natural acidification process induced by organic matter.

Finally, the last discrepancy can be seen in soil color, because the superficial layers (0-0.80m) of trenches are pale brownish-gray, whereas grave soils appear dark-brown. So, the presence of organic matter into the grave soils, due to decomposition process, may have been responsible of the darker coloration.

The well conservation of bones observed could be related to the fine-textured soil found in the necropolis, which inhibited cadaver breakdown, and, retaining moisture, can retard the decomposition process (HAGLUND & SORG, 1997). However, the moisture retained may have contributed to degradation of bone surface, because many bones appear fragmented, rougher, cracked, warp and laminate. Therefore, the amount of gravel recovered in each tomb was not enough to prevent waterlogging.

The scarce gravel soil detected did not affect the bone conservation, because, in general, bones buried in coarse gravels tend to lose large amounts of collagen and to have the consistency of powdery chalk. Also, the neutral-slightly alkaline pH of the soils could have preserved the bones, according to the literature, because acid conditions are detrimental to skeletal conservation. Acidic soils dissolve the inorganic matrix of carbonate-hydroxyapatite, which produces an organic material susceptible to leach by water (DENT *et alii*, 2004).

However, at histologic scale, the 64% of bones are badly preserved. The *post mortem* degradation of bone protein is mainly ascribed to microorganisms activities, which tend to metabolize amino acids with a higher number of carbon atoms as a source of energy. All bones investigated show traces of fungal and bacterial activities, responsible of organic degradation of collagen fibers and of carbonate-

hydroxyapatite remineralization. Degradation processes during the inhumation period can lead to partial or total structural alteration of bone tissue, depending on soil environment and time (HAGLUND & SORG, 1997).

The amounts of organic matter detected in grave soils is higher than those observed in trenches, confirming that bone degradation was certainly partially caused by microorganisms action present into the burial environment.

To find any traces of soil contamination into the bone tissue, 10 cross sections were prepared by mid-shaft diaphysis of either femora or tibia of 10 different individuals buried in earthy pits and analyzed by SEM-EDS.

Comparing the oxides detected on bone sections and into the soil samples, few matches were observed between them.

In tomb 16 the only positive match is manganese oxide, detected both on soil both on bone section. No traces of ilmenite or clay rich in iron oxide were observed on bone.

In tomb 17 clay rich in iron oxide and traces of zircon were detected both on soil both on bone. No rare earth elements and traces of titanium oxide present in soil were observed on bone. Bone cross section shows in addition barium sulfate.

In tomb 28 the only positive match is ilmenite; titanite was not detected on bone; sulfur oxide and clay rich in iron are present only in soil and not on bone. On the contrary, bone section has a large amount of manganese oxide.

In tomb 50 clay rich in iron was detected both on soil both on bone; no quartz and zircon were observed on bone, otherwise present in soil (fig. 4.7b); furthermore potassium oxide was not detected on bone but was observed in soil. On the contrary, rare earth elements, iron oxide and manganese oxide are only present on bone.

In tomb 55 clay rich in iron and manganese oxide was detected on bone and soil samples (fig. 4.7c); however, bone shows also zircon, instead soil has ilmenite. Nickel oxide was also detected in soil but not on bone.

In tomb 56 clay rich in iron and manganese oxide were detected both on bone both in soil samples; bone shows also barium sulfate, instead soil has traces of rare earth elements and titanium oxide. Zircon was detected only in soil.

In tomb 60 the only mineral positive match is zircon, because soil has also ilmenite and clay rich in iron. Among elements, the only positive match is manganese, because chromo oxide and titanium oxide were not detected on bone.

The bones coming from tomb 18, 19, 100 have not any correspondence with their soil samples, because the cross sections are clean; in fact, no oxides were detected by SEM-EDS analysis. On the contrary, their soils show in general clay rich in iron, titanium oxide, manganese oxide and rare earth elements, and in addition zircon, mica and ilmenite. For T.100 was also detected traces of thorium oxide into the soil (fig. 4.7d).

In general, in all grave soils analyzed, calcium phosphate was detected into the samples, probably due to a bone exchange (fig. 4.7a).

These results prove that it is difficult to compare bones with their burial environments, especially regards the oxides and minerals composition, because if the remains are well preserved, as in our case, do not undergo burial contamination. So, in the presence of bones with unknown origin is difficult to trace the burial context. On the contrary, it seems that bones always release calcium phosphate into the soil where they are laid, thus leaving a trace of their presence.



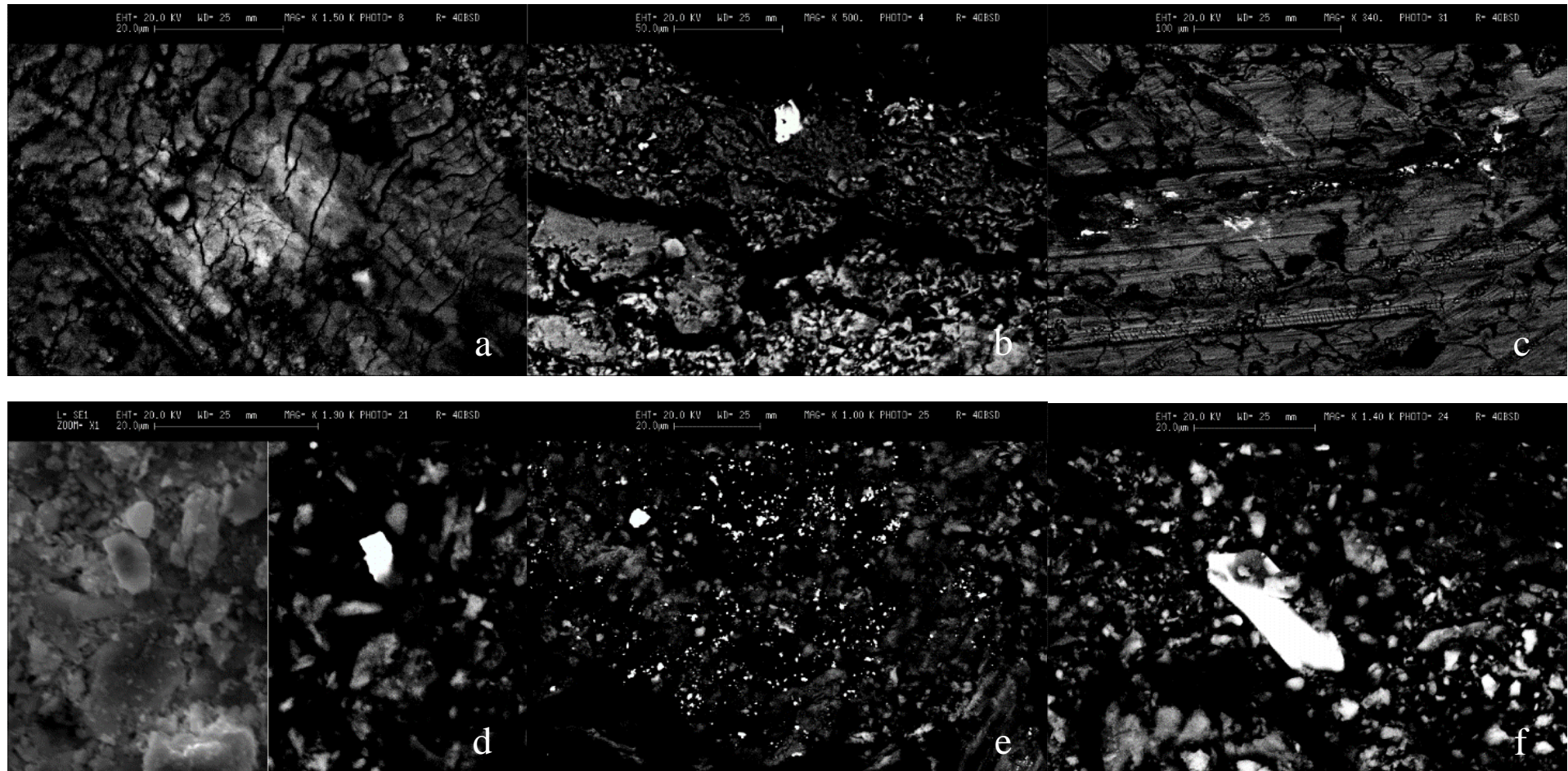


Fig. 4.6- a) detail of manganese oxide (bright color in BSE image) included into the chemical bone structure; b) detail of ilmenite (bright color in BSE view) detected on bone section; c) exogenous manganese oxide (bright color in BSE view) into the the bone fracture; d) detail of rare earth elements in BSE (bright color) (on right) and normal view (on left) on bone section; e) exogenous barium sulfate (bright color in BSE view) on the bone section; f) detail of zircon in BSE view on bone.

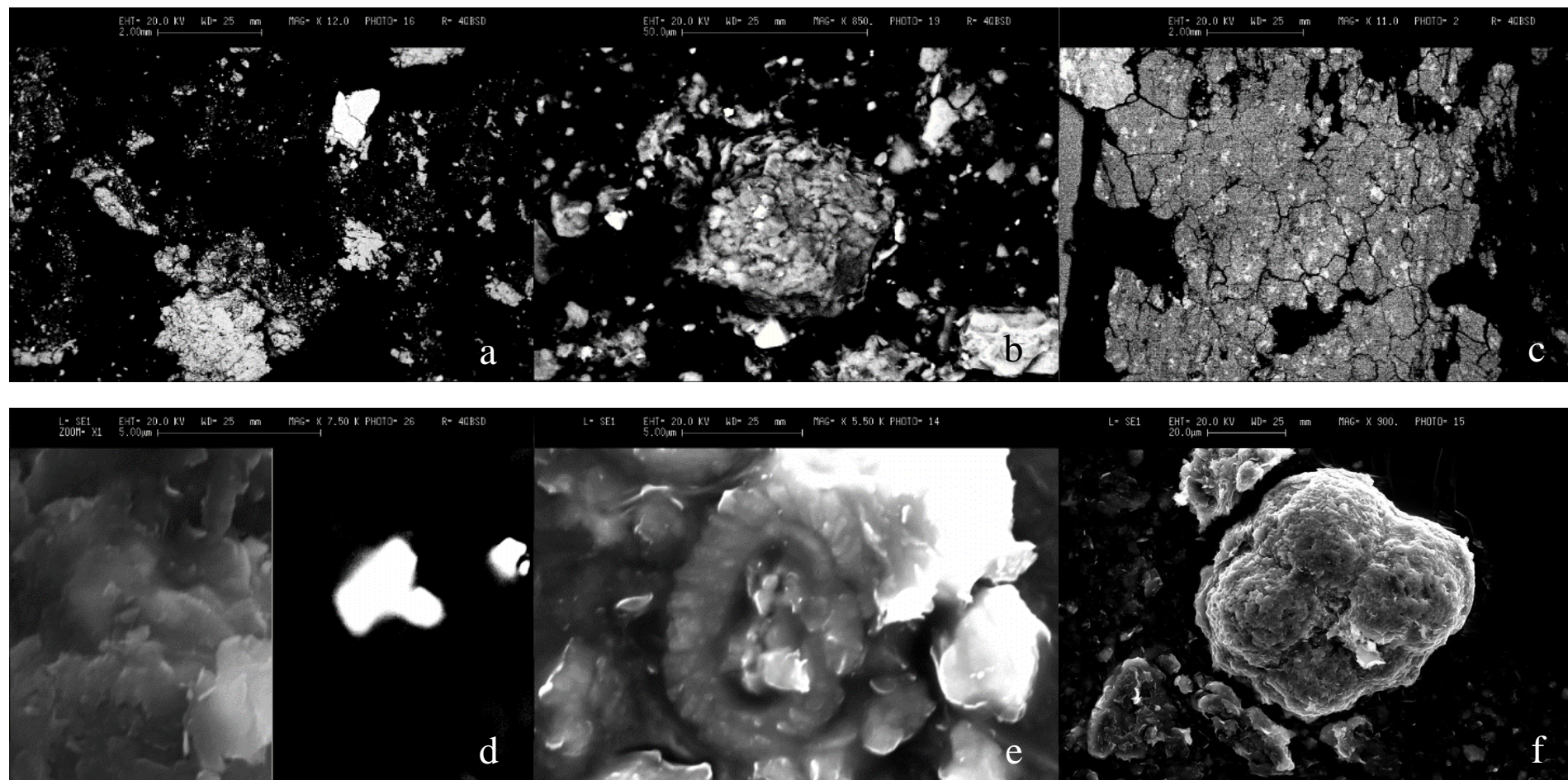


Fig. 4.7 - a) detail of calcium phosphate on soil sample in BSE image (at the right angle); b) detail of quartz grain on soil sample with iron oxide inclusions; c) clay of soil sample with a large amount of manganese oxide inclusions (bright particles); d) detail of rare earth elements with thorium oxide inclusion on soil sample in BSE (right) and normal view (left); e) detail of coccolith detected into the grave soil of tombs: 18, 28, 56, 100; f) foraminifer detected into the grave soil of tomb 28.

SEM-EDS analysis also allowed to estimate the chronology of the grave soil employed in the necropolis, because of the presence of coccoliths and one foraminifer in some tombs.

Coccoliths (fig. 4.7e) were found in 4 grave soils belonging to the tomb 18, 28, 56 and 100, instead one foraminifer was identified into the grave soil of tomb 28 (fig.4.7f).

Coccolithophores are marine, unicellular phytoplankton belonging to the phylum Haptophyta and the division of Prymnesiophyceae. Their morphology are characterized by an exoskeleton composed of calcite platelets (coccoliths). The taxonomy of coccolithophores is based on the morphology of the coccoliths and two major groups exists: holo- and heterococcoliths. In the first case the coccolith formation take place intracellularly, in the second case occur outside the cell (BAUMANN *et alii*, 2005). Living cell form a significant component of the marine algal plankton, and after death the calcareous coccoliths accumulate to form pelagic ooze sediments.

Coccolithophores influence biogeochemical cycle of organic carbon, because take atmospheric CO<sub>2</sub> for their photosynthesis, that is their prime nutritional mode, in the photic zone of the oceans, and produce CaCO<sub>3</sub> for their exoskeleton, which deposits on the ground ocean after death. So their impact on ocean chemistry, atmospheric composition and global carbon cycle via consumption of CO<sub>2</sub> during photosynthesis and generation of CO<sub>2</sub> during calcification.

Coccolithophores have one of the most abundant fossil records, continuous from their first occurrence in the Late Triassic to present day, and today 200 species exist. They are used as palaeoenvironmental and palaeoceanographical indicators, because are one of the main groups of marine phytoplankton, playing a key role in the marine ecosystem. Their morphology and size is influence by temperature, salinity, productivity and macronutrients of the oceans. Four zones can be recognized: subarctic, temperate, subtropical and subantarctic (YOUNG *et alii*, 1999; BAUMANN *et alii*, 2005).

Heterococcoliths are the most common coccolith type, and the shell, composed of CaCO<sub>3</sub>, have a basic disc-shaped morphology, with concave inner surface. Ultrastructure scale consist of 20-40 radial arrays inside an oval ring, and each entity is composed of a flat lower part and T-shaped upper part connected by a vertical stem (LOWENSTAM & WEINER, 1989).

*Emiliania huxleyi* is the heteococcoliths form most diffuse geographically, and probably detected in this study. It appears in the fossil record 268.000 years ago, and become dominant about 73.000 years ago.

Foraminiferida are an order of single-celled protozoa, included in the phylum Rhizopoda, that live on the sea floor (benthic foraminifera) or in the water column (planktonic foraminifera). The cell is enclosed within a shell, composed of secreted organic matter, minerals or agglutinated particles. The

shell size ranges from about 100 micron to few centimeters and can consist of single or multiple chambers interconnected by one or several openings (foramina).

Foraminifera are known from Early Cambrian, but became widespread during the Cenozoic. Actually they are over 90% of deep sea biomass, and are important biostratigraphical indicator in marine rocks from Late Paleozoic, Mesozoic and Cenozoic age.

Changes in the composition of the foraminiferal assemblages may be used to track changes in the circulation of the surface water and sea floor. They are especially important in studies of Mesozoic to Quaternary climate history because isotopes within their  $\text{CaCO}_3$  shells record changes in temperature and ocean chemistry.

The structure and the composition of the shell wall is a features used for classification at taxonomic level. Organic-walled are constituted by proteinaceous matter termed tectin; agglutinated shell are made by organic and mineral matter from the sea floor, selected for size, texture and composition, packed randomly or aligned; calcareous shell are the most abundant suborders, and three main type exists: porcelaneous, imperforate, microgranular and hyaline perforate, which differ about the chemical composition and arrangement of the walls. The general morphology varies widely and chamber shapes include globular, tubular, compressed lunate and wedge-shaped types.

The apertures, that in living organism connect the external pseudopodia with the internal endoplasm, allowing passage of food, vacuoles, nuclei and daughter cells, can have different shape, for example rounded, radiate, dendritic, cruciform and so on.

Another parameter of classification is the external surface, which can appear spinose, carinate, rugose, striate, costate, granulate or reticulate.

Benthic foraminifera are useful environmental indicators because have colonized almost all marine habitats and until now about 5000 living species are known. Their growth is influenced by light, food availability, substrate, salinity (about 35%), oxygen and temperature. Some shallow water benthic and planktonic foraminifera may host algal symbionts (e.g., dinoflagellates) that help the calcification process: during the photosynthesis in ocean photic zone, the  $\text{CO}_2$  stored during breathing allows precipitation of  $\text{CaCO}_3$  during shell formation. Modern assemblage can be arranged into biogeographic provinces: Artic, Subartic, Transitional, Tropical, Subtropical, Transitional, Subantartic and Antartic (ARMSTRONG & BRASIER, 2005).

In this work the foraminifer detected is very small in size, poor preserved; it is an internal mould, and does not show the original shell texture which is a features for classification at genus level. However, based on the general morphology it could be assigned to a planktonic foraminifera, such as *Paragloborotalia* or *Tenuitella* or *Neogloboquadrina* genus, which stratigraphic ranges are dated late Eocene-Miocene or Miocene-Holocene for the latter genus.

From these identifications, we can suppose that coccoliths and foraminifer preserved into the grave soils examined might come from the lithostratigraphic units of Travo, because the archaeological site examined is located in Val Luretta, which has a marine sedimentary origin, made by Poviago's Membro and Monteventano's Membro, dated back from Upper Pliocene to Lower Eocene. Also, Montepiano's marls emerge, dated back from Middle to Upper Eocene - Oligocene, overlying by Ranzano's sandstones, dated back from Upper to Lower Oligocene.

As consequence, these results confirm that the tombs analyzed were built with local soil, taken near the Trebbia River, as previously hypothesized.



## Chapter 5

# Conclusions

Human bones can undergo several diagenetic processes after death, depending on the local burial and environmental conditions. Bone begin a composite material, constituted by an intimate association of organic and mineral phases, assembled in a hierarchical organization, so *post mortem* degradation can occur at both structural and chemical scale.

The organic and inorganic components of bone tissue are unstable once removed from the body. Nevertheless, insights on the rate at which collagen and mineral components are lost can help to provide information on taphonomic history of bone assemblage and burial environment.

However, bone diagenesis is far to be completely understood, so more studies are required in this field.

This work describes the bone tissue appearance of bone from five different burial contexts, dated from the Late Roman period to 1990s. Bone tissue was described at the macroscopic, biomolecular, microscopic, ultramicroscopic, and chemical scale.

At macroscopic scale, the analyzed bones, despite their different burial settings and ages, appear all well preserved. So, this study shows that the origin of some macroscopic taphonomic characteristic is not time related but most probably local burial environmental factors contributed more strongly than time passing by.

Thus Behernsmeyer's classification, based on the presence/absence of macroscopic taphonomic characteristics, resulted to be not useful to determine if the examined bone specimens belonged to one of the archaeological, historical or contemporary burial contexts. In fact, Behernsmeyer's

classification has not intermediate stages, consequently most of the bones examined did not fit completely with the proposed scale and rates.

Since macroscopic appearance could not discriminate bones with different chronologies and from different burial sites, more invasive analyses were required. Bones that had similar macroscopic taphonomic characteristics, showed clear differences at biomolecular and histological scale.

The overall results of Luminol CL reaction show different responses among the bones examined; in general, recent bones appeared more chemiluminescent than archaeological ones. However, a positive reaction among the archaeological bones was observed, as well as no CL reaction was detected on some modern bones, as similarly reported in other studies. These phenomena could be due to local diagenetic factors, which preserved or altered the hemoglobin conservation. So, Luminol testing to determine burial ages should be relied upon with caution.

At the histological scale, archaeological bones appear more degraded than recent ones. However, a discrete variability among the samples coming from the same population was observed. The bones of the oldest population analyzed (Late Roman), with a PMI >1000 years, are partially or completely deteriorated. At the same time, traces of fungal and bacteria actions were observed into the tissue of the modern bones, with a PMI <50 years, because bone degradation occurred as soon as 3 months after death.

So, alteration of bone histology, observable both in optical light microscopy and in BSE-SEM, cannot be used alone to discriminate the ancient bones from the recent ones, because different environmental conditions may favor or inhibit osteon structure degradation and microbiological attack differently. Among the archaeological samples, the bones that show the highest degree of histological degradation were the ones buried in the ground. On the other hand, the bone samples that have the higher variability in histological structure preservation were those recovered from a crypt. It is thus possible that the local condition of the ossuary (low temperature and high moisture) could have slowed the bone decomposition. Interestingly, adipocere remnants were detected adhering to some human remains. Furthermore, micromorphological analysis showed that tissue alteration varied considerably within the same bone, within bones of the same individual, and among skeletons from the same archaeological site. Our results demonstrated also an independence between organic and inorganic osteological component conservation, but even false positives and negatives need to be taken into consideration.

Exogenous oxides and minerals inclusions were also detected by SEM-EDS in the natural pores and degraded zones of the bones examined. The quantitative analysis of exogenous oxides and minerals cannot be employed as indicator of the burial context or the time since death of the human remains, because of the high variability observed within the samples from the same population. Consequently



was not possible to identify the chemical fingerprints for any of the burial context analyzed: crypt, ground, coffin.

3D micro-computed tomography shows that total bone porosity increases with sample age. However, archaeological bones show a heterogeneous degree of porosity, irrespective of their chronology. In general, ancient bones have lower canals volume to size ratio than contemporary ones, presumably for the longer exposure to degrading agents. However, a little variability among the archaeological samples was also detected, proving that not only the age had a role on bone porosity but also local burial environment influenced the general porosity of bone tissue preservation.

A general decreases of organic and carbonate content of hydroxyapatite with age was observed by FT-IR. At the same time, the bone hydroxyapatite crystals of the most ancient bones (Late Roman) appear larger, with a more ordered structure than modern ones. In fact, once the collagen is removed, during diagenesis, the thin and plate-shape crystals inside the collagen fibril can become closer and fuse together, forming thicker and larger hydroxyapatite crystals. Furthermore, since hydroxyapatite crystals with high levels of carbonate are thermodynamically unstable, they tend to spontaneously lose the carbonate during bone diagenesis, thus evolving to more stable crystal lattices over time (see discussion for detailed references).

The analyses of the grave soils from Travo show some relationship between the soil properties (such as particle size, pH, carbonate content and organic matter), and the skeletal record. The fine texture and moisture retention of the necropolis soil inhibits mechanical and chemical decomposition. The neutral-slightly alkaline pH of the soil suppresses bone mineral dissolution. Interestingly the burial sediments have lower carbonate and higher organic matter content than the local surrounding soil. It is thus possible that the body decay enriched the local soil with organic matter and, at the same time, lowered the pH and the carbonate content.

On the other hand, the histological analysis shows that similar tissue degradation was observed in bones found in different burial contexts. Traces of fungal and bacterial activities supported by the rich organic matter content, supports the hypothesis that bone degradation was part caused by microorganisms action presents into the burial environment.

At chemical scale, soil contamination on bones was minimal, because few matches were detected between bones and their related soil, as regards of oxides and minerals composition. At the same time, traces of manganese oxide and barium sulfate were recovered on bones, and they could be related to decomposition process, because were not detected in the grave soils.

On the contrary, it seems that bones tend to release calcium phosphate into the soil where they are laid, thus leaving a trace of their presence.

In conclusion, the study shows a heterogeneous conservation of the human remains on the different scales investigated, irrespective of the background and age. A good macroscopic preservation does not necessarily mean a lack of degradation at microscopic and chemical/biomolecular scale or vice versa. So, these results demonstrate that the degradation of the organic and inorganic components of bone follows independent paths, that lead to a variety of preservation state.

## Chapter 6

# References

ARMSTRONG H. & BRASIER M. (2005) – *Microfossil*. 2<sup>nd</sup>.ed. Blackwell Publishing, USA, UK, Australia, 296 pp.

ARTIOLI G. (2010) - *Scientific methods and cultural heritage. An introduction to the application of materials science to archaeometry and conservation science*. Oxford University Press, New York, 536 pp.

ASCENZI M-G., ASCENZI A., BENVENUTI A., BURGHAMMER M., PANZAVOLTA S. & BIGI A. (2003) – *Structural differences between “dark” and “bright” isolated human osteonic lamellae*. *Journal of Structural Biology*, 141, 22-33.

ASTORI C., CIAVATTA C., SATANASSI A. & SEQUI P. (1994) - *Carbonio Organico*. In: *Metodi ufficiali di analisi chimica del suolo*. Ministero delle Risorse Agricole Alimentari e Osservatorio Nazionale Pedologico per la Qualità del Suolo, Roma.

AVERY, B.W. & BASCOMB, C. L. (1974) - *Soil Survey Laboratory Methods*. Soil Survey Technical Monograph, 6, Harpenden.

BAUMANN K-H., ANDRULEIT H., BOCKEL B., GEISEN M. & KINKEL H. (2005) – *The significance of extant coccolithophores as indicator of ocean water masses, surface water temperature and palaeoproductivity: a review*. *Palaontologische Zeitschrift*, 79 (1), 93-112.

BEHRENSMEYER A.K. (1978) - *Taphonomic and ecological information from bone weathering*. *Paleobiology*, 4 (2), 150-162.

BEHRENSMEYER A.K. & KIDWELL S.M. (1985) - *Taphonomy's Contributions to Paleobiology*. *Paleobiology*, 11 (1), 105-119.

BELL L. S. (1990) - *Paleopathology and Diagenesis: An SEM evaluation of structural changes using backscattered electron imaging*. *Journal of Archaeological Science*, 17, 85–102.

- BELL L.S. (1996) - *The speed of post mortem change to the human skeleton and its taphonomic significance*. Forensic Science International, 82 (2), 129-140.
- BERNA F., MATTHEWS A. & WEINER S. (2004) - *Solubilities of bone mineral from archaeological sites: the recrystallization window*. Journal of Archaeological Science, 31, 867–882.
- BOUSSON V., MEUNIER A., BERGOT C., VICAUT E., ROCHA M.A., MORAIS M.H., LAVAL-JEANTET A-M., & LAREDO J-D. (2001) - *Distribution of intracortical porosity in human midfemoral cortex by age and gender*. Journal of Bone and Mineral Research, 16 (7), 1308-1317.
- BRADY N.C. & WEIL R.R. (1999) - *The nature and properties of soils*, 12<sup>th</sup>. ed. Pearson, 881pp.
- BROMAGE T.G., GOLDMAN H.M., MCFARLIN S.C., WARSHAW J., BOYDE A. & RIGGS C.M. (2003) – *Circularly polarized light standards for investigation of collagen fiber orientation in bone*. The Anatomical Record (part B: New Anat.), 274B, 157-168.
- BRUN F., PACILÈ S., ACCARDO A., KOUROUSIAS G., DREOSSI D., MANCINI L., TROMBA G. & PUGLIESE R. (2015) - *Enhanced and flexible software tools for X-ray computed tomography at the Italian synchrotron radiation facility Elettra*. Fundamenta Informaticae, 141, 233-243.
- CAPPELLA A., GIBELLI D., MUCCINO E., SCARPULLA V., CERUTTI E., CARUSO V., SGUAZZA E., MAZZARELLI D. & CATTANEO C. (2015) - *The comparative performance of PMI estimation in skeletal remains by three methods (C-14, luminol test and OHI): analysis of 20 cases*. International Journal of Legal Medicine, 1-10.
- CAUDULLO G., CARUSO V., CAPPELLA A., SGUAZZA E., MAZZARELLI D., AMADASI A. & CATTANEO C. (2016) - *How valid is Luminol test in detecting modern skeletal bones? A test on several bone tissue typology: A caveat for PMI interpretation*. International Journal of Legal Medicine, 1-6.
- CHAPPARD C., BASILLAIS A., BENHAMOU L., BONASSIE A., BRUNET-IMBAULT B., BONNET N. & PEYRIN F. (2006) - *Comparison of synchrotron radiation and conventional x-ray microcomputed tomography for assessing trabecular bone microarchitecture of human femoral heads*. Medical Physics, 33, 3568-3577.
- COLLINS M. J., NIELSEN–MARSH C. M., HILLER J., SMITH C. I., ROBERTS J. P., PRIGODICH R. V., WEISS T.J., CSAPÒ J., MILLARD A.R. & TURNER–WALKER G. (2002) - *The survival of organic matter in bone: a review*. Archaeometry, 44 (3), 383–394.
- CONVERSI R. & MEZZADRI C. (2011) - *Testimonianze funerarie d'età longobarda nel Piacentino e studio preliminare della necropoli di Sant'Andrea di Travo (PC)*. In: POSSENTI (Ed.), Necropoli Longobarde in Italia. Indirizzi della ricerca e nuovi dati. Atti del convegno internazionale, pp. 214-244, Castello del Buonconsiglio, Trento, 26-28 Settembre 2011.

COOPER D. M. L., TURINSKY A. L., SENSEN C. W. & HALLGRIMSSON B. (2003) - *Quantitative 3D analysis of the canal network in cortical bone by micro-computed tomography*. Anatomical Record. Part B, New Anatomist, 274 (1), 169–179.

CREMASCHI (1990) - *Pedogenesi medio – olocenica ed uso dei suoli durante il Neolitico in Italia settentrionale*. In BIAGI (Ed.), The Neolithisation of the Alpine Region. “Monografie di natura bresciana”, 13.

DE BOER H.H., AARENTS M.J. & MAAT G.J.R. (2012) - *Staining ground sections of natural dry bone tissue for microscopy*. International Journal of Osteoarchaeology, 22 (4), 379–386.

DE CARLO F., GÜRSOY D., MARONE F., RIVERS M., PARKINSON D.Y., KHAN F., SCHWARZ N., VINE D.J., VOGT S., GLEBER S.C., NARAYANAN S., NEWVILLE M., LANZIROTTI T., SUN Y., HONG Y.P. & JACOBSEN C. (2014) - *Scientific data exchange: a schema for HDF5-based storage of raw and analyzed data*. Journal of Synchrotron Radiation, 21, 1224–1230.

DEER W.A., HOWIE R.A. & ZUSSMANN J. (1966) – *An introduction to the rock forming minerals*. Longman press, Harlow, 528 pp.

DENT B.B., FORBES S.L., STUART B.H. (2004) - *Review of human decomposition processes in soil*. Environmental Geology, 45, 576–585.

DIXON R., DAWSON L. & TAYLOR D. (2008) - *The experimental degradation of archaeological human bone by anaerobic bacteria and the implications for recovery of ancient DNA*. The 9<sup>th</sup> International Conference on Ancient DNA and Associated Biomolecules, 1–10.

DONG X.N & GUO W.E. (2004) - *The dependence of transversely isotropic elasticity of human femoral cortical bone on porosity*. Journal of Biomechanics, 37, 1281–1287.

DUCHAUFOR P. (1983) - *Pédologie 1: pédogènese et classification*. 2<sup>nd</sup>.ed. Masson, 491pp.

FELDKAMP L.A., GOLDSTEIN S.A., PARFITT A.M., JESION G. & KLEEREKOPER M. (1989) – *The direct examination of three-dimensional bone architecture in vitro by computed tomography*. Journal of bone and mineral research, 4 (1), 3-11.

GARLAND A.N. (1989) - *Microscopical analysis of fossil bone*. Applied Geochemistry, 4, 215-229.

GALE S.J. & HOARE P.G. (1991) - *Quaternary Sediments*. Belhaven Press, London.

GIORDANO A. (1999) – *Pedologia*. UTET, 364pp.

GUARINO F.M., ANGELINI F., VOLLONO C. & OREFICE C. (2006) - *Bone preservation in human remains from the Terme del Sarno at Pompeii using light microscopy and scanning electron microscopy*. Journal of Archaeological Science, 33 (4), 513–520.

HACKETT C.J. (1981) - *Microscopical focal destruction (tunnels) in exhumed human bones*. Medical Science Law, 21 (4), 243-265.

- HAGLUND W.D. & SORG M.H. (1997) – *Forensic Taphonomy. The postmortem fate of human remains*. CRC press, Boca Raton, Boston, London, New York, Washington D.C., 668 pp.
- HEDGES R. E. M. & MILLARD A. R. (1995) - *Bones and Groundwater: Towards the Modelling of Diagenetic Processes*. *Journal of Archaeological Science*, 22 (2), 155–164.
- HEDGES R.E.M. (2002) - *Bone diagenesis: an overview of processes*. *Archaeometry*, 44, 319–328.
- INTRONA F., DI VELLA G. & CAMPOBASSO C.P. (1999) - *The determination of postmortem interval from old skeletal remains by image analysis of Luminol test results*. *Journal of Forensic Science*, 44, 535-538.
- JANS M.M.E., KARS H., NIELSEN-MARSH C.M., SMITH C.I., NORD A.G., ARTHUR P. & EARL N. (2002) - *In situ preservation of archaeological Bone: a histological study within a multidisciplinary approach*. *Archaeometry*, 44 (3), 343–352.
- LOWENSTAM H.A. & WEINER S. (1989) - *On Biomineralization*. Oxford University Press, New York, Oxford, 324pp.
- MAAT G.J.R., VAN DEN BOS R.P.M. & AARENTS M. (2001) - *Manual preparation of ground sections for the microscopy of natural bone tissue: update and modification of Frost's 'rapid manual method'*. *International Journal of Osteoarchaeology*, 11 (5), 366–374.
- MARSDEN I. & PAGANI C. (2008) - *Milano, Viale Sabotino (MI), Indagini archeologiche*, in: *Notiziario 2006*, 119-122, Milano.
- MCRAE S.G. (1991) - *Pedologia pratica. Come studiare i suoli sul campo*. Zanichelli, Bologna.
- MINISTERO PER LE POLITICHE AGRICOLE (1999) - *Approvazione dei "Metodi ufficiali di analisi chimica del suolo"*. Decreto Ministeriale del 13/09/1999, Gazzetta Ufficiale Supplemento Ordine n° 248 del 21/10/1999.
- MÜLLER K., CHADEFaux C., THOMAS N. & REICHE I. (2011) - *Microbial attack of archaeological bones versus high concentrations of heavy metals in the burial environment . A case study of animal bones from a mediaeval copper workshop in Paris*. *Palaeogeography, Palaeoclimatology, Palaeoecology*, 310 (1-2), 39–51.
- MUNCH B., TRTIK P., MARONE F. & STAMPANONI M. (2009) - *Stripe and ring artifact removal with combined wavelet–Fourier filtering*. *Optic Express*, 17, 8567–8591.
- MUNSELL® COLOR (1994) - *Munsell Soil Color Charts*. Revised edition. Macbeth Division of Kollmorgen Instruments Corporation, New Windsor, NY.
- NIELSEN-MARSH C.M. & HEDGES R.E.M. (2000) – *Patterns of diagenesis in bone I: the effect of site environments*. *Journal of Archaeological Science*, 27, 1139-1150.

OSMAN K.T. (2013) – *Soils. Principles, properties and management*. Springer, Dordrecht Heidelberg New York London, 271pp.

PESCIO S. (2006-2007) - *Il supporto geoarcheologico allo scavo stratigrafico: il caso di studio del sito neolitico di Travo (PC)*. Tesi di Laurea, Dipartimento di Scienze della Terra “Ardito Desio”, Università degli Studi di Milano.

PFRETZSCHNER H. U. (2004) - *Fossilization of Haversian bone in aquatic environments*. *Comptes Rendus Palevol*, 3 (6-7), 605–616.

POKINES J.T. & SYMES S.A. (2010) – *Manual of forensic taphonomy*. CRC press, Boca Raton, London, New York, 471 pp.

RAMSTHALER F., EBACH S.C., BIRNGRUBER C.G. & VERHOFF M.A. (2011) - *Postmortem interval of skeletal remains through the detection of intraosseal hemin traces. A comparison of UV-fluorescence, Luminol, Hexagon-OBTI ®, and Combur® tests*. *Forensic Science International*, 209 (1-3), 59-63.

RAMSTHALER F., KREUTZ K., ZIPP K. & VERHOFF M.A. (2009) - *Dating skeletal remains with luminol-chemiluminescence. Validity, intra- and interobserver error*. *Forensic Science International*, 187, 47-50.

RHO J.Y., HOBATHO M.C. & ASHMAN R.B. (1995) - *Relations of mechanical properties to density and CT numbers in human bone*. *Medical Engineering and Physics*, 17 (5), 347-355.

ROGOZ A., SAWLOWICZ Z. & WOJTAL P. (2012) - *Diagenetic history of woolly mammoth (*Mammuthus Primigenius*) skeletal remains from the archaeological site Cracow Spadzista Street (B), Southern Poland*. *Palaios*, 27 (8), 541–549.

SANNAZARO M. (2001) - *La necropoli tardoantica: ricerche archeologiche nei cortili dell'Università Cattolica*, Milano, 257pp.

SANTOS R.V. & CLAYTON R.N. (1995) - *The carbonate content in high-temperature apatite: An analytical method applied to apatite from the Jacupiranga alkaline complex*. *American Mineralogist*, 80, 336-344.

STINER M.C., KUHN S.L., SUROVELL T.A., GOLDBERG P., MEIGNEN L., WEINER S., BARYOSEF O. (2001) - *Bone preservation in Hayonim Cave (Israel): a macroscopic and mineralogical study*. *Journal of Archeological Science*, 28, 643-659.

STOUT S.D. & TEITELBAUM S.L. (1976) - *Histological analysis of undecalcified thin section of archaeological bone*. *American Journal of Physical Anthropology*, 44, 263-269.

TIBETT M. & CARTER D.O. (2008) – *Soil analysis in forensic taphonomy. Chemical and biological effects of buried human remains*. CRC Press, Boca Raton, London, New York, 340 pp.

- TRUEMAN C. N. & MARTIN D.M. (2002) - *The long-term survival of bone: the role of bioerosion*. *Archaeometry*, 44 (3), 371–382.
- TRUEMAN C.N.G., BEHRENSMEYER A.K., TUROSS N. & WEINER S. (2004) - *Mineralogical and compositional changes in bones exposed on soil surfaces in Amboseli National Park, Kenya: diagenetic mechanisms and the role of sediment pore fluids*. *Journal of Archaeological Science*, 31, 721–739.
- TRUEMAN C.N.G., PRIVAT K. & FIELD J. (2008) - *Why do crystallinity values fail to predict the extent of diagenetic alteration of bone mineral?.* *Palaeogeography, Palaeoclimatology, Palaeoecology*, 266, 160–167.
- VAGLIENTI F., CATTANEO C. & MAZZAGATTI R. (2013) - *La popolazione di Milano dal Rinascimento*. Biblioteca Franceseana, 174pp.
- WALKLEY A. & BLACK I.A. (1934) - *An examination of the Degtjareff method for determining soil organic matter, and proposed modification of the chromic acid titration method*. *Soil Science*, 37(1), 29-38.
- WEBER K. (1966) - *Die Anwendung der Chemilumineszenz des Luminol, in Der gerichtlichen Medizin und Toxikologie. I. Der nachweis von Blutspuren, Dtsch. Z. Gesamte Gerichtl. Medicine*, 57, 410-423.
- WEINER S. & BAR-YOSEF O. (1990) - *States of preservation of bones from prehistoric sites in the Near East: a survey*. *Journal of Archaeological Science*, 17, 187–196.
- WEINER S. (2010) - *Microarchaeology. Beyond the visible archaeological record*. Cambridge University Press, Cambridge, New York, Melbourne, Madrid, Cape Town, Singapore, São Paulo, Delhi, Dubai, Tokyo, 396 pp.
- WEINER S. & WAGNER H.D. (1998) - *The material bone: structure-mechanical function relations*. *Annual Review of Materials Science*, 28, 271–298.
- WEISS L. (1983) - *Histology. Cell and tissue biology*. Elsevier Science Ltd, 5th edition, New York, Amsterdam, Oxford, 1219 pp.
- WILSON L.Y.N. & POLLARD A.M. (2002) - *Here Today, Gone Tomorrow? Integrated Experimentation and Geochemical Modeling in Studies of Archaeological Diagenetic Change Understanding Diagenetic Processes*. *Recent*, 35(8), 644–651.
- YOSHINO M., KIMIJIMA T., MIYASAKA S., SATO H. & SETA S. (1991) - *Microscopical study on estimation of time since death in skeletal remains*. *Forensic Science International*, 49 (2), 143-158.
- YOUNG J.R., DAVIS S.A., BROWN P.R. & MANN S. (1999) - *Coccolith ultrastructure and biomineralization*. *Journal of structural biology*, 126, 195-215.



## Chapter 7

# Appendices

### 7.1 - Appendix 1

Results of macroscopic analysis performed on bones coming from Population 1, 2, 3 and 4.

<i>Population 1</i>	
<b>Sample 1</b>	
<b>Features</b>	<b>Evaluation</b>
General state of bone	Complete right tibia
Cortical surface appearance	Complete (100%)
Fatty substance	Absent
Skin, muscles and ligaments	Absent
Spongy tissue	Slightly exposed on epiphyses. The color is Brown (5/2 7.5YR)
Tissue in medullary cavity	Absent
Cracking	Absent
Flaking	Absent
Color	Strong Brown (4/6 7.5YR), Reddish Yellow (6/8 7.5YR) and Yellow (8/6 10YR)
Bleaching	Absent
Odor	Absent
<b>Sample 2</b>	
<b>Features</b>	<b>Evaluation</b>

General state of bone	Complete right tibia
Cortical surface appearance	Complete (100%)
Fatty substance	Absent
Skin, muscles and ligaments	Absent
Spongy tissue	Exposed on proximal and distal epiphysis. The color is Brown (5/2 7.5YR)
Tissue in medullary cavity	Absent
Cracking	Longitudinal, on lateral and posterior diaphysis
Flaking	Absent
Color	Brown (5/2 7.5 YR), Very Pale Brown (8/4 10YR) and Yellowish Brown (5/6 10YR)
Bleaching	Absent
Odor	Absent

### Sample 3

Features	Evaluation
General state of bone	Complete left femur
Cortical surface appearance	Incomplete (<50%)
Fatty substance	Absent
Skin, muscles and ligaments	Absent
Spongy tissue	Exposed on greater trochanter, head and third distal shaft. The color is Brown (5/2 7.5YR)
Tissue in medullary cavity	Absent
Cracking	Longitudinal
Flaking	< 50% only on diaphysis
Color	Strong Brown (5/6 7.5YR), Brown (5/4 7.5YR), Very Pale Brown (8/4 10YR)
Bleaching	Absent
Odor	Absent

### Sample 4

Features	Evaluation
General state of bone	Incomplete right tibia at the proximal epiphysis
Cortical surface appearance	Complete (100%)
Fatty substance	Absent

Skin, muscles and ligaments	Absent
Spongy tissue	Exposed on proximal third shaft and anterior distal end. The color is Grayish Brown (10YR 5/2)
Tissue in medullary cavity	Absent
Cracking	Absent
Flaking	Absent
Color	Very Pale Brown (8/4 10YR) and Brownish Yellow (6/6 10YR)
Bleaching	Absent
Odor	Absent

#### Sample 5

<b>Features</b>	<b>Evaluation</b>
General state of bone	Incomplete right tibia at the distal end
Cortical surface appearance	Complete (100%)
Fatty substance	Absent
Skin, muscles and ligaments	Absent
Spongy tissue	Exposed on distal third and on proximal epiphysis. The color is Brown (5/2 7.5YR)
Tissue in medullary cavity	Absent
Cracking	Absent
Flaking	Absent
Color	Very Pale Brown (8/310YR), Yellowish Brown (5/4 10YR) and Grayish Brown (5/2 10YR)
Bleaching	Absent
Odor	Absent

#### Sample 6

<b>Features</b>	<b>Evaluation</b>
General state of bone	Incomplete right femur at the head
Cortical surface appearance	Complete (100%)
Fatty substance	Absent
Skin, muscles and ligaments	Absent
Spongy tissue	Exposed on anatomical neck. The color is Light Reddish Brown (6/3 5YR)
Tissue in medullary cavity	Absent

Cracking	Absent
Flaking	Absent
Color	Very pale Brown (8/4 10YR) and Brownish Yellow (6/8 10YR)
Bleaching	Absent
Odor	Absent

#### Sample 7

Features	Evaluation
General state of bone	Incomplete right femur at the third distal end
Cortical surface appearance	Complete (100%)
Fatty substance	Absent
Skin, muscles and ligaments	Absent
Spongy tissue	Exposed on head, neck and greater trochanter. The color is Very Pale Brown (7/4 10YR) and Yellowish Brown (5/6 10YR)
Tissue in medullary cavity	Absent
Cracking	Absent
Flaking	Absent
Color	Yellowish Brown (5/6 10YR) and Yellow (7/6 10YR)
Bleaching	Absent
Odor	Absent

#### Sample 8

Features	Evaluation
General state of bone	Incomplete left femur at the proximal epiphysis
Cortical surface appearance	Incomplete (<50%)
Fatty substance	Absent
Skin, muscles and ligaments	Absent
Spongy tissue	Exposed on anterior medial condyle and anterior medial condyle. The color is Brown (5/2 7.5YR)
Tissue in medullary cavity	Absent
Cracking	Absent
Flaking	Islet on anterior diaphysis
Color	Brown (4/4 7.5 YR) and Light Brown (6/4 7.5YR)

Bleaching	Absent
Odor	Absent

**Sample 9**

<b>Features</b>	<b>Evaluation</b>
General state of bone	Complete right femur
Cortical surface appearance	Complete (100%)
Fatty substance	Absent
Skin, muscles and ligaments	Absent
Spongy tissue	Exposed on lateral medial condyle and anterior lateral condyle. The colors are Brown (5/2 7.5YR) and Very Pale Brown (7/4 10YR)
Tissue in medullary cavity	Absent
Cracking	Absent
Flaking	Absent
Color	Reddish Yellow (6/8 7.5YR), Brown (5/4 7.5YR) and Very Pale Brown (7/3 10YR)
Bleaching	Absent
Odor	Absent

**Sample 10**

<b>Features</b>	<b>Evaluation</b>
General state of bone	Complete right femur
Cortical surface appearance	Incomplete (> 50%)
Fatty substance	Absent
Skin, muscles and ligaments	Absent
Spongy tissue	Exposed on anterior proximal epiphysis and lateral distal condyles. The colors are Light Reddish brown (6/3 5YR) and Reddish Brown (5/3 5YR)
Tissue in medullary cavity	Absent
Cracking	Longitudinal
Flaking	Diffused on anterior shaft
Color	White (8/1 10YR) and Yellow (8/6 10YR e 8/8 10YR)
Bleaching	Absent
Odor	Absent

**Population 2**

**Sample 1**

<b>Features</b>	<b>Evaluation</b>
General state of bone	Complete right tibia
Cortical surface appearance	Complete (100%)
Fatty substance	Absent
Skin, muscles and ligaments	Absent
Spongy tissue	Exposed on distal epiphysis. The colors are Brown (5/4 7.5YR) and Yellow (8/6 10Y)
Tissue in medullary cavity	Absent
Cracking	Longitudinal
Flaking	Absent
Color	Strong Brown (5/8 7.5YR), Very Pale Brown (8/4 10YR) and Yellow (8/6 10Y)
Bleaching	Absent
Odor	Absent

**Sample 2**

<b>Features</b>	<b>Evaluation</b>
General state of bone	Complete left tibia
Cortical surface appearance	Complete (> 50%)
Fatty substance	Absent
Skin, muscles and ligaments	Absent
Spongy tissue	Exposed on posterior proximal epiphysis, and on posterior and lateral distal epiphysis. The color is Brownish Yellow (6/6 10YR)
Tissue in medullary cavity	Absent
Cracking	Longitudinal
Flaking	Islet on distal third shaft
Color	Very Pale Yellow (8/6 10YR), Yellow (7/8 10YR), Brownish Yellow (6/8 10YR), Very Pale Brown (8/3 10YR)
Bleaching	Absent
Odor	Absent

**Sample 3**

<b>Features</b>	<b>Evaluation</b>
-----------------	-------------------

General state of bone	Incomplete right tibia at distal end
Cortical surface appearance	Incomplete (<50%)
Fatty substance	Absent
Skin, muscles and ligaments	Absent
Spongy tissue	Exposed on epiphyses. The colors are Very Pale Brown (8/4 10YR) and Light Yellowish Brown (6/4 10YR)
Tissue in medullary cavity	Absent
Cracking	Longitudinal, only on posterior shaft
Flaking	Absent
Color	Very Pale Brown (8/4 10YR) and Light Yellowish Brown (6/4 10YR)
Bleaching	Absent
Odor	Absent

#### Sample 4

Features	Evaluation
General state of bone	Complete right tibia
Cortical surface appearance	Complete (100%)
Fatty substance	Absent
Skin, muscles and ligaments	Absent
Spongy tissue	Exposed on posterior proximal epiphysis and later distal end. The color is Dusky Red (3/2 2.5YR)
Tissue in medullary cavity	Absent
Cracking	Absent
Flaking	Absent
Color	Weak Red (4/3 10R) and Red (4/6 2.5YR)
Bleaching	Absent
Odor	Absent

#### Sample 5

Features	Evaluation
General state of bone	Complete left tibia
Cortical surface appearance	Incomplete (< 50%)

Fatty substance	Absent
Skin, muscles and ligaments	Absent
Spongy tissue	Exposed on anterior and posterior proximal epiphysis and medial malleolus. The color is Red (4/6 2.5YR)
Tissue in medullary cavity	Absent
Cracking	Absent
Flaking	Islet on diaphysis
Color	Black (2.5/0 2.5YR), Red (4/6 2.5YR) and Weak Red (4/2 2.5YR)
Bleaching	Absent
Odor	Absent

#### Sample 6

<b>Features</b>	<b>Evaluation</b>
General state of bone	Incomplete left femur at the proximal epiphysis
Cortical surface appearance	Incomplete (< 50%)
Fatty substance	Absent
Skin, muscles and ligaments	Absent
Spongy tissue	Exposed on proximal epiphysis and anterior medial condyle. The colors are Reddish Brown (5/4 5YR) and Very Pale Brown (8/4 10YR)
Tissue in medullary cavity	Absent
Cracking	Longitudinal
Flaking	Absent
Color	Very Pale Brown (8/3 10YR), Brownish Yellow (6/6 10Y) and Yellowish Brown (5/6 10YR)
Bleaching	Absent
Odor	Absent

#### Sample 7

<b>Features</b>	<b>Evaluation</b>
General state of bone	Incomplete left femur at proximal epiphysis
Cortical surface appearance	Incomplete (< 50%)
Fatty substance	Absent
Skin, muscles and ligaments	Absent



Spongy tissue	Exposed on proximal epiphysis with Light Brown (6/4 7.5YR) and Very Pale Brown (7/3 10YR) colors, and on distal condyles with Brown (5/3 10YR) and Light Yellowish Brown (6/4 10YR) colors
Tissue in medullary cavity	Absent
Cracking	Longitudinal
Flaking	Absent
Color	Very Pale Brown (8/3 10YR), Dark Brown (4/3 10YR) and Brownish Yellow (6/6 10YR)
Bleaching	Absent
Odor	Absent

#### Sample 8

Features	Evaluation
General state of bone	Incomplete right femur at both epiphyses
Cortical surface appearance	Complete (100%)
Fatty substance	Absent
Skin, muscles and ligaments	Absent
Spongy tissue	Exposed on both epiphyses. The colors are Pale Brown (6/3 10YR) and Pinkish White (8/2 7.5YR)
Tissue in medullary cavity	Absent
Cracking	Absent
Flaking	Absent
Color	Light Brown (6/4 7.5YR) and Very Pale Brown (8/3 10YR)
Bleaching	Absent
Odor	Absent

#### Sample 9

Features	Evaluation
General state of bone	Incomplete left femur at the head
Cortical surface appearance	Incomplete (< 50%)
Fatty substance	Absent
Skin, muscles and ligaments	Absent
Spongy tissue	Exposed on proximal metaphysis with Light Brown (6/6 7.5 YR) and Reddish Yellow (6/8 10Y) colors, and on distal metaphysis with Yellonish Brown (5/8 10YR) and Dark Yellowish Brown (5/6 10YR) colors

Tissue in medullary cavity	Absent
Cracking	Longitudinal
Flaking	Absent
Color	Light Yellowish Brown (6/4 10YR), Yellowish Brown (5/6 10YR and 5/4 10YR)
Bleaching	Absent
Odor	Absent

**Sample 10**

<b>Features</b>	<b>Evaluation</b>
General state of bone	Incomplete right femur at both epiphyses
Cortical surface appearance	Incomplete (< 50%)
Fatty substance	Absent
Skin, muscles and ligaments	Absent
Spongy tissue	Exposed on both epiphysis. The color is Light Yellowish Brown (6/4 10YR)
Tissue in medullary cavity	Absent
Cracking	Longitudinal
Flaking	Absent
Color	Yellow (7/6 10Y) and Brownish Yellow (6/6 10YR)
Bleaching	Absent
Odor	Absent

**Population 3**

**Sample 1**

<b>Features</b>	<b>Evaluation</b>
General state of bone	Incomplete left femur at the epiphyses
Cortical surface appearance	Incomplete (<50%)
Fatty substance	Absent
Skin, muscles and ligaments	Absent
Spongy tissue	Exposed on both epiphyses. The color is Pale Yellow (8/3 2.5Y)
Tissue in medullary cavity	Absent
Cracking	Absent
Flaking	Absent

Color	Light Yellow Orange (8/4 10YR) with veins Brownish Black (3/2 7.5YR)
Bleaching	Present
Odor	Absent

**Sample 2**

<b>Features</b>	<b>Evaluation</b>
General state of bone	Incomplete right femur at the epiphyses
Cortical surface appearance	Incomplete (<50%)
Fatty substance	Absent
Skin, muscles and ligaments	Absent
Spongy tissue	Exposed on both epiphyses. The color is Pale Yellow (8/3 2.5Y)
Tissue in medullary cavity	Absent
Cracking	Absent
Flaking	Absent
Color	Pale yellow (8/4 2.5Y) and Dark brown (3/4 7.5YR)
Bleaching	Absent
Odor	Absent

**Sample 3**

<b>Features</b>	<b>Evaluation</b>
General state of bone	Incomplete right femur at the epiphyses
Cortical surface appearance	Incomplete (<50%)
Fatty substance	Absent
Skin, muscles and ligaments	Absent
Spongy tissue	Exposed on both epiphyses. The color is Pale Yellow (8/3 2.5Y)
Tissue in medullary cavity	Absent
Cracking	Absent
Flaking	Absent
Color	Small zones Pale Yellow (8/4 2.5Y), veins Dark Brown (3/4 7.5YR),
Bleaching	Absent
Odor	Absent

**Sample 4**

<b>Features</b>	<b>Evaluation</b>
-----------------	-------------------

General state of bone	Incomplete right femur at the distal third
Cortical surface appearance	Incomplete (<50%)
Fatty substance	Absent
Skin, muscles and ligaments	Absent
Spongy tissue	Exposed on distal third. The color is Pale Yellow (8/3 2.5Y).
Tissue in medullary cavity	Absent
Cracking	Absent
Flaking	Present
Color	Brownish Black (2/1 5YR) and Brown (4/4 7.5YR)
Bleaching	Absent
Odor	Absent

#### Sample 5

Features	Evaluation
General state of bone	Incomplete right femur at the epiphyses
Cortical surface appearance	Incomplete (<50%)
Fatty substance	Absent
Skin, muscles and ligaments	Absent
Spongy tissue	Exposed on both epiphyses. The color is Pale Yellow (8/3 2.5Y)
Tissue in medullary cavity	Absent
Cracking	Absent
Flaking	Present
Color	Light Grey (8/2 2.5Y), with small zones Dull Yellow Orange (7/4 10YR) and Brownish Black (3/1 10YR)
Bleaching	Present
Odor	Absent

#### Sample 6

Features	Evaluation
General state of bone	Incomplete left tibia at the epiphyses
Cortical surface appearance	Incomplete (<50%)
Fatty substance	Absent

Skin, muscles and ligaments	Absent
Spongy tissue	Exposed on both epiphyses. The color is Pale Yellow (8/3 2.5Y).
Tissue in medullary cavity	Absent
Cracking	Present
Flaking	Present
Color	Small zones Pale Yellow (8/4 2.5Y) and veins Dark Brown (3/4 7.5YR)
Bleaching	Absent
Odor	Absent

#### Sample 7

Features	Evaluation
General state of bone	Incomplete left tibia at the epiphyses
Cortical surface appearance	Incomplete (<50%)
Fatty substance	Absent
Skin, muscles and ligaments	Absent
Spongy tissue	Exposed on both epiphyses. The color is Light Grey (8/2 25Y).
Tissue in medullary cavity	Absent
Cracking	Absent
Flaking	Present
Color	Light Grey (8/2 25Y), with small zones Dull Yellow Orange (7/4 10YR)
Bleaching	Present
Odor	Absent

#### Sample 8

Features	Evaluation
General state of bone	Incomplete right tibia at proximal epiphyses
Cortical surface appearance	Incomplete (<50%)
Fatty substance	Absent
Skin, muscles and ligaments	Absent
Spongy tissue	Exposed on proximal epiphyses. The color is Pale Yellow (8/3 2.5Y).
Tissue in medullary cavity	Absent
Cracking	Absent

Flaking	Absent
Color	Small zones Pale Yellow (8/4 2.5Y), veins Dark Brown (3/4 7.5YR),
Bleaching	Absent
Odor	Absent

**Sample 9**

<b>Features</b>	<b>Evaluation</b>
General state of bone	Incomplete left tibia at the proximal epiphysis
Cortical surface appearance	Incomplete (<50%)
Fatty substance	Absent
Skin, muscles and ligaments	Absent
Spongy tissue	Exposed on proximal epiphysis. The color is Pale Yellow (8/3 2.5Y).
Tissue in medullary cavity	Absent
Cracking	Absent
Flaking	Present
Color	Small zones Bright Yellowish Brown (6/6 10YR), veins Brownish Black (3/1 7.5YR), Dark Brown (3/3 7.5YR)
Bleaching	Present
Odor	Absent

**Sample 10**

<b>Features</b>	<b>Evaluation</b>
General state of bone	Incomplete right tibia at the distal third
Cortical surface appearance	Incomplete (<50%)
Fatty substance	Absent
Skin, muscles and ligaments	Absent
Spongy tissue	Exposed on distal third. The color is Pale Yellow (8/3 2.5Y).
Tissue in medullary cavity	Absent
Cracking	Absent
Flaking	Present
Color	Small zones Bright Yellowish Brown (6/6 10YR) and Brownish Black (3/1 7.5YR)
Bleaching	Present
Odor	Absent

**Population 4**

**Sample 1**

<b>Features</b>	<b>Evaluation</b>
General state of bone	Complete left tibia
Cortical surface appearance	Complete (100%)
Fatty substance	Absent
Skin, muscles and ligaments	Absent
Spongy tissue	Exposed on anterior proximal epiphysis. The color is Black (2/1 10YR)
Tissue in medullary cavity	Absent
Cracking	Longitudinal
Flaking	Absent
Color	Black (2/1 10YR); Reddish Brown (4/4 5YR); Dark Brown (4/4 7.5YR)
Bleaching	Absent
Odor	Asbent

**Sample 2**

<b>Features</b>	<b>Evaluation</b>
General state of bone	Complete right tibia
Cortical surface appearance	Incomplete (<50%)
Fatty substance	Absent
Skin, muscles and ligaments	Absent
Spongy tissue	Exposed on both epiphyses. Yellowish color Dark Brown (4/4 10YR)
Tissue in medullary cavity	Absent
Cracking	Absent
Flaking	Islet and <50%, present on the most proximal portion of the mid-diaphysis in the medial face
Color	Dark Reddish Gray (4/2 5YR); Dark Yellowish Brown (4/4 10YR)
Bleaching	Absent
Odor	Absent

**Sample 3**

<b>Features</b>	<b>Evaluation</b>
General state of bone	Complete right tibia
Cortical surface appearance	Complete (100%)

Fatty substance	Absent
Skin, muscles and ligaments	Absent
Spongy tissue	Not exposed
Tissue in medullary cavity	Absent
Cracking	Absent
Flaking	Absent
Color	Dark Reddish Brown (3/4 2.5YR); Yellowish Brown (5/4 10YR); Dark Brown (3/3 10YR); Brownish Yellow (6/8 10Y)
Bleaching	Absent
Odor	Absent

#### Sample 4

<b>Features</b>	<b>Evaluation</b>
General state of bone	Complete left femur
Cortical surface appearance	Complete (100%)
Fatty substance	Absent
Skin, muscles and ligaments	Absent
Spongy tissue	Exposed on head and anterior great and less trochanter and on two distal lateral condyles. The color is Dusky Red (3/4 10R) and the loss is <50%
Tissue in medullary cavity	Absent
Cracking	Absent
Flaking	Absent
Color	Reddish Black (2.5/1 10R); Dusky Red (3/4 10R)
Bleaching	Absent
Odor	Absent

#### Sample 5

<b>Features</b>	<b>Evaluation</b>
General state of bone	Incomplete right femur at the head
Cortical surface appearance	Complete (100%)
Fatty substance	Absent
Skin, muscles and ligaments	Absent
Spongy tissue	Exposed on the proximal epiphysis. The color is Brown (5/3 10YR)



Tissue in medullary cavity	Absent
Cracking	Absent
Flaking	Absent
Color	Very Dark Brown (2/2 10YR); Brown (5/3 10YR); Olive Yellow (6/6 2.5Y)
Bleaching	Absent
Odor	Absent

#### Sample 6

<b>Features</b>	<b>Evaluation</b>
General state of bone	Complete right femur
Cortical surface appearance	Complete (100%)
Fatty substance	Absent
Skin, muscles and ligaments	Absent
Spongy tissue	Exposed on great trochanter. Brown color (7/4 7.5YR). The exposure is <50%
Tissue in medullary cavity	Absent
Cracking	Absent
Flaking	Absent
Color	Very Dark Brown (2/2 10YR); Brown (5/3 10YR); Olive Yellow (6/6 2.5Y)
Bleaching	Absent
Odor	Absent

#### Sample 7

<b>Features</b>	<b>Evaluation</b>
General state of bone	Complete right tibia
Cortical surface appearance	Incomplete (<50%)
Fatty substance	Absent
Skin, muscles and ligaments	Absent
Spongy tissue	Not exposed
Tissue in medullary cavity	Absent
Cracking	Absent
Flaking	Absent
Color	Black (2/1 10YR); Brown (7/4 7.5YR); Strong Brown (4/6 7.5YR)
Bleaching	Absent

Odor	Absent
<b>Sample 8</b>	
<b>Features</b>	<b>Evaluation</b>
General state of bone	Complete left femur
Cortical surface appearance	Incomplete (>50%)
Fatty substance	Absent
Skin, muscles and ligaments	Absent
Spongy tissue	Exposed on lateral and posterior distal end. The color is Black (2/1 10YR) and the loss is <50%
Tissue in medullary cavity	Absent
Cracking	Absent
Flaking	Diffused all over the bone and > 50%
Color	Black (2/1 10YR); Reddish Brown (4/4 5YR);
Bleaching	Absent
Odor	Absent
<b>Sample 9</b>	
<b>Features</b>	<b>Evaluation</b>
General state of bone	Incomplete right femur at the proximal epiphysis and lateral and medial condyles
Cortical surface appearance	Complete (100%)
Fatty substance	Absent
Skin, muscles and ligaments	Absent
Spongy tissue	Exposed on both epiphyses. The colors are Dark Yellowish Brown (4/4 10YR) and Dark Reddish Gray (4/2 5YR)
Tissue in medullary cavity	Absent
Cracking	Absent
Flaking	Absent
Color	Very Dark Brown (2/2 10YR); Brown (5/3 10YR); Olive Yellow (6/6 2.5Y)
Bleaching	Absent
Odor	Absent
<b>Sample 10</b>	
<b>Features</b>	<b>Evaluation</b>

---

General state of bone	Complete right tibia
Cortical surface appearance	Complete (100%)
Fatty substance	Absent
Skin, muscles and ligaments	Absent
Spongy tissue	Exposed on anterior proximal epiphysis. The color is Dark Reddish Gray (4/2 5YR)
Tissue in medullary cavity	Absent
Cracking	Absent
Flaking	Absent
Color	Black (2/1 10YR), Dark Yellowish Brown (3/4 10YR), Very Pale Brown (7/4 10YR)
Bleaching	Absent
Odor	Asbent

---

## 7.2 - Appendix 2

Comparison of the results carried out by macroscopic, microscopic and chemiluminescence analyses performed on bones from Population 1, 2, 3 and 4.

Population	Sample	Macroscopic classification (Behrensmeier's stage)	Calcified microscopy (OHI score)	Decalcified microscopy (DHI score)	Luminol test (chemiluminescence score)
1	1	0	0/1	1	+
	2	1	0	1	+
	3	1	0/1	1	-
	4	0	1	3	+
	5	0	0/1	1	-
	6	0	1	2	-
	7	0	0	1	-
	8	2	0	1	-
	9	0	0	1	-
	10	2	1	1	-
2	1	1	0	1	-
	2	1	1/2	1	-
	3	1	1	1	-
	4	1	3	1	-
	5	2	4/5	3	-
	6	3	2/3	2	-
	7	3	0	1	+
	8	2	0	1	-
	9	4	1/2	3	-
	10	3	3	2	-
3	1	0	1	2	-
	2	0	3	2	-
	3	0	4	3	+
	4	3/4	4	3	-
	5	0	4	3	-
	6	2	3	3	-
	7	2	3	1	+
	8	0	3/4	2	-
	9	0	2/3	3	+

---

	10	3	3/4	3	-
	1	0	3/4	3	-
	2	2	4	3	++
	3	0	4	3	++
	4	2	3	2	-
4	5	1	4	3	++
	6	1	4	3	+
	7	2	3	3	++
	8	1	4/5	3	++
	9	0	3/4	3	++
	10	0	4	3	++

---

### 7.3 - Appendix 3

Oxides detected by SEM-EDS analysis performed on archaeological and recent bones coming from Population 1, 2, 3 and 4.

Population	Analysis	Oxide																												
		Na <sub>2</sub> O	MgO	Al <sub>2</sub> O <sub>3</sub>	SiO <sub>2</sub>	P <sub>2</sub> O <sub>5</sub>	SO <sub>3</sub>	K <sub>2</sub> O	CaO	TiO <sub>2</sub>	MnO	FeO	SnO <sub>2</sub>	BaO	Cr <sub>2</sub> O <sub>3</sub>	CuO	PbO	Bi <sub>2</sub> O <sub>3</sub>	Sb <sub>2</sub> O <sub>3</sub>	La <sub>2</sub> O <sub>3</sub>	Ce <sub>2</sub> O <sub>3</sub>	Nd <sub>2</sub> O <sub>3</sub>	ZnO	NiO	SrO	CoO	ThO			
1	1	48.5	0.2	0.5	0.0	0.0	21.9	0.3	0.0	0.1	28.3	0.0	0.0	0.0	0.0	0.0	0.0	0.0	0.0	0.0	0.0	0.0	0.0	0.1	0.0	0.0	0.0	0.0	0.0	
	2	42.7	0.0	0.4	0.0	0.0	25.2	0.5	0.0	31.2	0.0	0.0	0.0	0.0	0.0	0.0	0.0	0.0	0.0	0.0	0.0	0.0	0.0	0.0	0.0	0.0	0.0	0.0	0.0	
	3	21.3	0.6	0.5	0.0	0.0	33.6	0.5	0.0	43.5	0.0	0.0	0.0	0.0	0.0	0.0	0.0	0.0	0.0	0.0	0.0	0.0	0.0	0.0	0.0	0.0	0.0	0.0	0.0	0.0
	4	1.7	0.3	0.1	0.2	26.0	1.1	0.3	30.5	0.3	0.0	39.5	0.0	0.0	0.0	0.0	0.0	0.0	0.0	0.0	0.0	0.0	0.0	0.0	0.0	0.0	0.0	0.0	0.0	
	5	1.5	0.4	0.2	0.2	44.6	1.1	0.0	18.3	0.0	20.2	13.4	0.0	0.0	0.0	0.0	0.0	0.0	0.0	0.0	0.0	0.0	0.0	0.0	0.0	0.0	0.0	0.0	0.0	
	6	0.0	0.4	0.1	1.6	15.6	0.2	0.4	14.3	0.0	0.4	65.7	0.0	0.0	0.0	0.0	0.0	0.0	0.0	0.0	0.0	0.0	0.0	0.0	1.3	0.0	0.0	0.0	0.0	
	7	0.4	0.8	4.4	6.9	1.2	0.1	0.6	2.4	42.3	2.4	38.6	0.0	0.0	0.0	0.0	0.0	0.0	0.0	0.0	0.0	0.0	0.0	0.0	0.0	0.0	0.0	0.0	0.0	
	8	0.3	0.7	2.4	81.6	8.6	0.0	0.8	5.7	0.0	0.0	0.0	0.0	0.0	0.0	0.0	0.0	0.0	0.0	0.0	0.0	0.0	0.0	0.0	0.0	0.0	0.0	0.0	0.0	
	9	1.3	0.0	18.2	59.9	0.4	0.0	18.9	0.7	0.5	0.0	0.0	0.0	0.0	0.0	0.0	0.0	0.0	0.0	0.0	0.0	0.0	0.0	0.0	0.0	0.0	0.0	0.0	0.0	
	10	14.8	0.1	18.8	63.9	1.1	0.0	0.1	1.1	0.0	0.0	0.0	0.0	0.0	0.0	0.0	0.0	0.0	0.0	0.0	0.0	0.0	0.0	0.0	0.0	0.0	0.0	0.0	0.0	











## 7.4 - Appendix 4

Minerals detected by SEM-EDS analysis performed on archaeological and recent bones coming from Population 1, 2, 3 and 4.

Population	Analysis	Minerals											
		K-feldspar	Barite	Ilmenite	Potassium chloride	Rutile	Pyrite	Chlorite	Zircon	Albite	Quartz	Clay	
1	36	0	0	1	0	0	0	0	0	0	0	0	0
	37	0	0	0	0	0	0	0	0	1	0	0	0
	38	1	0	0	0	0	0	0	0	0	0	0	0
	39	0	0	0	0	0	0	0	0	0	1	0	0
	40	0	0	0	0	0	0	0	0	0	0	1	0
	41	0	0	0	0	0	0	0	0	0	0	0	1
	42	0	0	0	0	0	0	0	0	0	0	0	1
	43	0	0	0	0	0	0	0	0	0	0	0	1
	44	0	0	0	0	0	0	0	0	0	0	0	0
	45	0	1	0	0	0	0	0	0	0	0	0	1
	46	0	1	0	0	0	0	0	0	0	1	0	1
	47	0	0	0	0	0	0	0	0	0	0	0	0
	48	0	0	1	0	0	0	0	0	0	0	0	1
	49	0	0	0	0	0	0	1	0	0	0	0	0
	50	0	1	0	0	0	0	0	0	0	1	0	1
	51	0	1	0	0	0	0	0	0	0	0	0	1
2	52	0	0	0	0	1	0	0	0	0	0	0	0
	53	0	1	0	1	0	0	0	0	0	0	0	0

	54	0	0	0	0	0	0	0	0	0	0	1	0
	55	0	0	0	0	1	0	0	0	0	0	0	0
3	56	0	0	0	0	1	1	0	0	0	0	0	0
	57	0	1	0	0	0	0	1	0	0	0	0	0
	58	1	0	0	0	0	0	0	0	0	0	0	0
4	59	0	1	1	0	0	0	0	0	0	0	0	0

## 7.5 - Appendix 5

Morphological parameters observed on archaeological and recent bones coming from Population 1, 2, 3 and 4 with SEM.

Population	Sample	preserved osteons			degraded areas			remineralized zones	cracks related to bone structure			cracks not related to bone structure				
		internal cortical border	central cortical	external cortical border	internal cortical border	central cortical	external cortical border		central cortical	external cortical border	internal cortical border	central cortical	external cortical border			
1	1		X		X	X	X	X	X	X	X	X	X	X	X	
	2	X	X		X	X	X	X	X	X	X	X	X	X	X	
	3		X		X	X	X	X	X		X		X	X	X	
	4		X		X	X	X	X	X	X			X	X	X	
	5				X	X	X	X	X						X	
	6		X		X	X	X	X	X				X	X	X	
	7				X	X	X	X	X				X	X	X	
	8				X	X	X	X	X				X	X	X	
	9	X		X	X	X	X	X	X	X				X	X	X
	10			X	X	X	X	X	X	X	X	X	X	X	X	X

2	1				X	X	X	X	X	X					
	2	X		X	X	X	X		X		X	X	X	X	X
	3	X	X	X	X	X	X	X	X	X	X	X	X	X	X
	4	X	X	X			X				X	X	X	X	X
	5	X	X	X			X	X		X	X	X	X	X	X
	6		X	X	X	X	X	X	X	X	X	X	X	X	X
	7	X			X	X	X	X	X	X	X	X	X	X	X
	8	X	X	X			X			X	X	X	X	X	X
	9				X	X	X	X	X	X				X	X
	10	X	X	X	X		X	X		X	X	X	X	X	X
3	1	X	X	X	X	X	X	X	X	X	X	X	X	X	X
	2	X	X	X	X		X	X		X	X	X	X	X	X
	3	X	X	X	X		X	X		X				X	X
	4	X	X	X							X	X	X	X	X
	5		X	X	X	X	X	X	X	X	X	X	X	X	
	6	X	X	X		X	X		X	X	X	X	X	X	X
	7		X		X		X	X	X	X			X	X	X
	8	X	X	X	X		X				X	X	X	X	X
	9	X	X	X	X	X	X	X	X	X	X	X	X	X	X
	10	X	X	X							X	X	X	X	X
4	1	X	X	X						X	X	X	X	X	
	2	X	X	X			X			X	X	X	X	X	
	3	X	X	X						X	X	X	X	X	
	4	X	X	X			X	X	X	X	X	X	X	X	
	5	X	X	X						X	X	X	X	X	
	6	X	X	X						X	X	X	X	X	

---

7	X	X	X			X	X	X	X	X	X
8	X	X	X		X	X	X	X	X	X	X
9	X	X	X						X	X	X
10	X	X	X			X	X	X	X	X	X

---

## 7.6 - Appendix 6

Tomographic results carried out by imaging analysis of 24 bone samples coming from Milan.

Morphometric parameter	Population 1						Population 2						Population 3						Population 4					
	sample 2	sample 3	sample 4	sample 5	sample 8	sample 10	sample 1	sample 2	sample 3	sample 5	sample 8	sample 10	sample 3	sample 4	sample 5	sample 8	sample 9	sample 10	sample 1	sample 2	sample 4	sample 5	sample 7	sample 10
% Total bone porosity	6.7	16.3	11.2	13.0	12.8	11.9	8.0	16.2	23.9	2.8	21.4	19.7	16.2	6.1	19.6	9.0	7.0	2.7	15.3	14.0	20.4	26.2	7.3	17.7
% Canals porosity	1.3	2.9	5.8	8.5	2.5	0.8	1.8	3.7	8.1	1.2	1.3	18.7	1.4	4.9	1.5	5.0	4.6	1.9	13.0	12.4	18.2	25.5	3.6	17.1
% Lacunae porosity	/	/	/	/	/	/	/	/	/	1.7	/	0.3	0.7	1.2	/	1.7	0.4	0.6	1.5	1.4	/	0.7	1.4	0.4
% Remineralized areas	15.6	6.7	4.8	10.4	8.6	3.7	3.6	10.8	10.0	0.0	6.9	0.0	3.00	0.0	0.8	0.0	0.0	0.0	0.0	0.0	3.6	0.0	0.0	0.0
Canals volume ( $\mu\text{m}^3$ )	2.4	0.6	6.3	27.4	1.9	1.3	1.1	1.6	1.2	1.6	1.4	15.7	1.1	2.7	1.1	1.6	4.5	1.2	10.3	6.3	20.5	28.5	4.5	22.9

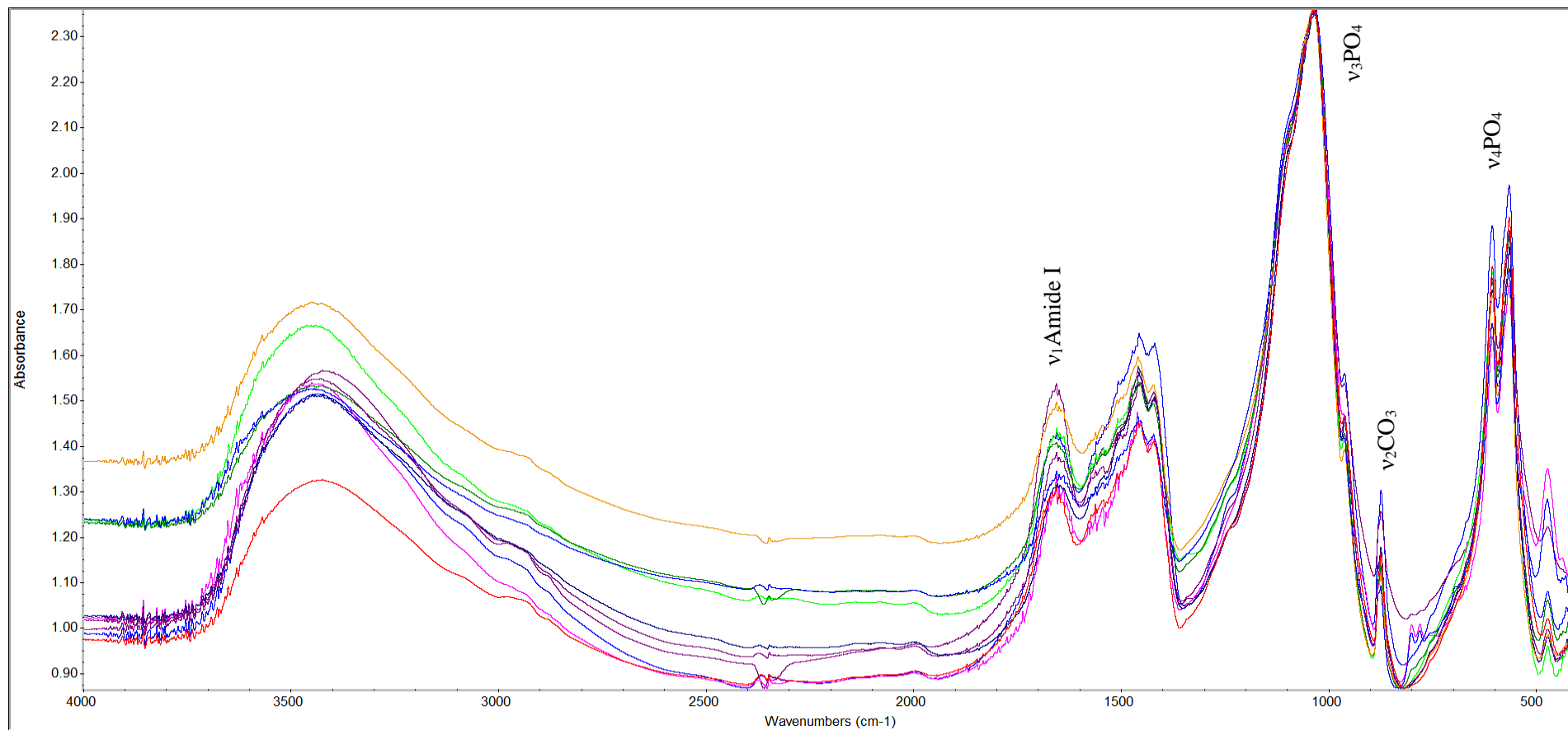


Lacunae volume ( $\mu\text{m}^3$ )	/	/	/	/	/	/	/	/	/	/	1e <sup>-03</sup>	/	4.6e <sup>-04</sup>	6.6e <sup>-04</sup>	5.1e <sup>-04</sup>	/	2.5 e <sup>-04</sup>	7.5 e <sup>-04</sup>	3.2 e <sup>-04</sup>	1.1 e <sup>-03</sup>	4.3 e <sup>-04</sup>	/	5.4 e <sup>-04</sup>	1 e <sup>-03</sup>	6.5 e <sup>-04</sup>
Canals surface ( $\mu\text{m}^2$ )	193.7	81.1	356	903.6	119.1	165.5	108.9	155.7	164.9	199.6	133.2	568	121.7	220.8	109.4	155.5	304	124.3	456.8	330.7	744.2	1021.2	481.3	924.7	
Lacunae surface ( $\mu\text{m}^2$ )	/	/	/	/	/	/	/	/	/	0.8	/	0.4	0.6	0.4	/	0.2	0.5	0.3	0.8	0.3	/	0.4	1	0.5	
Canals surface/ canls volume	124.9	150.1	115.7	114.4	166.4	136.0	127.1	134.5	181.1	143.1	140.4	79.7	130.7	140.9	114.4	144.6	102.9	165.5	87.7	92.4	103.7	93.3	154.1	90.5	
Lacunae surface/ lacunae volume	/	/	/	/	/	/	/	/	/	915.2	/	1030.5	1020.2	981.7	/	1097.5	953	1059.5	886	974.8	/	907.5	1023.9	953.9	
3D canals length ( $\mu\text{m}$ )	793.1	650.9	1012.3	1020.3	518.2	527.3	643.9	688.6	666.4	764.1	424.3	1253.3	676	950.7	697.4	796.2	785.1	901.8	652.7	874.1	900.4	1364.8	729	926.6	
3D canals width ( $\mu\text{m}$ )	0.07	0.08	0.1	0.18	0.08	0.08	0.1	0.08	0.1	0.09	0.08	0.2	0.07	0.1	0.1	0.1	0.1	0.1	0.1	0.1	0.1	0.2	0.1	0.1	
3D lacunae length ( $\mu\text{m}$ )	/	/	/	/	/	/	/	/	/	2.6	/	1.8	2.2	2.7	/	3.4	2.1	3.0	1.9	3.1	/	2.5	1.3	1.9	

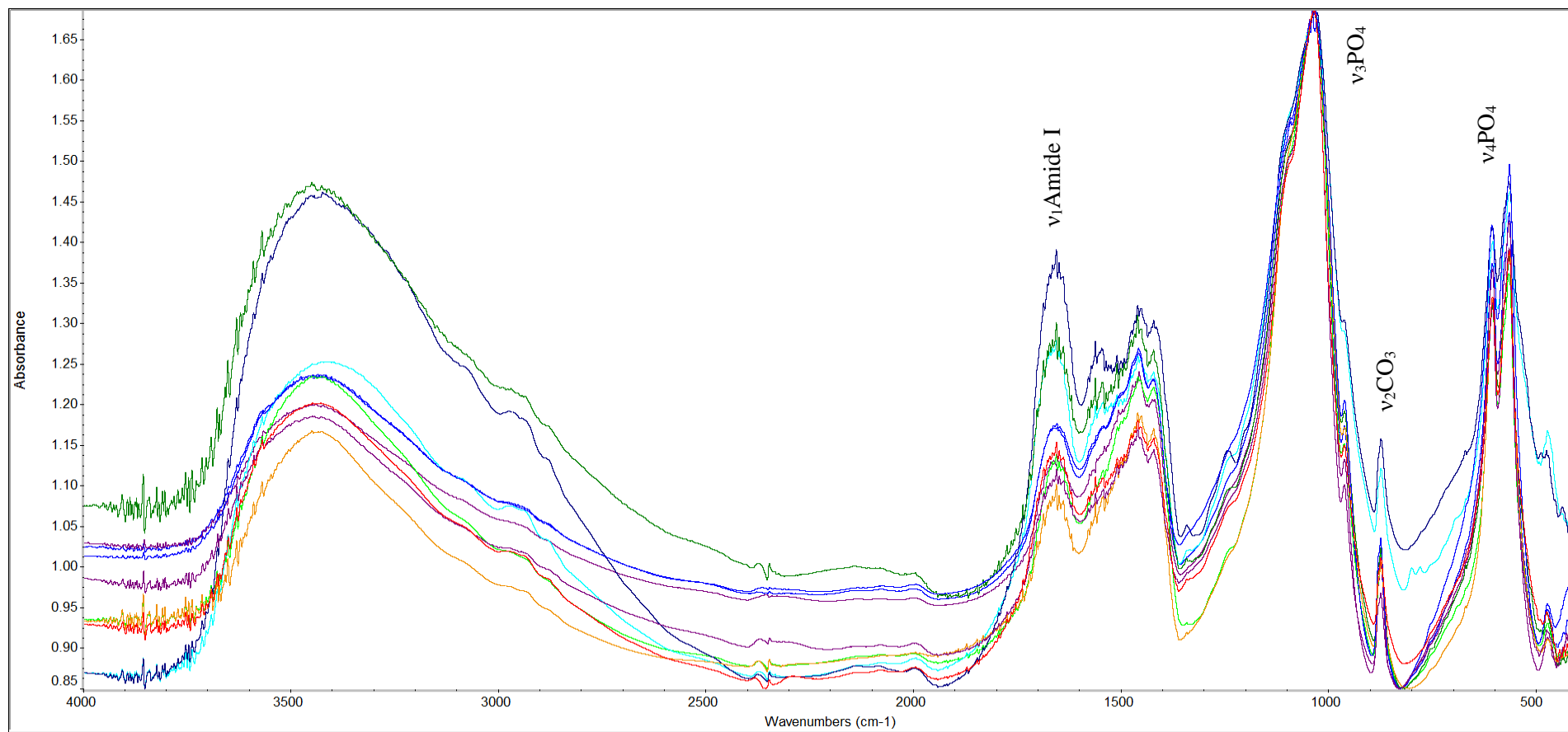
3D lacunae width ( $\mu\text{m}$ )	/	/	/	/	/	/	/	/	/	/	0.3	/	0.1	0.2	0.3	0.3	0.2	0.3	0.2	0.3	/	0.2	0.1	0.2
canals aspect ratio	0	0.4	0.4	1.9	3.4	0	1.6	0.4	6.4	0	2.3	0.7	2.3	2.5	1.2	1.5	0	0.8	0.8	0.4	0	0.9	3.4	2.6
lacunae aspect ratio	/	/	/	/	/	/	/	/	/	9.6	/	7.6	9.3	7.1	/	5.3	7.7	6.2	9	6	/	5.6	13.2	7.6

## 7.7 - Appendix 7

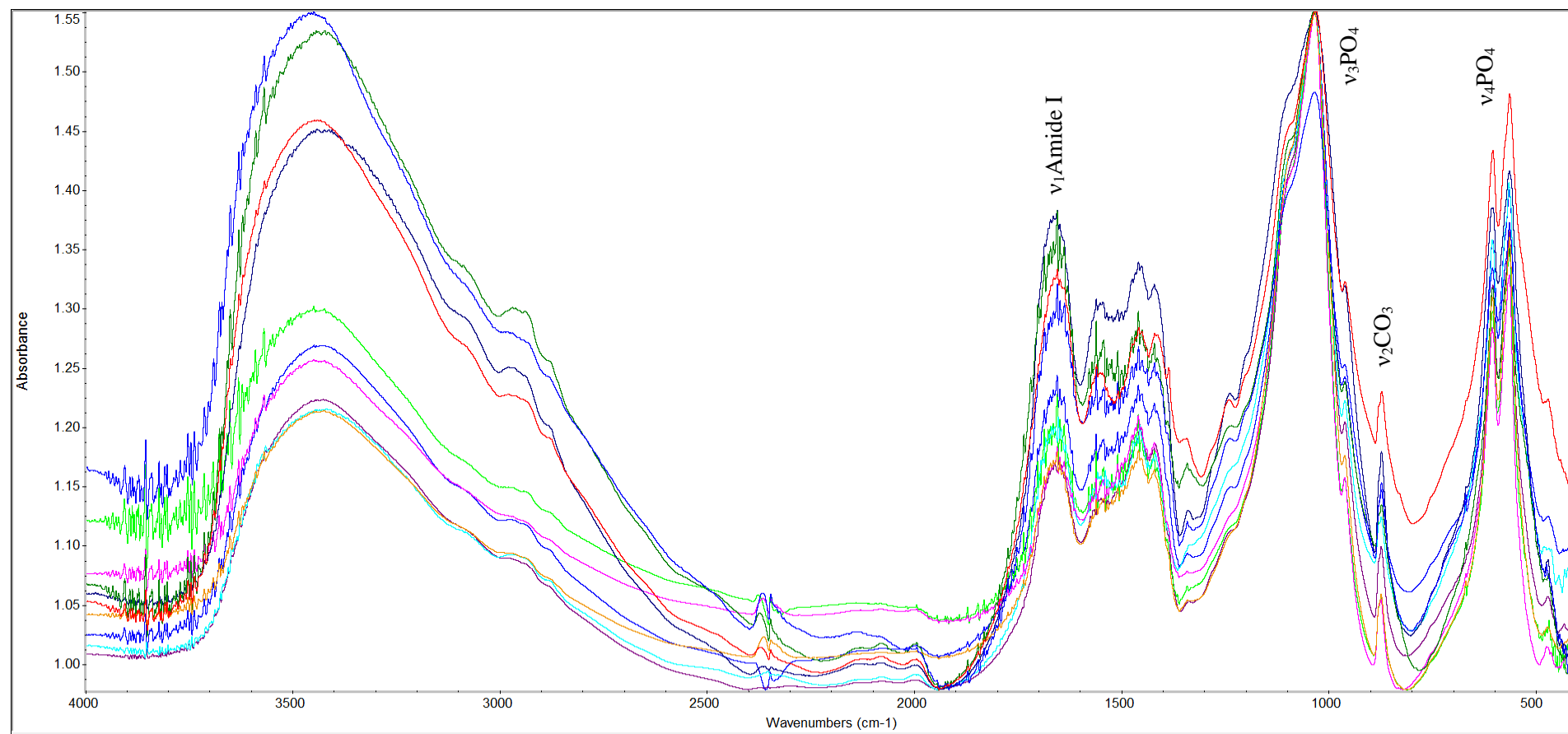
IR spectra detected by FT-IR spectrometer from the 40 bone powders coming from Population 1, 2, 3 and 4.



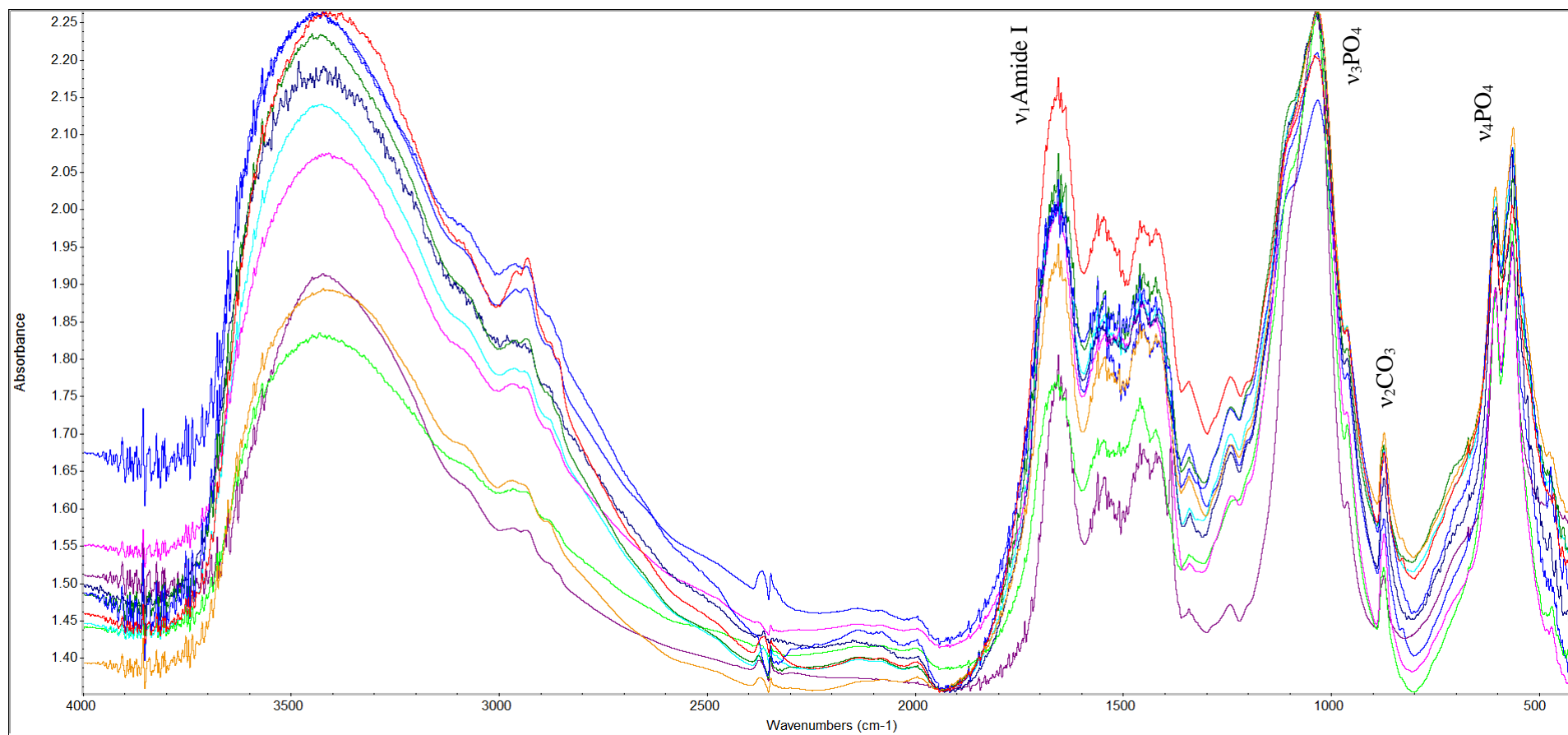
- Population 1 -



- Population 2 -



- Population 3 -



- Population 4 -

## 7.8 - Appendix 8

Results obtained by measuring the ratios of  $\nu_1\text{AmI}/\nu_3\text{PO}_4$  and  $\nu_2\text{CO}_3/\nu_3\text{PO}_4$  and the infrared splitting factor (IRSF) from the spectra detected with FT-IR spectrometry for each bone powders coming from Population 1, 2, 3 and 4.

Population	Sample	$\nu_1\text{AmI}/\nu_3\text{PO}_4$ ratio	$\nu_2\text{CO}_3/\nu_3\text{PO}_4$ ratio	IRSF
1	1	0.36	0.49	2.61
	2	0.41	0.38	2.79
	3	0.30	0.38	2.74
	4	0.21	0.26	3.62
	5	0.25	0.40	2.82
	6	0.27	0.35	2.85
	7	0.27	0.34	2.84
	8	0.21	0.29	3.08
	9	0.31	0.41	2.78
	10	0.28	0.35	2.80
2	1	0.29	0.39	2.85
	2	0.25	0.36	2.87
	3	0.31	0.42	2.87
	4	0.50	0.42	2.81
	5	0.69	0.52	2.61
	6	0.42	0.42	2.76
	7	0.26	0.36	2.85
	8	0.29	0.39	2.76
	9	0.27	0.32	3.01
	10	0.34	0.35	2.92
3	1	0.43	0.36	2.85
	2	0.33	0.34	2.91
	3	0.35	0.29	3.02
	4	0.68	0.48	2.79
	5	0.32	0.30	2.99
	6	0.39	0.31	2.96
	7	0.28	0.31	2.99
	8	0.71	0.58	2.53
	9	0.64	0.51	2.61
	10	0.65	0.48	2.81
4	1	0.81	0.55	2.71
	2	0.49	0.32	2.98
	3	0.67	0.51	2.69
	4	0.42	0.36	2.88
	5	0.78	0.54	2.64

---

6	0.74	0.53	2.82
7	0.85	0.59	2.61
8	0.70	0.50	2.72
9	0.80	0.58	2.62
10	1.04	0.73	2.52

---



## 7.9 - Appendix 9

Results of the SEM-EDS analysis performed on bone sections and grave soils from the archaeological site of Travo.

<b>Tomb 16</b>											
<b>Soil US 201</b>											
	MgO	Al <sub>2</sub> O <sub>3</sub>	SiO <sub>2</sub>	P <sub>2</sub> O <sub>5</sub>	SO <sub>3</sub>	K <sub>2</sub> O	CaO	TiO <sub>2</sub>	MnO	FeO	NiO
analysis 1, clay rich in MnO and FeO	2.84	16.89	37.27	1.30	0.11	3.60	3.87	1.01	24.64	7.85	0.62
	MgO	Al <sub>2</sub> O <sub>3</sub>	SiO <sub>2</sub>	P <sub>2</sub> O <sub>5</sub>	SO <sub>3</sub>	K <sub>2</sub> O	CaO	TiO <sub>2</sub>	MnO	FeO	NiO
analysis 2, clay rich in FeO	3.22	21.67	60.60	0.65	4.36	2.39	0.37	0.08	6.63	0.03	
	MgO	Al <sub>2</sub> O <sub>3</sub>	SiO <sub>2</sub>	P <sub>2</sub> O <sub>5</sub>	K <sub>2</sub> O	CaO	TiO <sub>2</sub>	MnO	FeO	NiO	
analysis 3, calcium phosphate	1.83	15.89	37.24	1.86	4.13	4.66	0.71	25.97	7.16	0.56	
FeO											
MnO											
ilmenite											
<b>Bone US 128</b>											
	MgO	Al <sub>2</sub> O <sub>3</sub>	SiO <sub>2</sub>	P <sub>2</sub> O <sub>5</sub>	SO <sub>3</sub>	K <sub>2</sub> O	CaO	TiO <sub>2</sub>	MnO	FeO	NiO
analysis 1, clay rich in MnO	0.20	0.01	0.01	36.24	0.46	0.04	44.65	0.53	15.28	2.14	0.44
	MgO	Al <sub>2</sub> O <sub>3</sub>	SiO <sub>2</sub>	P <sub>2</sub> O <sub>5</sub>	SO <sub>3</sub>	K <sub>2</sub> O	CaO	TiO <sub>2</sub>	MnO	FeO	NiO
analysis 2, clay rich in FeO	2.57	21.77	58.33	0.43	0.03	6.37	2.70	0.62	0.00	7.16	0.03
MnO											
<b>Tomb 17</b>											
<b>Soil US 203</b>											
	MgO	Al <sub>2</sub> O <sub>3</sub>	SiO <sub>2</sub>	P <sub>2</sub> O <sub>5</sub>	SO <sub>3</sub>	K <sub>2</sub> O	CaO	TiO <sub>2</sub>	MnO	FeO	NiO
analysis 1, clay	1.35	11.00	80.50	0.05	0.04	2.49	0.84	0.17	0.20	3.16	0.20
	MgO	Al <sub>2</sub> O <sub>3</sub>	SiO <sub>2</sub>	P <sub>2</sub> O <sub>5</sub>	SO <sub>3</sub>	K <sub>2</sub> O	CaO	TiO <sub>2</sub>	MnO	FeO	NiO
analysis 2, clay rich in FeO	2.63	21.14	41.66	0.70	0.26	3.79	2.46	0.66	0.09	26.46	0.14
	MgO	Al <sub>2</sub> O <sub>3</sub>	SiO <sub>2</sub>	P <sub>2</sub> O <sub>5</sub>	SO <sub>3</sub>	K <sub>2</sub> O	CaO	TiO <sub>2</sub>	MnO	FeO	
analysis 3, calcium phosphate	0.69	3.47	8.17	35.61	0.51	0.77	49.14	0.04	0.06	1.54	

analysis 4, FeO	MgO	Al <sub>2</sub> O <sub>3</sub>	SiO <sub>2</sub>	P <sub>2</sub> O <sub>5</sub>	SO <sub>3</sub>	K <sub>2</sub> O	CaO	TiO <sub>2</sub>	MnO	FeO			
	1.91	8.01	7.90	2.24	0.34	0.44	1.00	0.28	0.23	77.65			
analysis 5, clay	MgO	Al <sub>2</sub> O <sub>3</sub>	SiO <sub>2</sub>	P <sub>2</sub> O <sub>5</sub>	K <sub>2</sub> O	CaO	TiO <sub>2</sub>	MnO	FeO				
	1.86	28.76	52.12	0.10	10.73	1.13	0.92	0.10	4.27				
TiO <sub>2</sub>													
chlorite													
ilmenite													
rare earth elements													
zircon													
<b>Bone US 113</b>													
analysis 1, clay rich in FeO	Na <sub>2</sub> O	MgO	Al <sub>2</sub> O <sub>3</sub>	SiO <sub>2</sub>	P <sub>2</sub> O <sub>5</sub>	SO <sub>3</sub>	K <sub>2</sub> O	CaO	TiO <sub>2</sub>	MnO	FeO	NiO	Ce <sub>2</sub> O <sub>3</sub>
	1.17	3.51	9.79	59.12	1.14	0.05	15.74	2.59	0.84	0.00	5.93	0.10	0.03
analysis 2, zircon	MgO	Al <sub>2</sub> O <sub>3</sub>	SiO <sub>2</sub>	P <sub>2</sub> O <sub>5</sub>	K <sub>2</sub> O	CaO	TiO <sub>2</sub>	MnO	FeO	ZrO <sub>2</sub>			
	0.23	0.74	32.19	0.95	0.39	1.81	0.07	0.07	0.64	62.91			
analysis 3, barium sulfate	Na <sub>2</sub> O	MgO	Al <sub>2</sub> O <sub>3</sub>	SiO <sub>2</sub>	P <sub>2</sub> O <sub>5</sub>	SO <sub>3</sub>	K <sub>2</sub> O	CaO	TiO <sub>2</sub>	MnO	FeO	BaO	
	0.89	2.45	0.59	3.34	21.33	15.10	0.12	24.82	3.03	0.00	2.73	25.60	
<b>Tomb 18</b>													
<b>Soil US 205</b>													
analysis 1, clay rich in FeO	Na <sub>2</sub> O	MgO	Al <sub>2</sub> O <sub>3</sub>	SiO <sub>2</sub>	P <sub>2</sub> O <sub>5</sub>	SO <sub>3</sub>	K <sub>2</sub> O	CaO	TiO <sub>2</sub>	MnO	FeO	NiO	ZnO
	1.75	2.81	10.42	26.30	0.20	0.00	5.97	3.11	9.00	0.27	39.17	0.33	0.65
analysis 2, clay	Na <sub>2</sub> O	MgO	Al <sub>2</sub> O <sub>3</sub>	SiO <sub>2</sub>	P <sub>2</sub> O <sub>5</sub>	SO <sub>3</sub>	K <sub>2</sub> O	CaO	TiO <sub>2</sub>	MnO	FeO	ZnO	
	6.01	5.13	17.07	49.22	0.56	0.13	1.60	15.25	0.82	0.08	4.10	0.03	
analysis 3, quartz with FeO	Na <sub>2</sub> O	MgO	Al <sub>2</sub> O <sub>3</sub>	SiO <sub>2</sub>	P <sub>2</sub> O <sub>5</sub>	SO <sub>3</sub>	K <sub>2</sub> O	CaO	TiO <sub>2</sub>	FeO	NiO		
	5.13	3.95	17.19	59.35	0.60	0.08	2.82	2.66	0.66	7.39	0.16		
FeO													
TiO <sub>2</sub>													
mica													
<b>Bone US 115</b>													
No oxides or minerals were detected													
<b>Tomb 19</b>													
<b>Soil US 207</b>													

analysis 1, clay rich in FeO	Na <sub>2</sub> O	MgO	Al <sub>2</sub> O <sub>3</sub>	SiO <sub>2</sub>	P <sub>2</sub> O <sub>5</sub>	SO <sub>3</sub>	K <sub>2</sub> O	CaO	TiO <sub>2</sub>	MnO	FeO	NiO	
	5.26	4.33	24.33	51.80	0.26	0.09	5.84	1.57	0.30	0.00	6.18	0.04	
analysis 2, clay	Na <sub>2</sub> O	MgO	Al <sub>2</sub> O <sub>3</sub>	SiO <sub>2</sub>	P <sub>2</sub> O <sub>5</sub>	SO <sub>3</sub>	K <sub>2</sub> O	CaO	TiO <sub>2</sub>	MnO	FeO	NiO	ZnO
	3.64	0.76	0.14	0.10	41.30	0.68	0.05	52.10	0.00	0.00	0.82	0.15	0.26
analysis 3, MnO	Na <sub>2</sub> O	MgO	Al <sub>2</sub> O <sub>3</sub>	SiO <sub>2</sub>	P <sub>2</sub> O <sub>5</sub>	SO <sub>3</sub>	K <sub>2</sub> O	CaO	TiO <sub>2</sub>	MnO	FeO	NiO	ZnO
	6.34	4.13	16.57	40.48	0.95	0.04	2.97	2.92	0.59	16.20	8.43	0.21	0.19
calcium phosphate													
ilmenite													
mica													
<b>Bone US 118</b>													
no oxides or minerals were detected													

<b>Tomb 28</b>													
<b>Soil US 243</b>													
analysis 1, clay rich in Fe	MgO	Al <sub>2</sub> O <sub>3</sub>	SiO <sub>2</sub>	P <sub>2</sub> O <sub>5</sub>	SO <sub>3</sub>	K <sub>2</sub> O	CaO	TiO <sub>2</sub>	MnO	FeO	NiO		
	3.56	23.33	55.27	0.74	0.14	4.44	4.39	0.26	0.15	7.69	0.03		
analysis 2, clay	MgO	Al <sub>2</sub> O <sub>3</sub>	SiO <sub>2</sub>	P <sub>2</sub> O <sub>5</sub>	SO <sub>3</sub>	K <sub>2</sub> O	CaO	TiO <sub>2</sub>	FeO	NiO			
	2.92	13.56	31.70	0.13	0.70	2.39	42.59	0.10	5.51	0.38			
calcium phosphate													
SO <sub>3</sub>													
TiO <sub>2</sub>													
FeO													
titanite													
chlorite													
ilmenite													
<b>Bone US 163</b>													
analysis 1, ilmenite	MgO	Al <sub>2</sub> O <sub>3</sub>	SiO <sub>2</sub>	P <sub>2</sub> O <sub>5</sub>	SO <sub>3</sub>	K <sub>2</sub> O	CaO	TiO <sub>2</sub>	MnO	FeO			
	0.55	5.63	13.50	0.04	0.01	3.53	0.58	41.65	1.46	33.06			
MnO													
<b>Tomb 50</b>													
<b>Soil US 826</b>													
analysis 1, clay rich in Fe	MgO	Al <sub>2</sub> O <sub>3</sub>	SiO <sub>2</sub>	P <sub>2</sub> O <sub>5</sub>	SO <sub>3</sub>	K <sub>2</sub> O	CaO	TiO <sub>2</sub>	MnO	FeO	NiO		

	0.41	0.49	1.44	24.02	0.00	0.85	8.05	0.29	4.74	59.66	0.04			
analysis 2, clay	MgO	Al <sub>2</sub> O <sub>3</sub>	SiO <sub>2</sub>	P <sub>2</sub> O <sub>5</sub>	SO <sub>3</sub>	K <sub>2</sub> O	CaO	TiO <sub>2</sub>	MnO	FeO				
	3.60	24.10	55.61	0.41	0.01	4.88	2.70	0.37	0.04	8.29				
calcium phosphate														
FeO														
K <sub>2</sub> O														
zircon														
quartz														
<b>Bone US 827</b>														
analysis 1, rare earth elements	Na <sub>2</sub> O	MgO	SiO <sub>2</sub>	P <sub>2</sub> O <sub>5</sub>	SO <sub>3</sub>	CaO	TiO <sub>2</sub>	CaO	TiO <sub>2</sub>	FeO	NiO	La <sub>2</sub> O <sub>3</sub>	Ce <sub>2</sub> O <sub>3</sub>	Nd <sub>2</sub> O <sub>3</sub>
	0.51	1.87	5.75	34.57	0.41	3.23	0.04	3.23	0.04	0.42	0.12	17.05	29.25	6.78
FeO														
MnO														
<b>Tomb 55</b>														
<b>Soil US 841</b>														
analysis 1, clay wrich in MnO, FeO, NiO	MgO	Al <sub>2</sub> O <sub>3</sub>	SiO <sub>2</sub>	P <sub>2</sub> O <sub>5</sub>	SO <sub>3</sub>	K <sub>2</sub> O	CaO	TiO <sub>2</sub>	MnO	FeO	NiO			
	0.36	1.71	5.87	5.98	0.31	1.39	12.17	1.27	61.49	8.13	1.33			
analysis 2, clay rich in FeO	MgO	Al <sub>2</sub> O <sub>3</sub>	SiO <sub>2</sub>	P <sub>2</sub> O <sub>5</sub>	SO <sub>3</sub>	K <sub>2</sub> O	CaO	TiO <sub>2</sub>	MnO	FeO	NiO			
	3.70	27.62	52.93	0.37	0.28	5.98	1.62	0.39	0.23	6.73	0.13			
analysis 3,clay rich in MnO and FeO	MgO	Al <sub>2</sub> O <sub>3</sub>	SiO <sub>2</sub>	P <sub>2</sub> O <sub>5</sub>	K <sub>2</sub> O	CaO	TiO <sub>2</sub>	MnO	FeO	NiO				
	1.83	14.86	35.31	1.78	3.00	5.22	0.75	25.51	11.08	0.68				
analysis 4, clay rich in MnO and FeO	MgO	Al <sub>2</sub> O <sub>3</sub>	SiO <sub>2</sub>	P <sub>2</sub> O <sub>5</sub>	SO <sub>3</sub>	K <sub>2</sub> O	CaO	TiO <sub>2</sub>	MnO	FeO	NiO			
	1.66	13.59	34.82	1.33	0.12	3.20	5.22	0.29	27.35	11.90	0.52			
analysis 5, calcium phosphate	MgO	Al <sub>2</sub> O <sub>3</sub>	SiO <sub>2</sub>	P <sub>2</sub> O <sub>5</sub>	SO <sub>3</sub>	K <sub>2</sub> O	CaO	TiO <sub>2</sub>	MnO	FeO	NiO			
	1.88	11.38	27.25	18.41	0.29	1.84	24.30	0.18	8.59	5.54	0.33			
ilmenite														
chlorite														
<b>Bone US 842</b>														
analysis 1, MnO	MgO	Al <sub>2</sub> O <sub>3</sub>	SiO <sub>2</sub>	P <sub>2</sub> O <sub>5</sub>	SO <sub>3</sub>	K <sub>2</sub> O	CaO	TiO <sub>2</sub>	MnO	FeO	NiO			
	0.52	0.28	0.42	17.12	0.13	0.21	25.19	1.38	52.07	1.77	0.91			
FeO														

zircon													
<b>Tomb 56</b>													
<b>Soil US 844</b>													
analysis 1, calcium phosphate	Na <sub>2</sub> O	MgO	Al <sub>2</sub> O <sub>3</sub>	SiO <sub>2</sub>	P <sub>2</sub> O <sub>5</sub>	SO <sub>3</sub>	K <sub>2</sub> O	CaO	TiO <sub>2</sub>	MnO	FeO		
	4.77	4.74	20.86	52.03	2.38	0.34	3.61	4.62	0.42	0.04	6.19		
analysis 2, clay	Na <sub>2</sub> O	MgO	Al <sub>2</sub> O <sub>3</sub>	SiO <sub>2</sub>	P <sub>2</sub> O <sub>5</sub>	SO <sub>3</sub>	K <sub>2</sub> O	CaO	TiO <sub>2</sub>	MnO	FeO	ZnO	
	1.71	0.49	1.17	2.94	16.89	0.17	0.67	67.08	0.14	3.84	4.37	0.53	
analysis 3, MnO	Na <sub>2</sub> O	MgO	Al <sub>2</sub> O <sub>3</sub>	SiO <sub>2</sub>	P <sub>2</sub> O <sub>5</sub>	SO <sub>3</sub>	K <sub>2</sub> O	CaO	TiO <sub>2</sub>	MnO	FeO	NiO	
	4.95	2.48	8.41	19.72	22.30	0.45	1.39	32.23	0.46	3.65	3.93	0.03	
FeO													
TiO <sub>2</sub>													
rare earth elements													
zircon													
chlorite													
<b>Bone US 845</b>													
analysis 1, MnO	MgO	Al <sub>2</sub> O <sub>3</sub>	SiO <sub>2</sub>	P <sub>2</sub> O <sub>5</sub>	SO <sub>3</sub>	K <sub>2</sub> O	CaO	TiO <sub>2</sub>	MnO	FeO	NiO		
	0.32	0.27	0.25	29.15	0.42	0.02	41.18	0.34	26.41	0.01	1.63		
analysis 2, MnO	MgO	Al <sub>2</sub> O <sub>3</sub>	SiO <sub>2</sub>	P <sub>2</sub> O <sub>5</sub>	SO <sub>3</sub>	K <sub>2</sub> O	CaO	TiO <sub>2</sub>	MnO	FeO	NiO		
	0.34	0.09	0.08	35.27	0.45	0.00	47.16	0.30	15.83	0.09	0.38		
analysis 4, FeO	Na <sub>2</sub> O	MgO	Al <sub>2</sub> O <sub>3</sub>	SiO <sub>2</sub>	P <sub>2</sub> O <sub>5</sub>	SO <sub>3</sub>	K <sub>2</sub> O	CaO	TiO <sub>2</sub>	MnO	FeO	NiO	
	1.04	0.17	0.57	1.25	18.89	0.57	0.36	18.86	0.09	0.19	57.90	0.10	
barium sulfate													
<b>Tomb 60</b>													
<b>Soil US 857</b>													
analysis 1, calcium phosphate	MgO	Al <sub>2</sub> O <sub>3</sub>	SiO <sub>2</sub>	P <sub>2</sub> O <sub>5</sub>	SO <sub>3</sub>	CaO	TiO <sub>2</sub>	MnO	FeO	NiO			
	0.17	0.23	0.00	43.54	0.88	54.53	0.00	0.00	0.32	0.32			
analysis 2, clay	MgO	Al <sub>2</sub> O <sub>3</sub>	SiO <sub>2</sub>	P <sub>2</sub> O <sub>5</sub>	SO <sub>3</sub>	K <sub>2</sub> O	CaO	TiO <sub>2</sub>	MnO	FeO			
	1.38	10.82	78.25	0.16	0.10	1.85	2.71	0.42	0.08	4.23			
analysis 3, zircon	MgO	Al <sub>2</sub> O <sub>3</sub>	SiO <sub>2</sub>	K <sub>2</sub> O	CaO	TiO <sub>2</sub>	MnO	FeO	NiO	ZrO <sub>2</sub>			
	0.22	1.51	34.97	0.20	0.66	0.21	0.22	1.90	0.40	59.71			
analysis 4, ilmenite with Zn	Na <sub>2</sub> O	MgO	Al <sub>2</sub> O <sub>3</sub>	SiO <sub>2</sub>	P <sub>2</sub> O <sub>5</sub>	SO <sub>3</sub>	K <sub>2</sub> O	CaO	TiO <sub>2</sub>	MnO	FeO	NiO	ZnO

	3.81	1.59	3.93	7.82	0.23	0.15	0.37	0.47	43.91	3.94	30.85	0.11	2.80		
analysis 5, clay	Na <sub>2</sub> O	MgO	Al <sub>2</sub> O <sub>3</sub>	SiO <sub>2</sub>	P <sub>2</sub> O <sub>5</sub>	SO <sub>3</sub>	K <sub>2</sub> O	CaO	TiO <sub>2</sub>	FeO	ZnO				
	7.42	2.05	14.18	22.73	21.38	0.55	1.24	28.10	0.09	2.22	0.04				
Cr															
TiO <sub>2</sub>															
FeO															
ilmenite with MnO															
ilmenite															
chlorite															
<b>Bone US 858</b>															
zircon															
MnO															
<b>Tomb 100</b>															
<b>Soil US 8246</b>															
analysis 1, calcium phosphate	Na <sub>2</sub> O	MgO	Al <sub>2</sub> O <sub>3</sub>	SiO <sub>2</sub>	P <sub>2</sub> O <sub>5</sub>	SO <sub>3</sub>	K <sub>2</sub> O	CaO	FeO	NiO	ZnO				
	2.57	0.50	0.19	0.07	42.01	0.74	0.18	53.22	0.30	0.12	0.10				
analysis 2, clay	Na <sub>2</sub> O	MgO	Al <sub>2</sub> O <sub>3</sub>	SiO <sub>2</sub>	P <sub>2</sub> O <sub>5</sub>	SO <sub>3</sub>	K <sub>2</sub> O	CaO	TiO <sub>2</sub>	MnO	FeO	NiO	ZnO		
	5.34	4.45	20.13	51.76	1.85	0.17	3.54	3.59	1.01	0.06	7.86	0.07	0.17		
analysis 3, rare earth elements with thorium	Na <sub>2</sub> O	MgO	SiO <sub>2</sub>	P <sub>2</sub> O <sub>5</sub>	SO <sub>3</sub>	K <sub>2</sub> O	CaO	TiO <sub>2</sub>	MnO	FeO	NiO	La <sub>2</sub> O <sub>3</sub>	Ce <sub>2</sub> O <sub>3</sub>	Nd <sub>2</sub> O <sub>3</sub>	ThO
	9.16	4.65	26.39	18.24	0.17	1.34	2.29	0.26	0.21	2.29	0.07	10.97	17.17	5.42	1.35
TiO <sub>2</sub>															
FeO															
zircon															
<b>Bone US 8245</b>															
no oxides and minerals were detected															

## *Acknowledgements*

*Questo progetto di tesi è il prodotto di tre anni di lavoro svoltisi tra il Dipartimento di Scienze della Terra “Ardito Desio” e il Labanof (Laboratorio di Antropologia e Odontologia Forense), entrambi afferenti all’Università degli Studi di Milano.*

*Vorrei ringraziare il dott. Luca Trombino e la prof.ssa Cristina Cattaneo per avermi fatto da tutor e co-tutor rispettivamente, permettendo così la realizzazione di questo dottorato.*

*Un dovuto ringraziamento va a tutte quelle persone, professori, ricercatori, tecnici e studenti che hanno contribuito a portare a termine questo progetto nelle sue varie fasi.*

*Per quanta riguarda le persone efferenti all’Università degli Studi di Milano, Dipartimento di Scienze della Terra “Ardito Desio”, si ringrazia il dott. Agostino Rizzi per aver eseguito le analisi al SEM, il dott. Curzio Malinverno per aver preparato le sezioni sottili inglobate in resina per l’analisi al microscopio elettronico a scansione, la prof.ssa Maria Rose Petrizzo per la consulenza sui foraminiferi e infine la dott.ssa Nicoletta Marinoni per avermi aiutato con i programmi computerizzati di elaborazione delle immagini tomografiche prodotte al sincrotrone di ELETTRA (TS).*

*Si ringrazia quindi la linea SYRMEP dell’Elettra sincrotrone di Trieste, tutti i tecnici, dottorandi e collaboratori che vi lavorano o vi hanno lavorato, per aver contribuito l’acquisizione dei dati tomografici.*

*Vorrei ringraziare inoltre il prof. Francesco Berna della Simon Fraser University (Canada) per avermi accolto nella sua università e aiutato con le analisi FTIR e m-FTIR.*

*Un dovuto ringraziamento va inoltre alla Dott.ssa Emanuela Maderna, della Fondazione I.R.C.S.S. Istituto Neurologico Carlo Besta di Milano, per aver contribuito alla realizzazione delle sezioni sottili decalcificate.*

*Vorrei inoltre ringraziare gli enti che hanno messo a disposizione il materiale per questo lavoro, ossia la Soprintendenza per i Beni Archeologici della Lombardia, la Fondazione IRCCS Ca’ Granda Ospedale Maggiore Policlinico di Milano, la Soprintendenza Archeologica Belle Arti e Paesaggio per le province di Parma e Piacenza, il Museo Civico di Travo, e il Comune di Milano.*